1985

Tensile and compressive buckling of plates weakened by mechanical imperfections /

Yi-Der Lee
Lehigh University

TENSILE AND COMPRESSIVE BUCKLING OF PLATES WEAKENED BY MECHANICAL IMPERFECTIONS

by

Yi-Der Lee

A Thesis

Presented to the Graduate Committee

of Lehigh University

in Candidacy for the Degree of

Master of Science

in

Applied Mechanics

Lehigh University

1985

This thesis is accepted and approved in partial fulfillment of the requirement for the degree of Master of Science.

August 26, 1985
(date)

Professor in Charge

Chairman of Department

ACKNOWLEDGEMENTS

The author is indebted to Professor G. C. Sih for his constant guidance under which this thesis was initiated and completed. Acknowledgements are also due to his fellow graduate students, Messrs. D. Y. Tzou, C. H. Chue and C. K. Chao of the Institute of Fracture and Solid Mechanics. Their discussions and inputs have proved to be most valuable. Mrs. Barbara DeLazaro's effort for typing this thesis is also gratefully acknowledged.

To my parents and fiancée, I owe their understanding and constant encouragement.

TABLE OF CONTENTS

TABLE OF CONTENTS - (CONTINUED)

LIST OF TABLES

LIST OF TABLES - (CONTINUED)

LIST OF TABLES - (CONTINUED)

LIST OF FIGURES

LIST OF FIGURES - (CONTINUED)

-x-

LIST OF FIGURES - (CONTINUED)

ABSTRACT

Plates are susceptible to buckling under compression when the thickness dimension becomes sufficiently small. Such mode of structure failure can prevail even if the plates were extended in tension. Wrinkling of stretched thin sheets is a commonly observed phenomenon that leads to complex deflection patterns, particularly in regions close to the mechanical imperfections. Theoretical predictions of the buckled displacement modes for plates weakened by mechanical defects are presented in this work.

Variational calculus is applied to formulate a theory governing the tensile and compressive buckling of thin plates weakened by cavities. By means of the method of finite element, any general shape of mechanical defects can be treated. Analyzed in detail are the cases of a circular hole and narrow elliptical cavity. Various buckled displacement modes are determined and displayed graphically by making use of the graphic package TEMPLAT. The critical buckling loads are found to decrease with increasing cavity size. Moreover, local wrinkling of the plate surface becomes less pronounced for the higher buckling modes. The present method of solution applies equally well to plates that are initially curved.

INTRODUCTION

The local intensification of stress and/or energy field near mechanical defects such as cracks, notches, inclusions, etc., is now well-known. Most of the analyses pertaining to plate-like structure consider the deformation to take place either in a plane or out-of-plane in the global sense. These modes of deformation are usually referred to as plane extension and plate bending such that the load increment is assumed to increase slowly with the displacement. There is another important class of problems that are referred to as "buckling" in which the elements in a plate that lie originally in the same plane are suddenly deformed or deflected in the transverse direction. This may occur nonuniformly as a function of the in-plane space variables, particularly in regions near local defects or cavities regardless of whether the load is applied in tension or compression. Buckling or surface wrinkling will occur if the plate is sufficiently thin.

Classical plates buckling under compressive, shear and bending loads have been solved by application of the finite element method [1,2]. These formulations, however, are not valid when defects are present in the plate. The additional influence of the local boundaries that change with deformation or deflection makes the problem considerably more complex.

The fourth order differential equation governing the transverse displacement of thin plates [3] interacting with the in-plane resultant stresses can be used. A new functional subjected to the changing

boundary conditions on the cavity or defect will be developed by application of the variational principle [4]. The formulation is carried out in matrix form with appropriate triangular finite elements selected such that displacement and slope compatibility of connecting elements are satisfied. The three curvature components at each of the three corner nodes are also introduced as variational parameters. This results in an 18 degrees of freedom for each element.

The plate geometry considered in this work is that of a rectangular plate with a cavity of any general shape. The edges of the plate are simply supported and can be subjected to tensile or compressive loads. Element stiffness and geometric stiffness matrices are developed [5,6] to transform the functional to a large scale standard eigenvalue problem [6] which can be solved by the IMSL subroutine. Results for the various different buckling displacement modes are obtained for the cases of a circular hole and narrow elliptical cavity. The influence of local wrinkling around cavities on the buckling load is discussed in detail. Whether the cavity would fail by fracture prior to or during buckling can be investigated by invoking the strain energy density criterion [7,8].

FUNCTIONAL GOVERNING THE BUCKLING OF THIN PLATES

The equilibrium equation in the z-direction for a thin plate element under the action of in-plane forces, Figure 1, can be written as [3]

$$\frac{\partial^4 w}{\partial x^4} + 2\frac{\partial^4 w}{\partial x^2 \partial y^2} + \frac{\partial^4 w}{\partial y^4} = \frac{1}{D}\left(N_x \frac{\partial^2 w}{\partial x^2} + 2N_{xy}\frac{\partial^2 w}{\partial x \partial y} + N_y \frac{\partial^2 w}{\partial y^2}\right) \qquad (1)$$

where $w(x,y)$ is the plate deflection in the z-direction, D the flexural rigidity, and N_x, N_{xy}, N_y the in-plane forces per unit length of plate boundary. Consider a small variation of the plate deflection, δw, and assume that the in-plane forces N_x, N_{xy}, N_y remain constant during buckling [9-11]. Let the rectangular plate with a cavity be simply-supported. Integrating equation (1) over the surface of the plate A yields

$$D\int_A\int \left(\frac{\partial^4 w}{\partial x^4} + 2\frac{\partial^4 w}{\partial x^2 \partial y^2} + \frac{\partial^4 w}{\partial y^4}\right)\delta w dA = \int_A\int \left(N_x \frac{\partial^2 w}{\partial x^2} + 2N_{xy}\frac{\partial^2 w}{\partial x \partial y} + N_y \frac{\partial^2 w}{\partial y^2}\right)\delta w dA \qquad (2)$$

Carrying out the lengthy process of integrations by parts, the result is

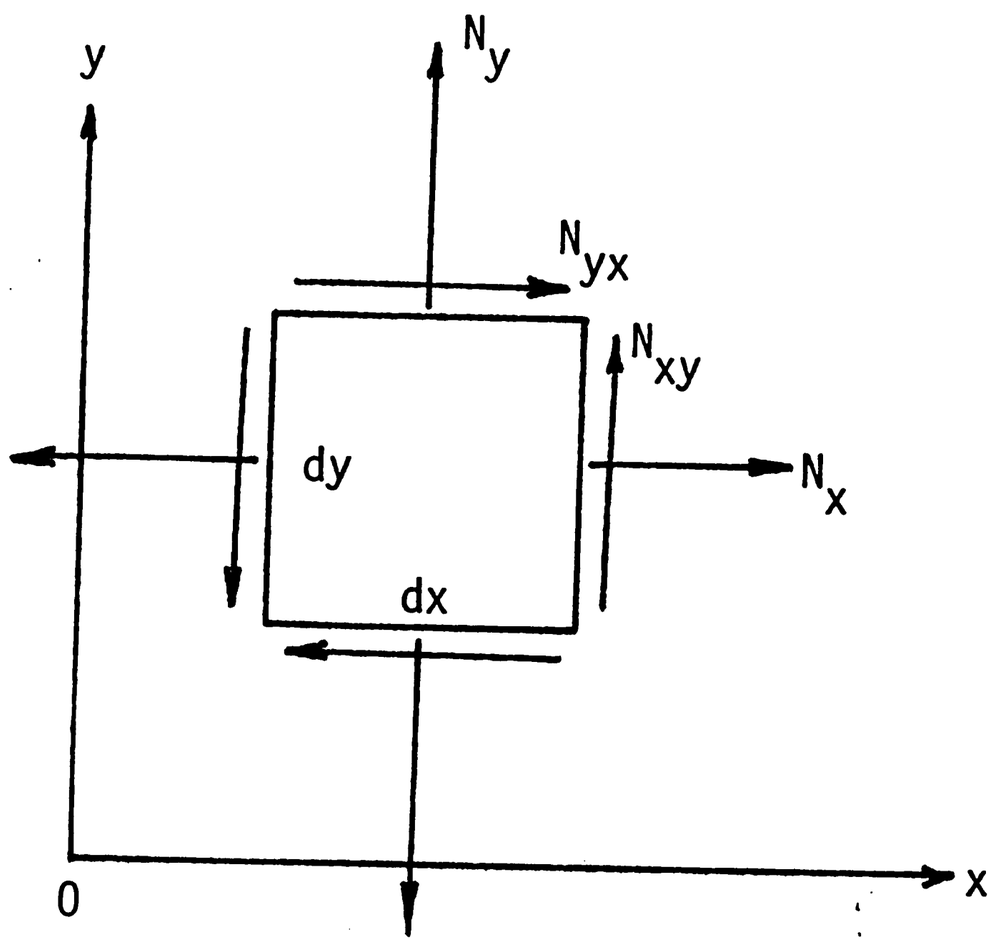

Figure 1 - Notation for in-plane forces.

$$\frac{D}{2}\int_A\int \delta[(\frac{\partial^2 w}{\partial x^2})^2 + (\frac{\partial^2 w}{\partial y^2})^2 + 2\nu\ \frac{\partial^2 w}{\partial x^2}\ \frac{\partial^2 w}{\partial y^2} + 2(1-\nu)(\frac{\partial^2 w}{\partial x \partial y})^2]dA$$

$$+ D\int_A\int \frac{\partial}{\partial x}\ [\delta w(\frac{\partial^3 w}{\partial x^3} + \frac{\partial^3 w}{\partial x \partial y^2})]dA$$

$$+ D\int_A\int \frac{\partial}{\partial y}\ [\delta w(\frac{\partial^3 w}{\partial y^3} + \frac{\partial^3 w}{\partial x^2 \partial y})]dA$$

$$- D\int_A\int \frac{\partial}{\partial x}\ [\delta(\frac{\partial w}{\partial x})(\frac{\partial^2 w}{\partial x^2} + \nu\ \frac{\partial^2 w}{\partial y^2})$$

$$+ (1-\nu)\delta(\frac{\partial w}{\partial y})\ \frac{\partial^2 w}{\partial x \partial y}]dA$$

$$- D\int_A\int \frac{\partial}{\partial y}\ [\delta(\frac{\partial w}{\partial y})(\frac{\partial^2 w}{\partial y^2} + \nu\ \frac{\partial^2 w}{\partial x^2})$$

$$+ (1-\nu)\delta(\frac{\partial w}{\partial x})\ \frac{\partial^2 w}{\partial x \partial y}]dA = -\frac{1}{2}\int_A\int \delta[N_x(\frac{\partial w}{\partial x})^2$$

$$+ N_y(\frac{\partial w}{\partial y})^2 + 2N_{xy}\ \frac{\partial w}{\partial x}\ \frac{\partial w}{\partial y}]dA - \int_A\int \frac{\partial w}{\partial x}\ (\frac{\partial N_x}{\partial x}$$

$$+ \frac{\partial N_{xy}}{\partial y})\delta w dA - \int_A\int \frac{\partial w}{\partial y}\ (\frac{\partial N_{xy}}{\partial x} + \frac{\partial N_y}{\partial y})\delta w dA$$

$$+ \int_A\int \frac{\partial}{\partial x}\ [(N_x\ \frac{\partial w}{\partial x} + N_{xy}\ \frac{\partial w}{\partial y})\delta w]dA$$

$$+ \int_A\int \frac{\partial}{\partial y}\ [(N_y\ \frac{\partial w}{\partial y} + N_{xy}\ \frac{\partial w}{\partial x})\delta w]dA \qquad (3)$$

with ν being the Poisson's ratio. Rearrangement of equation (3) leads to

$$\delta\{\frac{D}{2}\int_A\int [(\frac{\partial^2 w}{\partial x^2})^2 + (\frac{\partial^2 w}{\partial y^2})^2 + 2\nu\,\frac{\partial^2 w}{\partial x^2}\,\frac{\partial^2 w}{\partial y^2} + 2(1-\nu)(\frac{\partial^2 w}{\partial x \partial y})^2]dA$$

$$+ \frac{1}{2}\int_A\int [N_x(\frac{\partial w}{\partial x})^2 + N_y(\frac{\partial w}{\partial y})^2 + 2N_{xy}\,\frac{\partial w}{\partial x}\,\frac{\partial w}{\partial y}]dA\}$$

$$+ \int_A\int \frac{\partial}{\partial x}\{\delta w[D(\frac{\partial^3 w}{\partial x^3} + \frac{\partial^3 w}{\partial x \partial y^2}) - (N_x\,\frac{\partial w}{\partial x}$$

$$+ N_{xy}\,\frac{\partial w}{\partial y})]\}dA + \int_A\int \frac{\partial}{\partial y}\{\delta w[D(\frac{\partial^3 w}{\partial y^3} + \frac{\partial^3 w}{\partial y \partial x^2})$$

$$- (N_{xy}\,\frac{\partial w}{\partial x} + N_y\,\frac{\partial w}{\partial y})]\}dA + \int_A\int [\frac{\partial w}{\partial x}(\frac{\partial N_x}{\partial x} + \frac{\partial N_{xy}}{\partial y})$$

$$+ \frac{\partial w}{\partial y}(\frac{\partial N_{xy}}{\partial x} + \frac{\partial N_y}{\partial y})]\delta w dA - D\int_A\int \frac{\partial}{\partial x}[(\frac{\partial^2 w}{\partial x^2}$$

$$+ \nu\,\frac{\partial^2 w}{\partial y^2})\delta(\frac{\partial w}{\partial x}) + (1-\nu)\frac{\partial^2 w}{\partial x \partial y}\,\delta(\frac{\partial w}{\partial y})]dA$$

$$- D\int_A\int \frac{\partial}{\partial y}[(\frac{\partial^2 w}{\partial y^2} + \nu\,\frac{\partial^2 w}{\partial x^2})\delta(\frac{\partial w}{\partial y})$$

$$+ (1-\nu)\frac{\partial^2 w}{\partial x \partial y}\,\delta(\frac{\partial w}{\partial x})]dA = 0 \qquad (4)$$

The integrands in equation (4) can be identified with the shearing forces per unit length $\tilde{Q}_x$, $\tilde{Q}_y$ and the bending and twisting moments per unit length M_x, M_y, M_{xy}. Refer to Figure 2 for notations. Note that

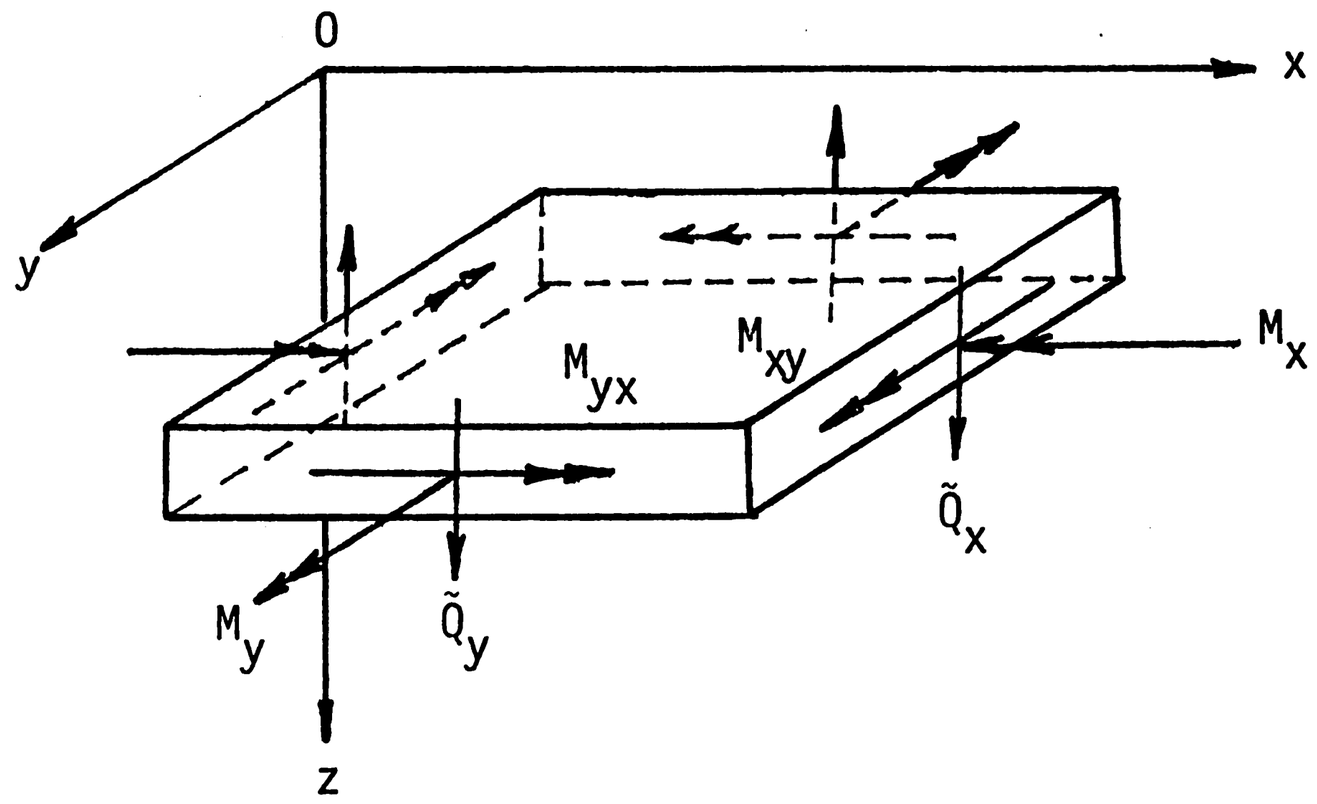

Figure 2 - Notation for stress resultants and loading.

$$M_x = - D(\frac{\partial^2 w}{\partial x^2} + \nu \frac{\partial^2 w}{\partial y^2})$$

$$M_y = - D(\frac{\partial^2 w}{\partial y^2} + \nu \frac{\partial^2 w}{\partial x^2}) \qquad (5)$$

$$M_{xy} = - D(1-\nu)\frac{\partial^2 w}{\partial x \partial y}$$

and

$$\tilde{Q}_x = Q_x + N_x \frac{\partial w}{\partial x} + N_{xy} \frac{\partial w}{\partial y}$$

$$\tilde{Q}_y = Q_y + N_{xy} \frac{\partial w}{\partial x} + N_y \frac{\partial w}{\partial y} \qquad (6)$$

in which Q_x and Q_y stand for

$$Q_x = - D(\frac{\partial^3 w}{\partial x^3} + \frac{\partial^3 w}{\partial x \partial y^2}) \qquad (7)$$

$$Q_y = - D(\frac{\partial^3 w}{\partial y^3} + \frac{\partial^3 w}{\partial y \partial x^2})$$

Invoking the equilibrium of the in-plane resultant stresses,

$$\frac{\partial N_x}{\partial x} + \frac{\partial N_{xy}}{\partial y} = 0 \qquad (8)$$

$$\frac{\partial N_{xy}}{\partial x} + \frac{\partial N_y}{\partial y} = 0$$

it can be shown that equation (4) reduces to

$$\delta\{\frac{1}{2}\int_A\int [(\frac{\partial^2 w}{\partial x^2})^2 + (\frac{\partial^2 w}{\partial y^2})^2 + 2\nu \frac{\partial^2 w}{\partial x^2}\frac{\partial^2 w}{\partial y^2} + 2(1-\nu)(\frac{\partial^2 w}{\partial x \partial y})^2]dA$$

$$+ \frac{1}{2}\int_A\int [N_x(\frac{\partial w}{\partial x})^2 + N_y(\frac{\partial w}{\partial y})^2 + 2N_{xy}\frac{\partial w}{\partial x}\frac{\partial w}{\partial y}]dA\}$$

$$- \oint_c (\tilde{Q}_x \ell + \tilde{Q}_y m)\delta w ds + \oint_c (M_x \ell + M_{xy} m)\delta(\frac{\partial w}{\partial x})ds$$

$$+ \oint_c (M_{xy}\ell + M_y m)\delta(\frac{\partial w}{\partial y})ds = 0 \qquad (9)$$

where ℓ and m are the direction cosines defined in Figure 4. The contour c in Figure 3 is composed of the plate boundary c_1 and notch boundary c_2. With reference to any contour with normal n and tangent s, the following relations may be established:

$$\oint_c (\tilde{Q}_x \ell + \tilde{Q}_y m)\delta w ds = \oint_c \tilde{Q}_n \delta w ds \qquad (10)$$

and

$$\oint_c (M_x \ell + M_{xy} m)\delta(\frac{\partial w}{\partial x})ds + \oint_c (M_{xy}\ell + M_y m)\delta(\frac{\partial w}{\partial y})ds$$

$$= \oint_c M_n \delta(\frac{\partial w}{\partial n})ds + \oint_c M_{ns}\delta(\frac{\partial w}{\partial s})ds$$

$$= \oint_c M_n \delta(\frac{\partial w}{\partial n})ds + (M_{ns}\delta w)_c - \oint_c \frac{\partial M_{ns}}{\partial s}\delta w ds \qquad (11)$$

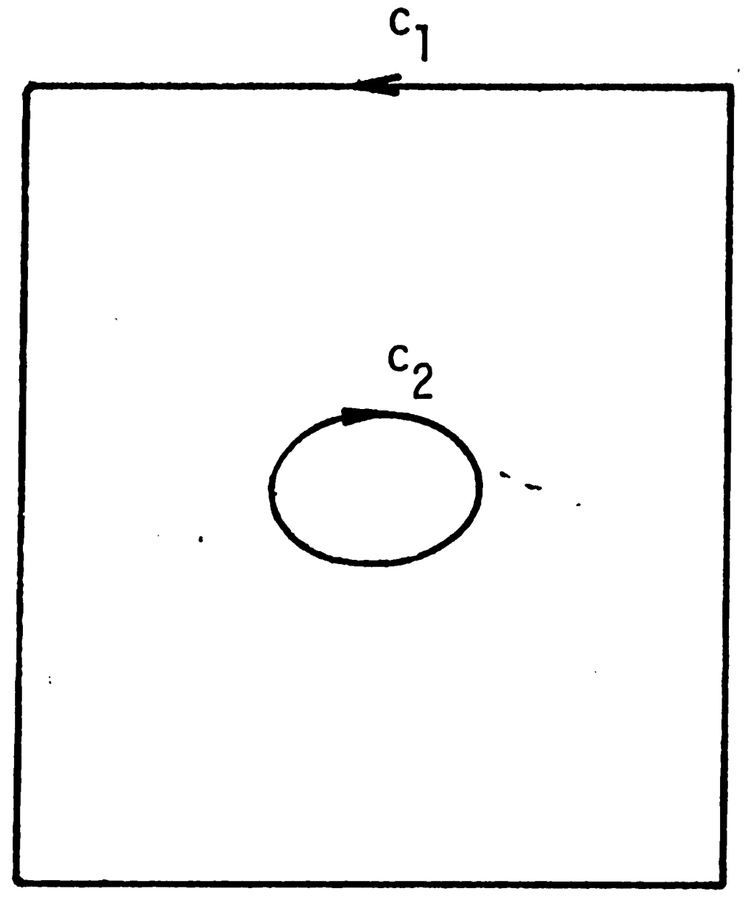

Figure 3 - Boundary contours for this problem.

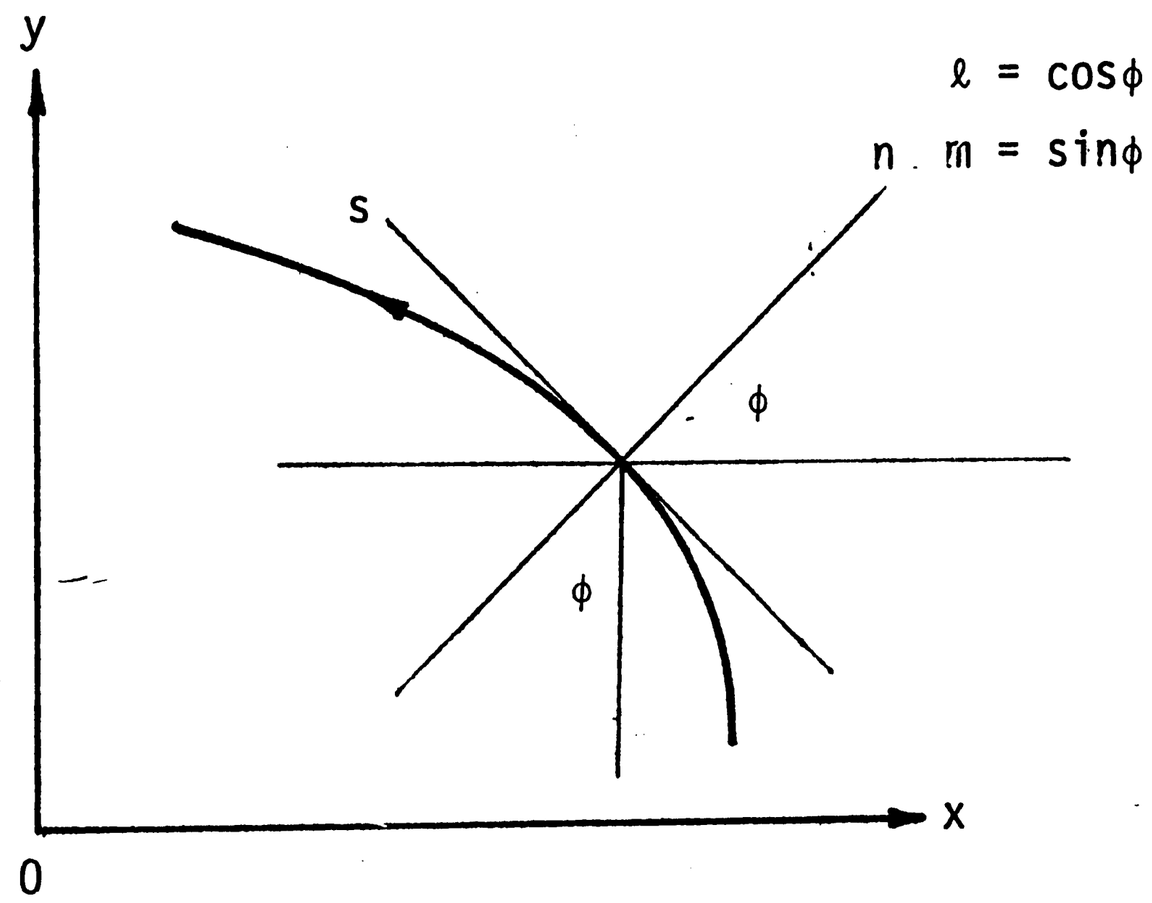

Figure 4 - Definition of a rectangular coordinate on the boundary.

For a closed contour, $(M_{ns}\delta w)_c$ will vanish. Hence, equation (9) becomes

$$\delta\{\frac{D}{2}\int_A\int [(\frac{\partial^2 w}{\partial x^2})^2 + (\frac{\partial^2 w}{\partial y^2})^2 + 2\nu\,\frac{\partial^2 w}{\partial x^2}\,\frac{\partial^2 w}{\partial y^2} + 2(1-\nu)(\frac{\partial^2 w}{\partial x \partial y})^2]dA$$

$$+ \frac{1}{2}\int_A\int [N_x(\frac{\partial w}{\partial x})^2 + N_y(\frac{\partial w}{\partial y})^2 + 2N_{xy}\,\frac{\partial w}{\partial x}\,\frac{\partial w}{\partial y}]dA\}$$

$$- \oint_c (\tilde{Q}_n + \frac{\partial M_{ns}}{\partial s})\delta w ds + \oint_c M_n \delta(\frac{\partial w}{\partial n})ds = 0 \qquad (12)$$

The integrands of the two contour integrals in equation (12) provide the boundary conditions on the plate. For simply supported edges, the following conditions prevail

$$\left.\begin{aligned} \tilde{Q}_n + \frac{\partial M_{ns}}{\partial s} &= 0 \\ M_n &= 0 \end{aligned}\right\} \text{ on } c_1 \text{ and } c_2 \qquad (13)$$

A functional F can thus be defined

$$F = \frac{D}{2}\int_A\int [(\frac{\partial^2 w}{\partial x^2})^2 + (\frac{\partial^2 w}{\partial y^2})^2 + 2\nu\,\frac{\partial^2 w}{\partial x^2}\,\frac{\partial^2 w}{\partial y^2} + 2(1-\nu)(\frac{\partial^2 w}{\partial x \partial y})^2]dA$$

$$+ \frac{1}{2}\int_A\int [N_x(\frac{\partial w}{\partial x})^2 + N_y(\frac{\partial w}{\partial y})^2 + 2N_{xy}\,\frac{\partial w}{\partial x}\,\frac{\partial w}{\partial y}]dA \qquad (14)$$

which consists of the sum of the strain energy and the potential energy.

FINITE ELEMENT FORMULATION

A. Shape Function

The general procedure of the finite element method can be found in [1,2]. It involves discretizing the plate into a number of finite elements. The triangular element [12] with nodal points i, j and k is adopted in this work. The deflection w, slopes $\frac{\partial w}{\partial x}$, $\frac{\partial w}{\partial y}$, and three curvatures $\frac{\partial^2 w}{\partial x^2}$, $\frac{\partial^2 w}{\partial y^2}$, $\frac{\partial^2 w}{\partial x \partial y}$ at each of the three corner nodes can be regarded as independent displacement components, Figure 5. The functional F in equation (14) may be written in matrix form by introducing an appropriate interpolation function.

Let $\{\xi\}$ be defined in terms of the independent displacement components of a typical element, i.e.,

$$\{\xi\}^T = \{w_i, \left(\frac{\partial w}{\partial x}\right)_i, \left(\frac{\partial w}{\partial y}\right)_i, \left(\frac{\partial^2 w}{\partial x^2}\right)_i, \left(\frac{\partial^2 w}{\partial y^2}\right)_i, \left(\frac{\partial^2 w}{\partial x \partial y}\right)_i, w_j, \ldots$$

$$\ldots, \left(\frac{\partial^2 w}{\partial y^2}\right)_k, \left(\frac{\partial^2 w}{\partial x \partial y}\right)_k \} \qquad (15)$$

where the superscript T denotes the transpose of a matrix. The quantities in equation (15) are evaluated at each node. The displacement function will be represented by a fifth order polynomial in x and y. A total of 21 terms are obtained. It can be expressed in terms of the displacement pattern function $p_i(x,y)$ and generalized displacement parameter q_i as

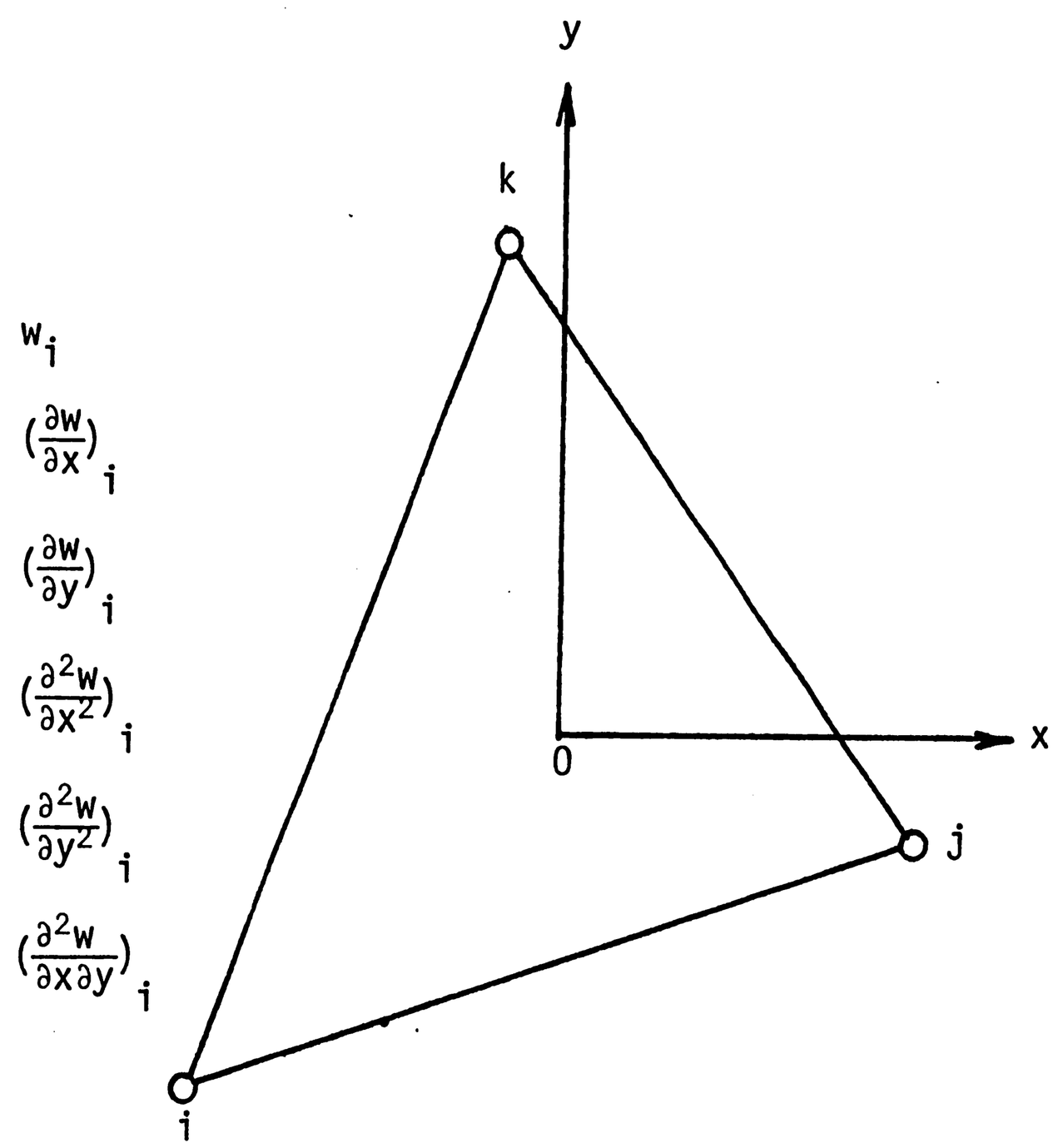

Figure 5 - Degree of freedom for each node in every element.

$$w = q_1 + q_2x + q_3y + q_4x^2 + q_5xy + \ldots + q_{20}xy^4 + q_{21}y^5$$

$$= \sum_{i=1}^{21} p_i(x,y)q_i = \{p\}^T\{q\} \tag{16}$$

Without going into details, the transverse displacement can be written as

$$w = \{p\}^T[R]\{\xi\} \tag{17}$$

where [R] is a matrix whose elements depend on the coordinates of the corner nodes in the element. Refer to Appendix I for the derivation and notation.

B. Matrix Representation

The functional in equation (14) is composed of two portions, one for the strain energy over the plate surface and the other dealing with the potential energy of the in-plane stress resultants N_x, N_y, N_{xy}. The following notations will be adopted:

$$\{\epsilon\} = \begin{Bmatrix} -\frac{\partial^2 w}{\partial x^2} \\ -\frac{\partial^2 w}{\partial y^2} \\ 2\frac{\partial^2 w}{\partial x \partial y} \end{Bmatrix} = [E][R]\{\xi\} \tag{18}$$

$$\{\sigma\} = \begin{Bmatrix} M_x \\ M_y \\ M_{xy} \end{Bmatrix} = D \begin{bmatrix} 1 & \nu & 0 \\ \nu & 1 & 0 \\ 0 & 0 & \frac{1-\nu}{2} \end{bmatrix} \{\varepsilon\} = [G]\{\varepsilon\} = [B][R]\{\xi\} \tag{19}$$

$$\{\phi\} = \begin{Bmatrix} \frac{\partial w}{\partial x} \\ \\ \frac{\partial w}{\partial y} \end{Bmatrix} = [H][R]\{\xi\} \tag{20}$$

$$[S] = \begin{bmatrix} N_x & N_{xy} \\ \\ N_{yx} & N_y \end{bmatrix} \tag{21}$$

where

$$[E] = \begin{Bmatrix} -\frac{\partial^2}{\partial x^2} \\ -\frac{\partial^2}{\partial y^2} \\ 2\frac{\partial^2}{\partial x \partial y} \end{Bmatrix} \{p\}^T \tag{22}$$

$$[G] = D\begin{bmatrix} 1 & \nu & 0 \\ \nu & 1 & 0 \\ 0 & 0 & \frac{1-\nu}{2} \end{bmatrix} \tag{23}$$

$$[B] = [G][E] \tag{24}$$

$$[H] = \begin{Bmatrix} \frac{\partial}{\partial x} \\ \\ \frac{\partial}{\partial y} \end{Bmatrix} \{p\}^T \tag{25}$$

Equation (14) can thus be discretized [1] in the form

$$F = \frac{1}{2}\int_A\int \{\varepsilon\}^T[G]\{\varepsilon\}dA + \frac{1}{2}\int_A\int \{\phi\}^T[S]\{\phi\}dA \tag{26}$$

or

$$F = \frac{1}{2}\{\xi\}^T[R]^T\left(\int_A\int [E]^T[G][E]dA\right)[R]\{\xi\} +$$

$$+ \frac{1}{2}\{\xi\}^T[R]^T\left(\int_A\int [H]^T[S][H]dA\right)[R]\{\xi\} \tag{27}$$

Let the first surface integral be denoted by $[K_S]$ (element stiffness matrix) and the second by $[K_G]$ (geometric stiffness matrix). The

Rayleigh-Ritz method may be applied to equation (27). An eigenvalue problem is thus obtained with

$$([K_S] + \lambda[K_G])\{\xi\} = 0 \tag{28}$$

and λ is the incremental factor of the in-plane resultant stresses N_x, N_y and N_{xy}.

The method of solution consists first of solving the two-dimensional in-plane stress field for a given loading. The global element and geometric stiffness matrices are then found to formulate the eigenvalue problem. The eigenvalue λ determines the buckling load. Use is made of numerical integration in the area coordinates with four sampling points [13]. Positive definiteness of the geometric stiffness matrix is achieved by dividing equation (28) by λ prior to iteration. The displacement, rotations and curvatures at each node for each eigenmode are then obtained. Graphical representation of data is carried out by the TEMPLAT package available at Lehigh.

DISCUSSION OF RESULTS

Different combinations of load and cavity shape are considered while the overall plate dimensions are taken as 36 cm x 50 cm x 0.2 cm. The uniaxial load in the y-direction as shown in Figures 6 to 9 can be tensile or compressive. The Young's modulus of elasticity is $E = 7.1 \times 10^4$ MPa and the Poisson's ratio is $\nu = 0.33$. Considered are the following boundary conditions

$$
\begin{aligned}
&w = 0,\ \frac{\partial^2 w}{\partial x^2} = 0 \qquad \text{(free rotation); at } x = \pm 18 \text{ cm} \\
&w = 0,\ \frac{\partial^2 w}{\partial y^2} = 0 \qquad \text{(free rotation); at } y = \pm 25 \text{ cm} \\
&\tilde{Q}_n + \frac{\partial M_{ns}}{\partial s} = 0 \qquad \text{(free edge); at cavity boundary}
\end{aligned}
\tag{29}
$$

Because of load and geometric symmetry, only one-quarter of the plate needs to be analyzed. Figures 10 to 13 give the finite element grid patterns for each one of the four cases.

A. Small Circular Hole (r = 3 cm)

Consider first the configuration of a small circular hole of radius r = 3 cm subjected to uniaxial tensile and compressive stress. Buckling displacement modes corresponding to critical tensile loads of 2.000×10^6, 4.483×10^6, 6.543×10^6 and 8.309×10^6 N/m are found. The results are displayed in Figures 14 to 17 inclusive only for the center portion of the plate. Wrinkling of the surface is most notice-

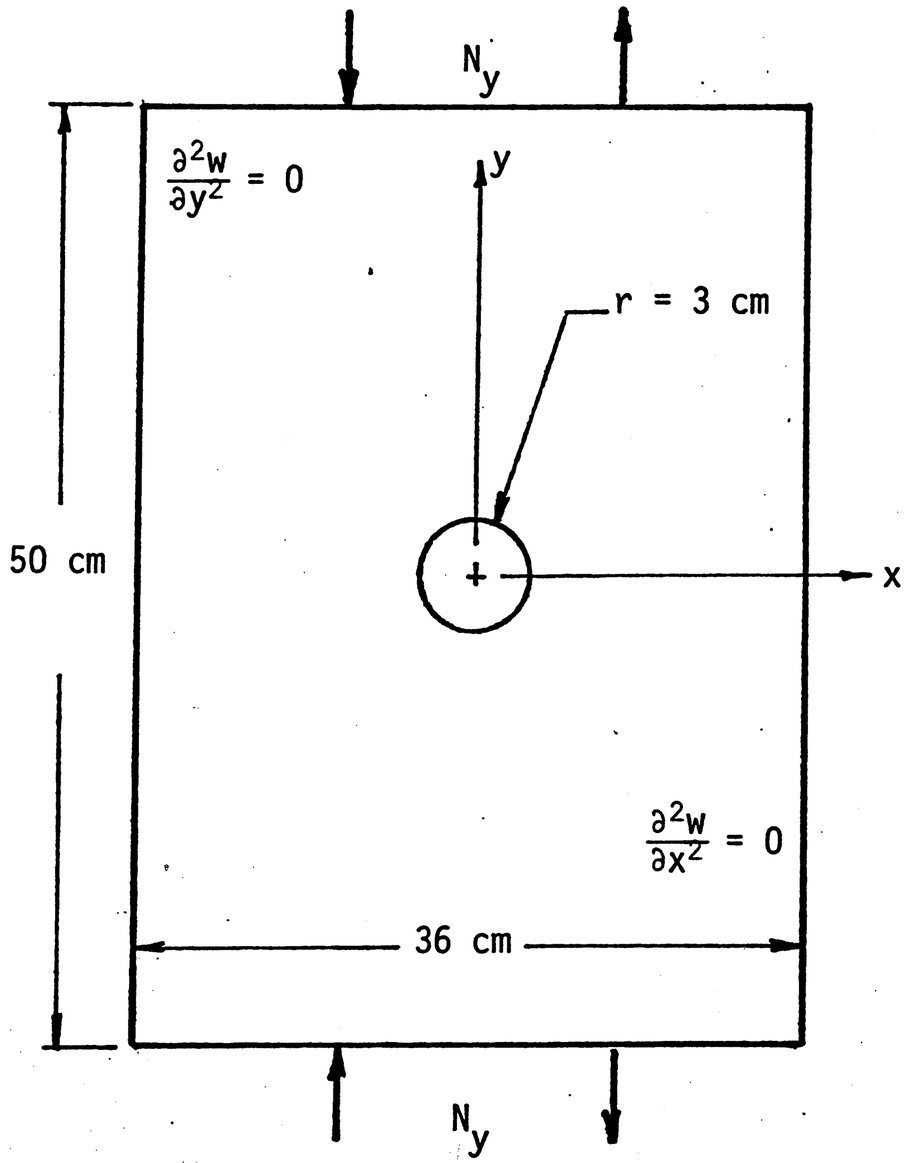

Figure 6 - Plate with a small circular hole r = 3 cm.

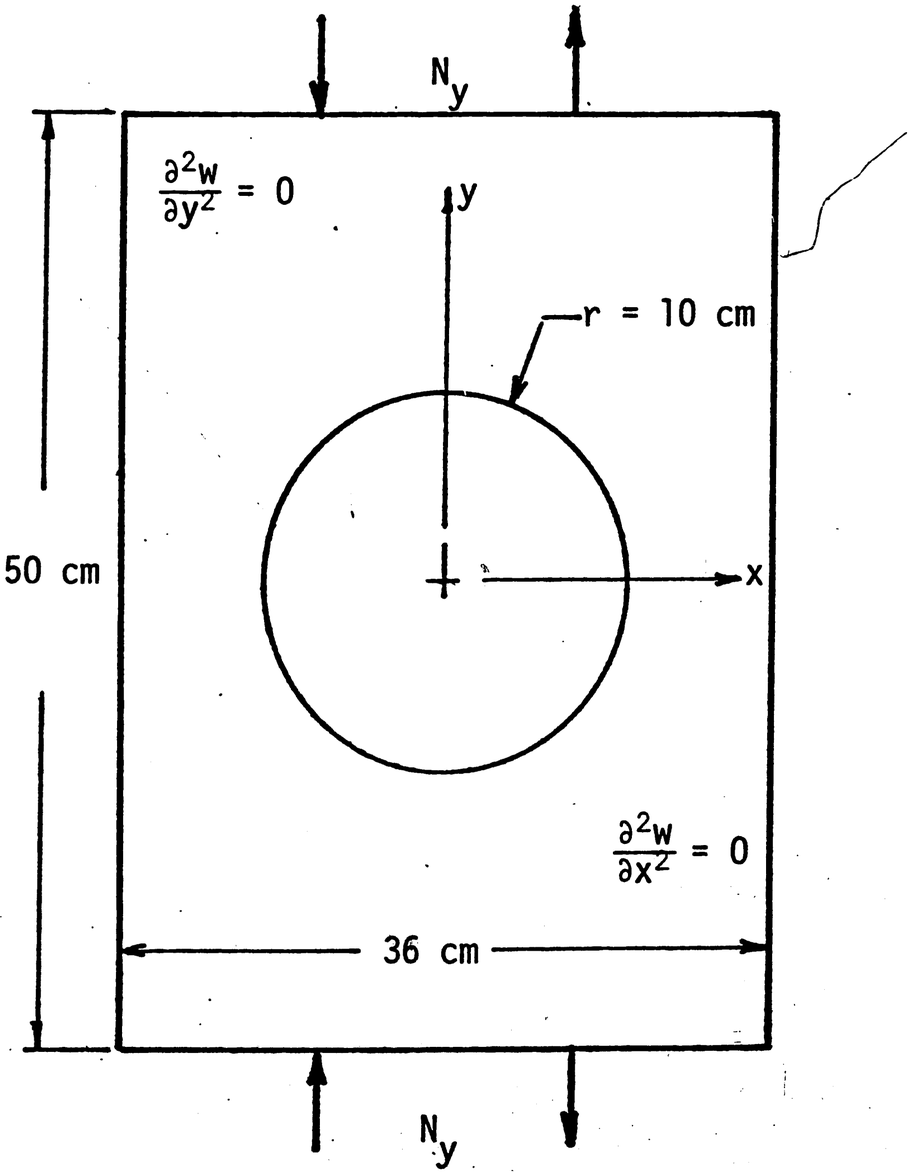

Figure 7 - Plate with a large circular hole r = 10 cm.

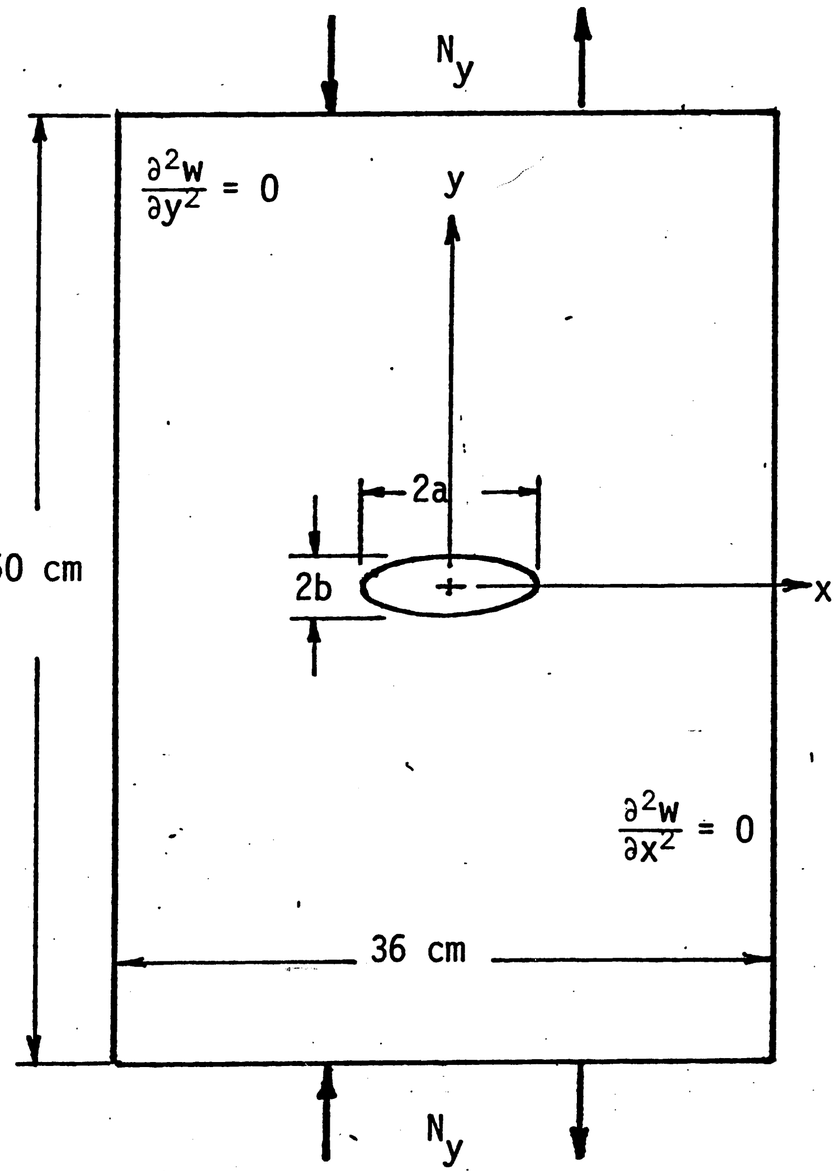

Figure 8 - Plate with a narrow horizontal elliptical cavity; b/a = 0.1, a = 10 cm.

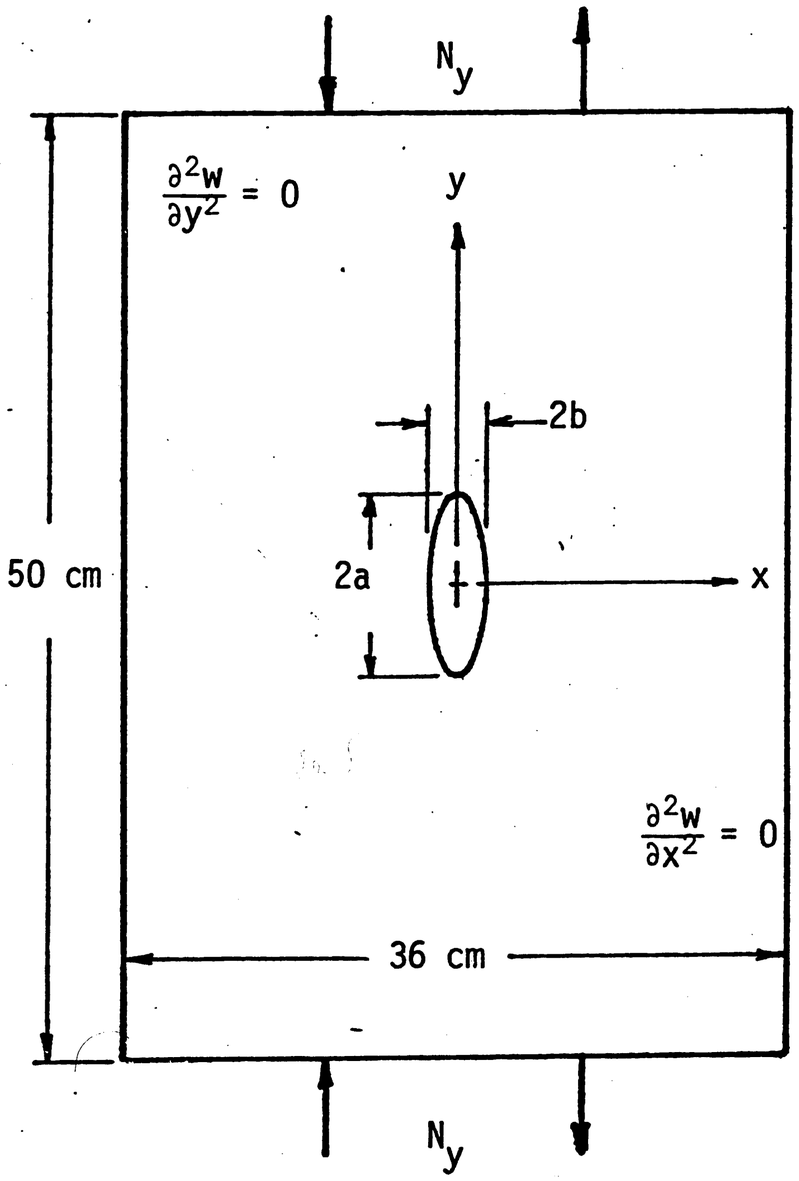

Figure 9 - Plate with a narrow vertical elliptical cavity; b/a = 0.1, a = 10 cm.

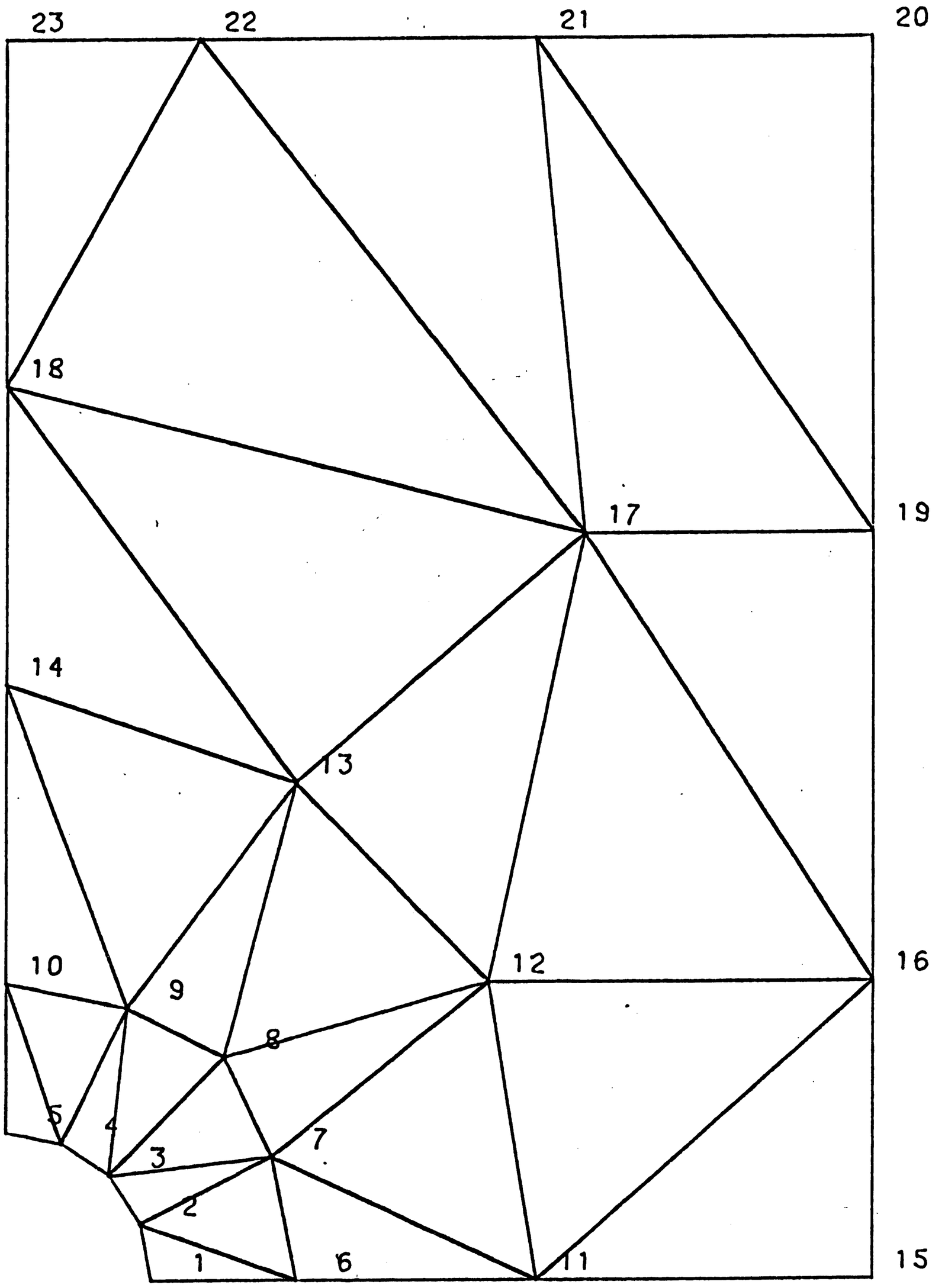

Figure 10 - Finite element grid pattern for small circular hole.

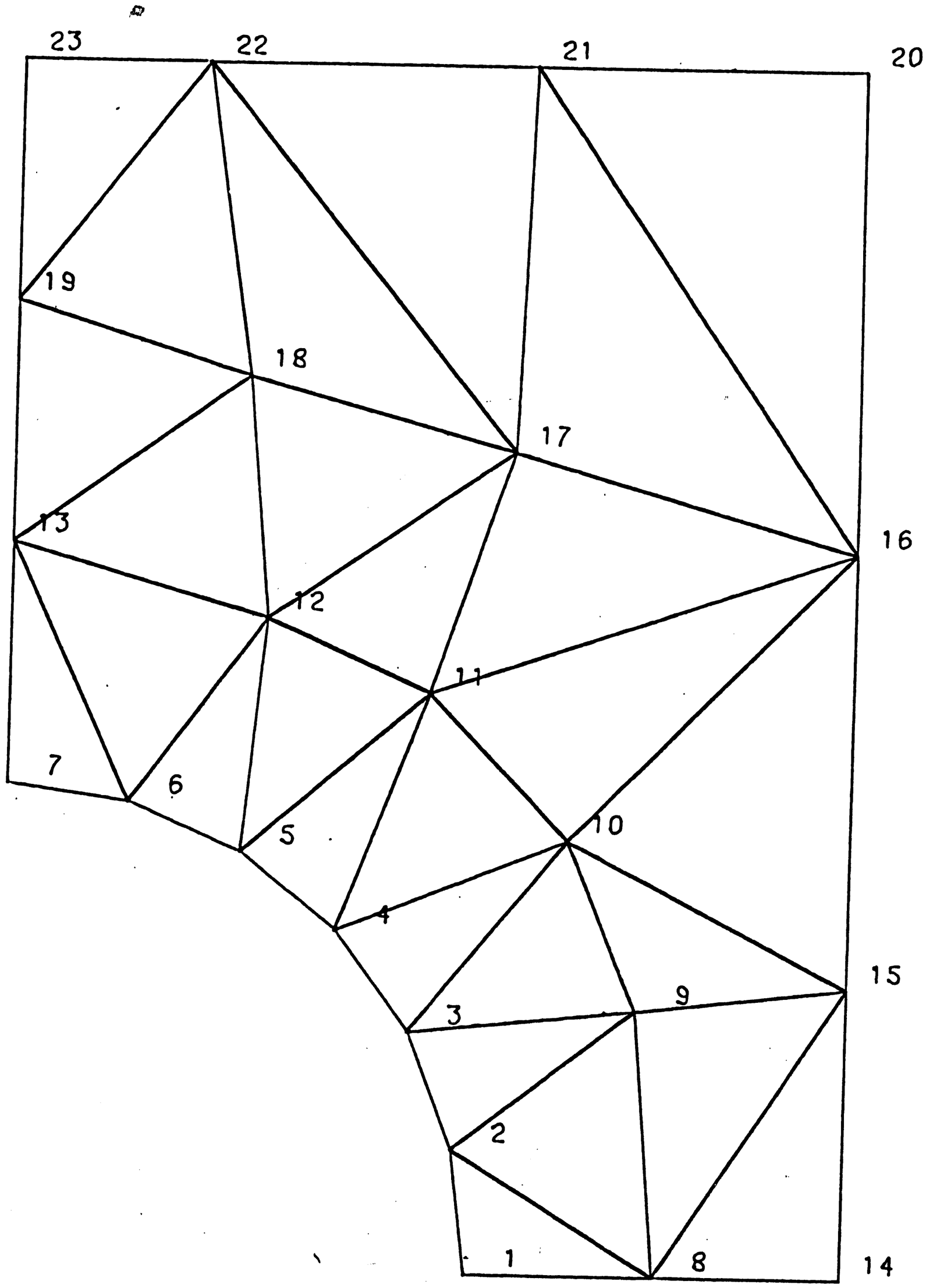

Figure 11 - Finite element grid pattern for large circular hole.

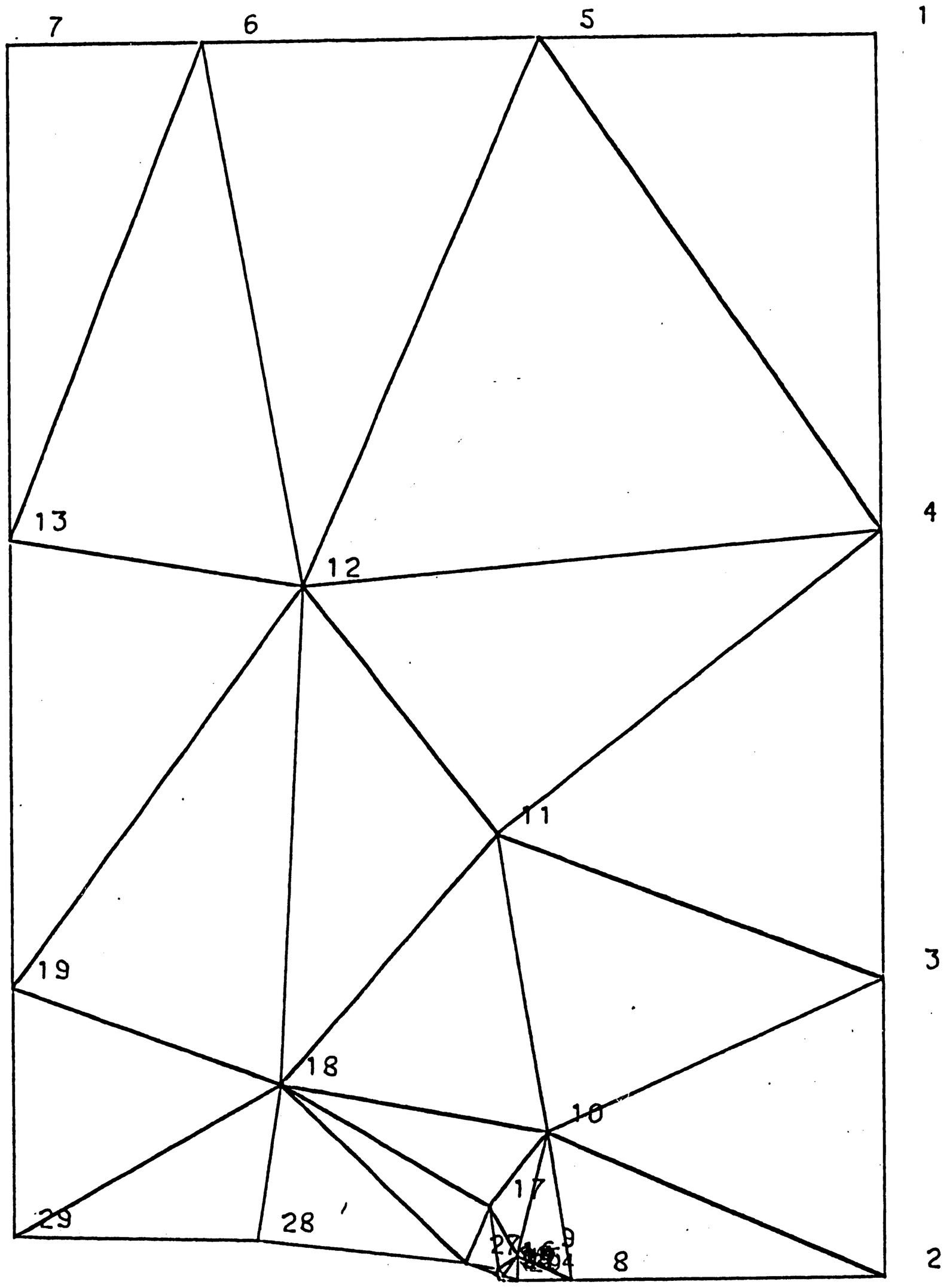

Figure 12 - Finite element grid pattern for narrow horizontal elliptical cavity.

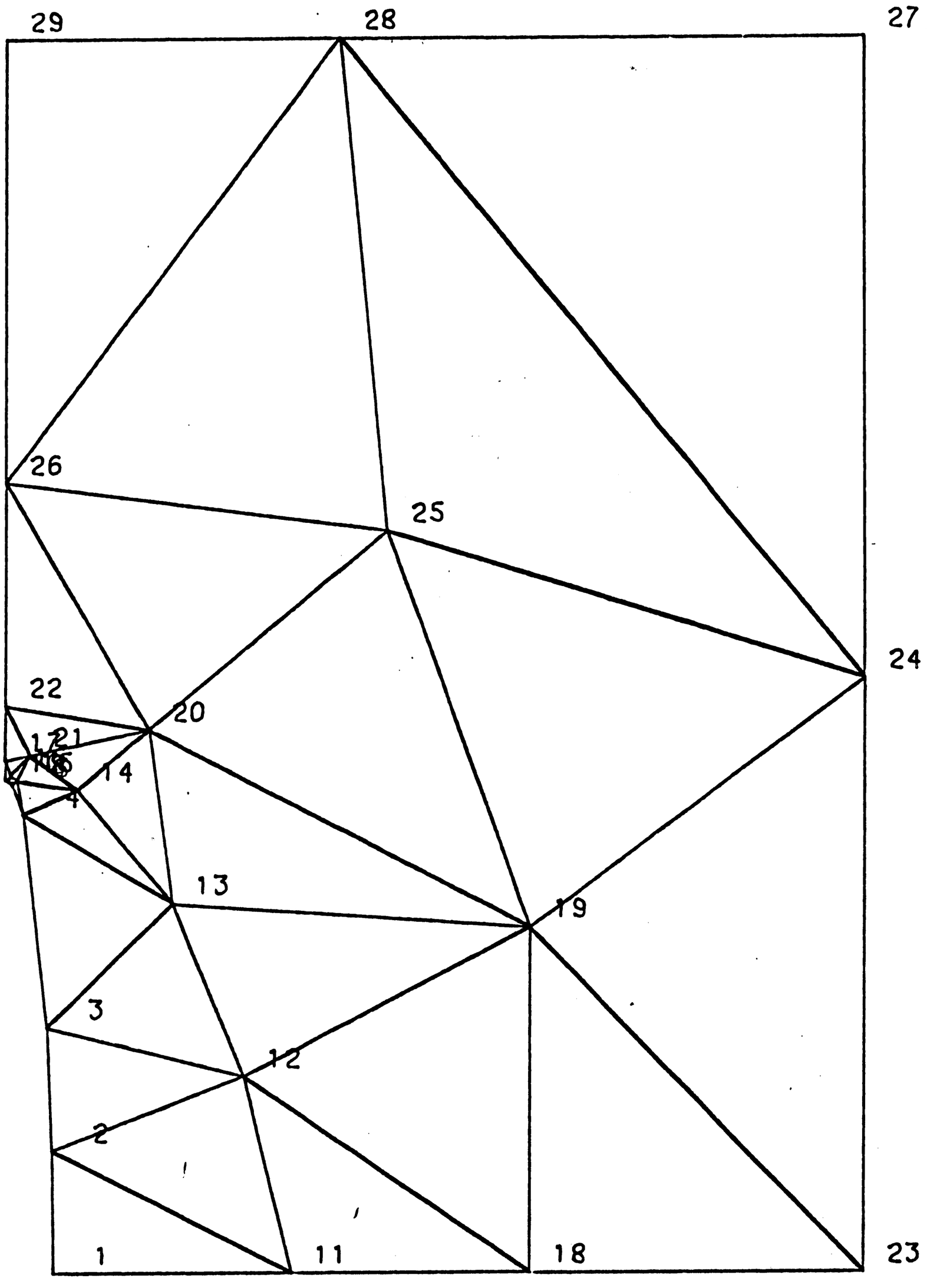

Figure 13 - Finite element grid pattern for narrow vertical elliptical cavity.

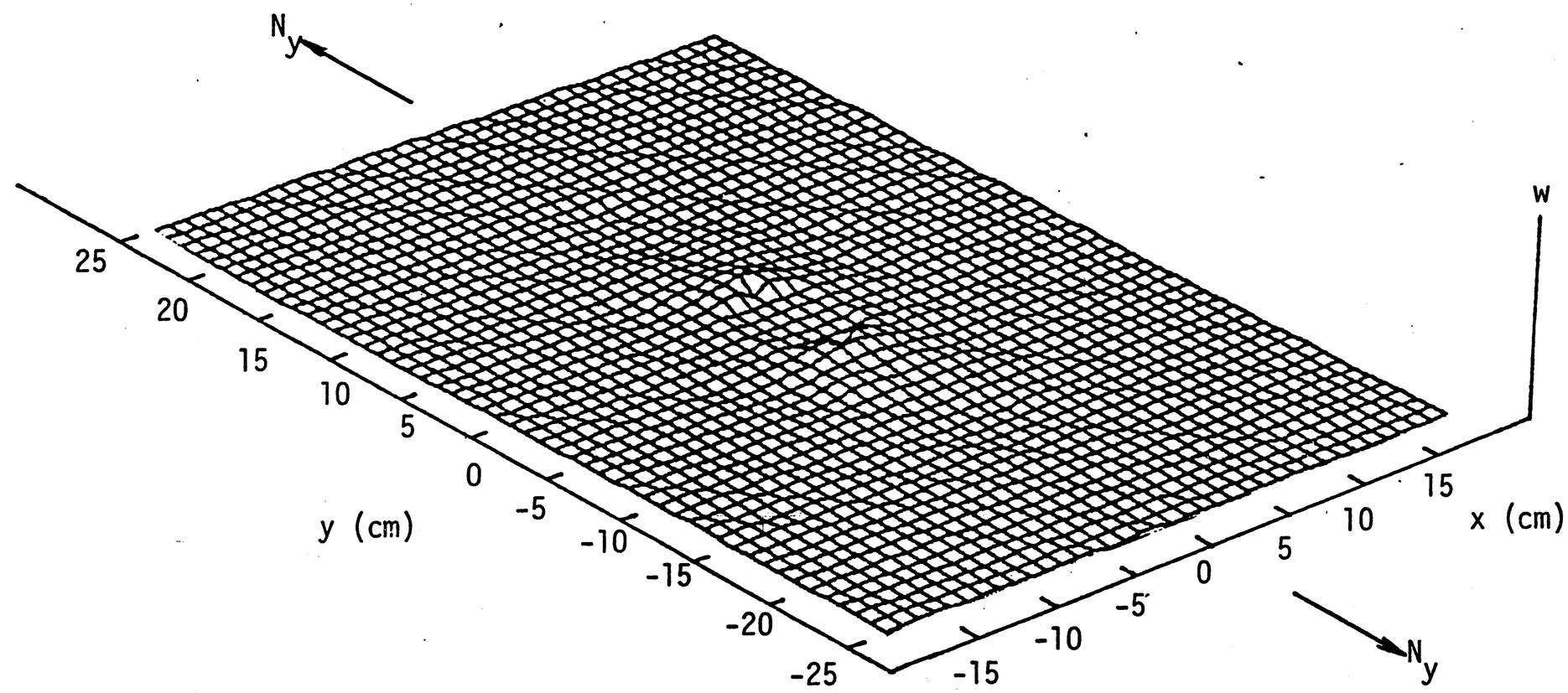

Figure 14 - The lowest tensile buckling mode of a plate with a small circular hole, r = 3 cm; buckling load = 2.000×10^6 N/m.

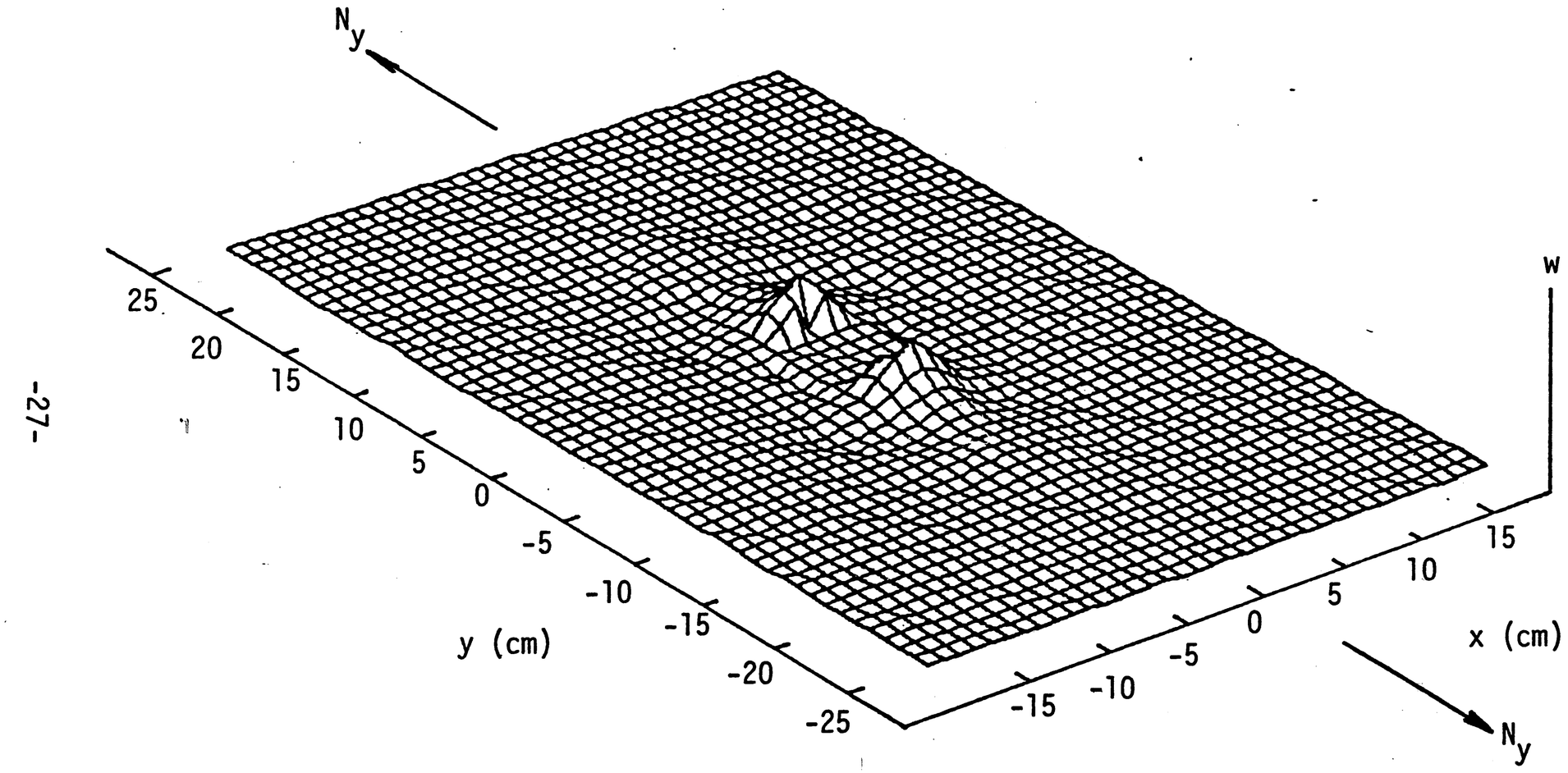

Figure 15 - The second lowest tensile buckling mode of a plate with a small circular hole, r = 3 cm; buckling load = 4.483×10^6 N/m.

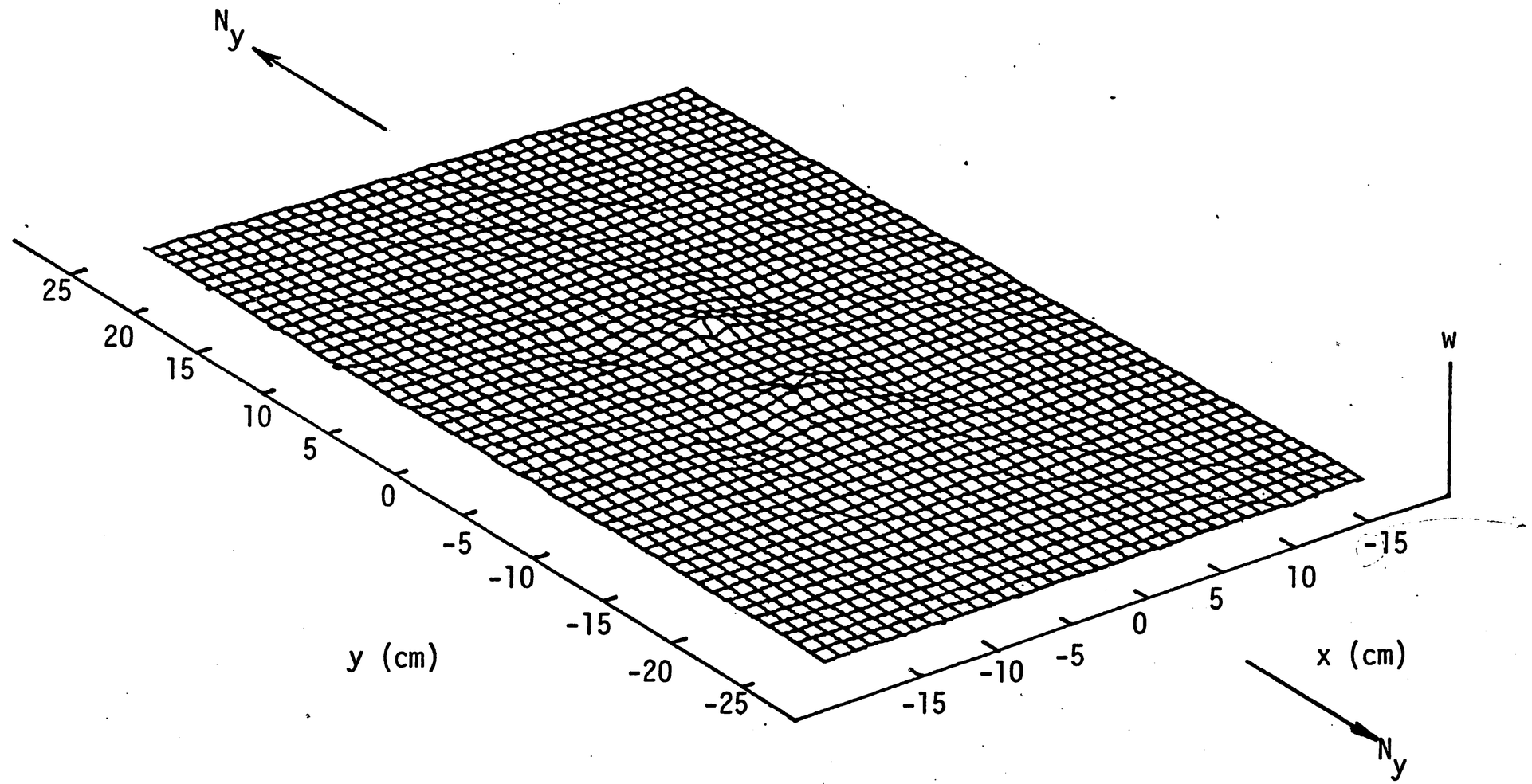

Figure 16 - The third lowest tensile buckling mode of a plate with a small circular hole, r = 3 cm; buckling load = 6.543×10^6 N/m.

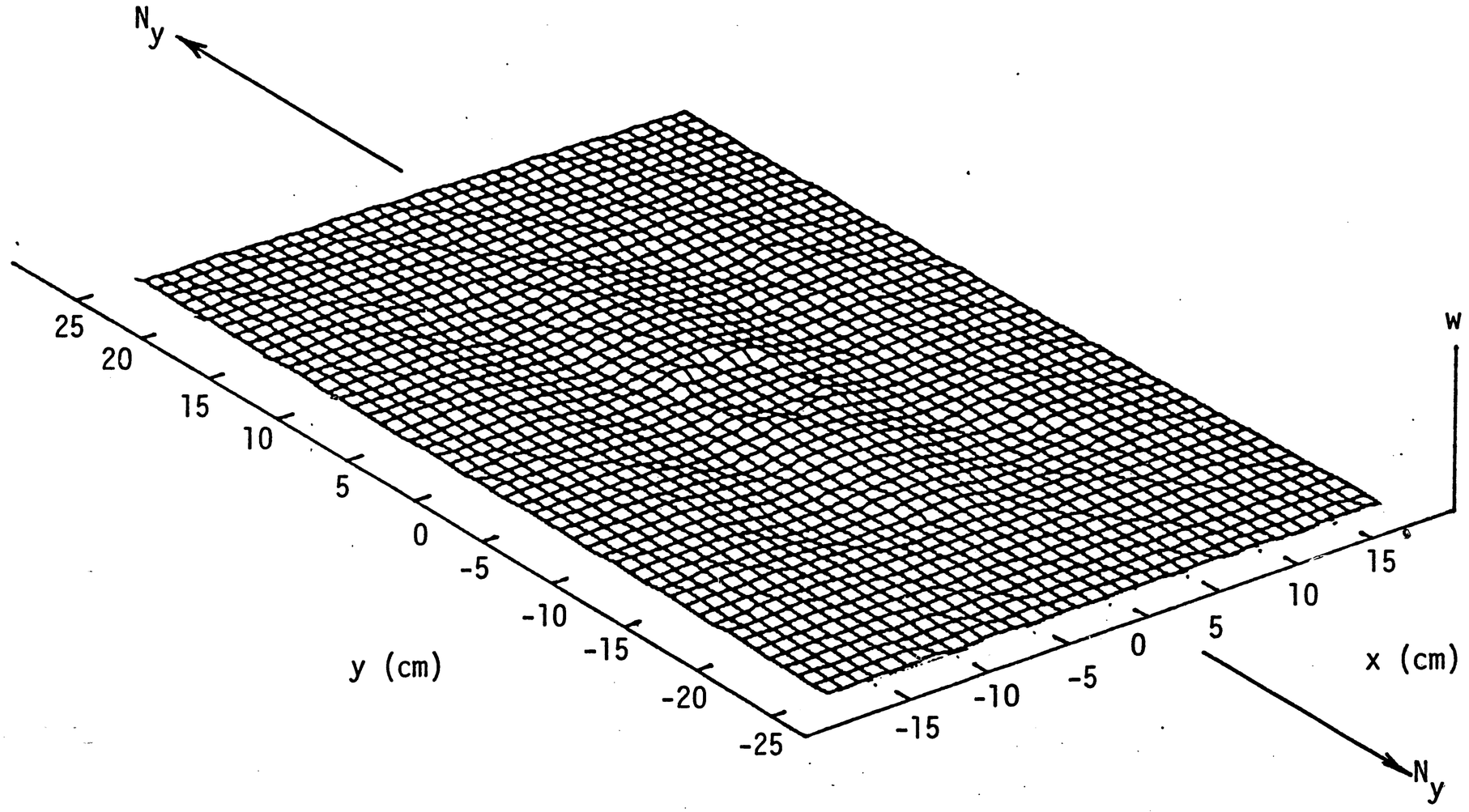

Figure 17 - The fourth lowest tensile buckling mode of a plate with a small circular hole; r = 3 cm; buckling load = 8.309×10^6 N/m.

able at the top and bottom side of the hole and it gradually diminishes at distances further away. The most noticeable out-of-plane local deflection pattern is seen in Figure 15 with a buckling load of 4.483×10^6 N/m. The higher modes show that wrinkling is gradually diffused throughout the plate.

When the load is reversed in compression, buckling becomes much more pronounced. This is indicated in Figures 18 to 21 for critical loads of 1.693×10^4, 2.658×10^4, 5.923×10^4 and 1.116×10^5 N/m even though the magnitude of the local load is approximately two orders of magnitude lower. Figure 18 corresponds to the first compressive buckling mode which shows little or no local wrinkling of the surface near the circular hole. The plate deformed as if the hole were not present. Ripples in the plate start to develop at the higher buckling loads with decreasing wave length. This can be clearly seen in Figures 19 to 21. For more details, refer to the numerical results in Tables 1 to 16 inclusive.

B. Large Circular Hole (r = 10 cm)

When the circular hole size is increased more than three times, i.e., from r = 3 cm to 10 cm, the buckling local displacement fields change dramatically. Figures 22 to 25 correspond to critical tensile loads of 1.140×10^5, 4.031×10^5, 7.006×10^5 and 8.707×10^5 N/m. These values are lower than those in Figures 14 to 17 for the smaller circular hole. Larger hole size tends to enhance buckling with more pronounced out-of-plane displacement. It is interesting to note that

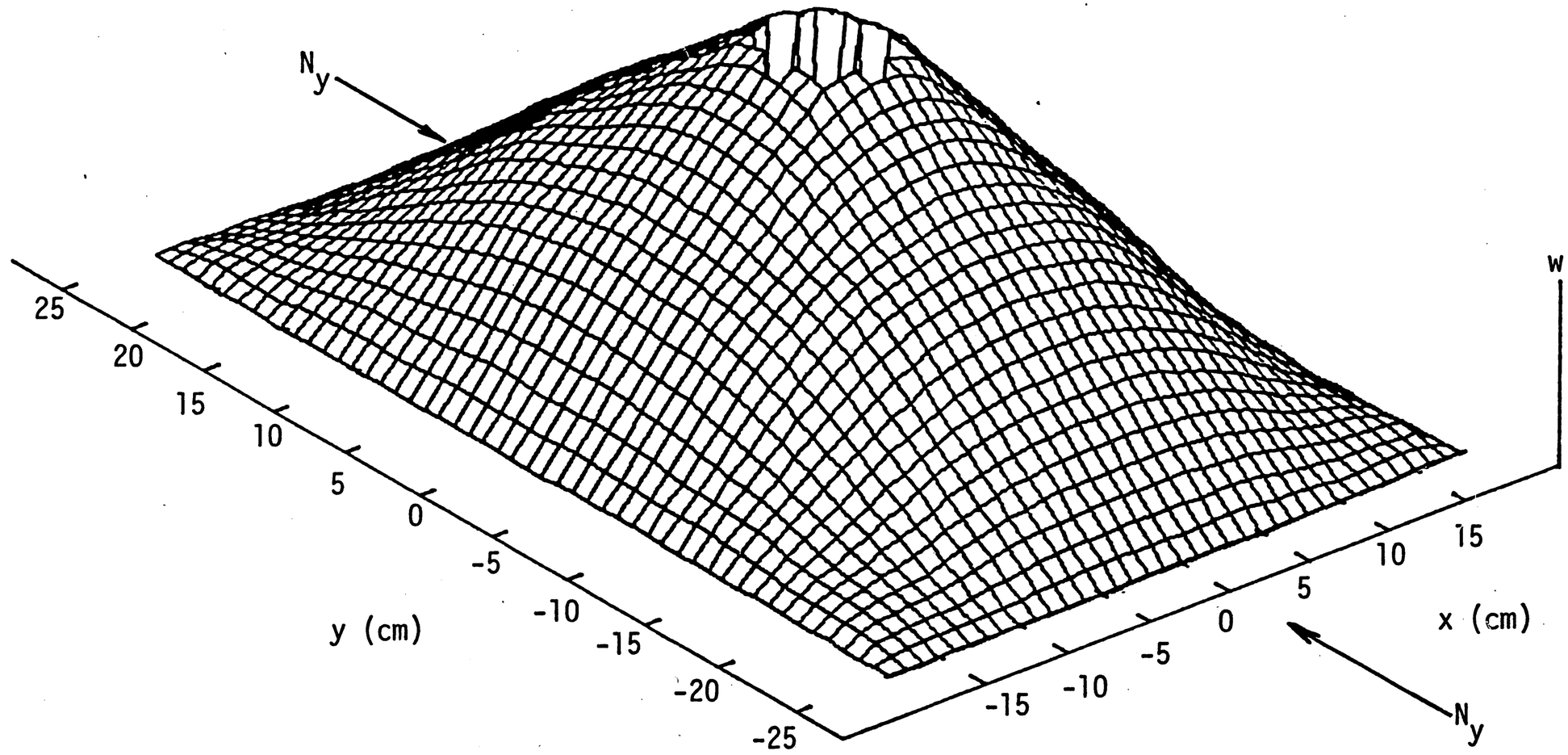

Figure 18 - The lowest compressive buckling mode of a plate with a small circular hole, r = 3 cm; buckling load = 1.693×10^4 N/m.

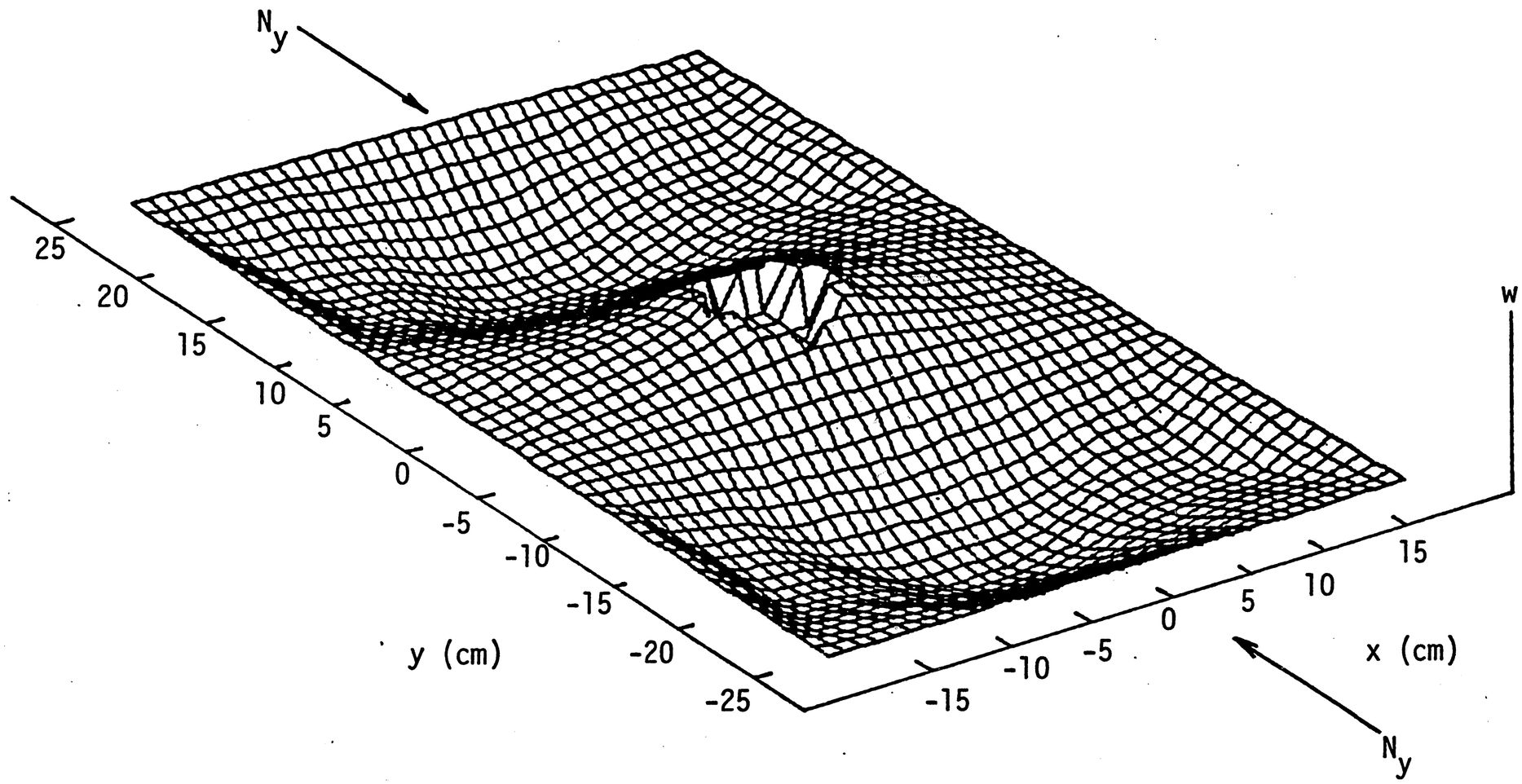

Figure 19 - The second lowest compressive buckling mode of a plate with a small circular hole, r = 3 cm; buckling load = 2.658×10^4 N/m.

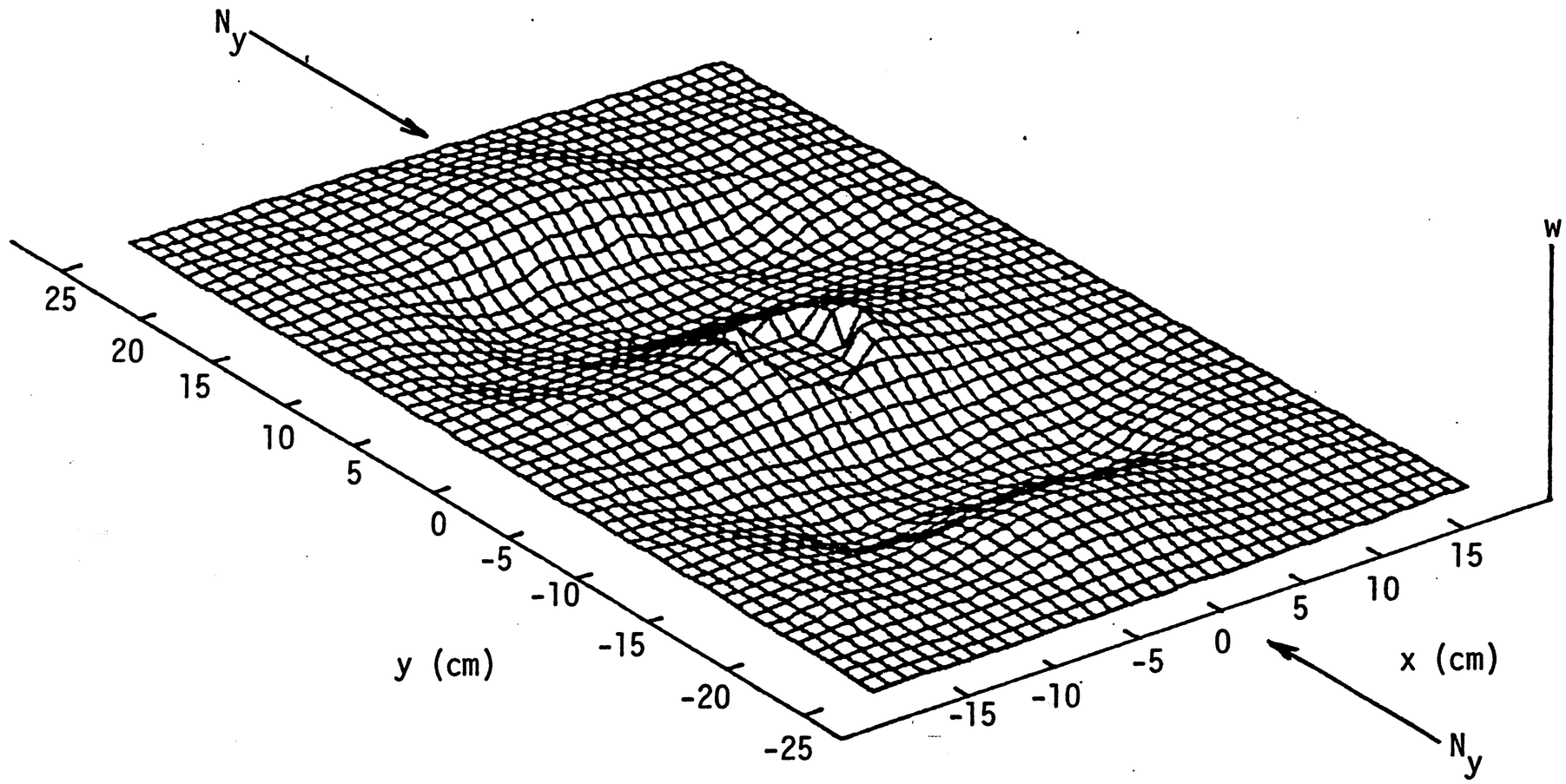

Figure 20 - The third lowest compressive buckling mode of a plate with a small circular hole, r = 3 cm; buckling load = 5.923×10^4 N/m.

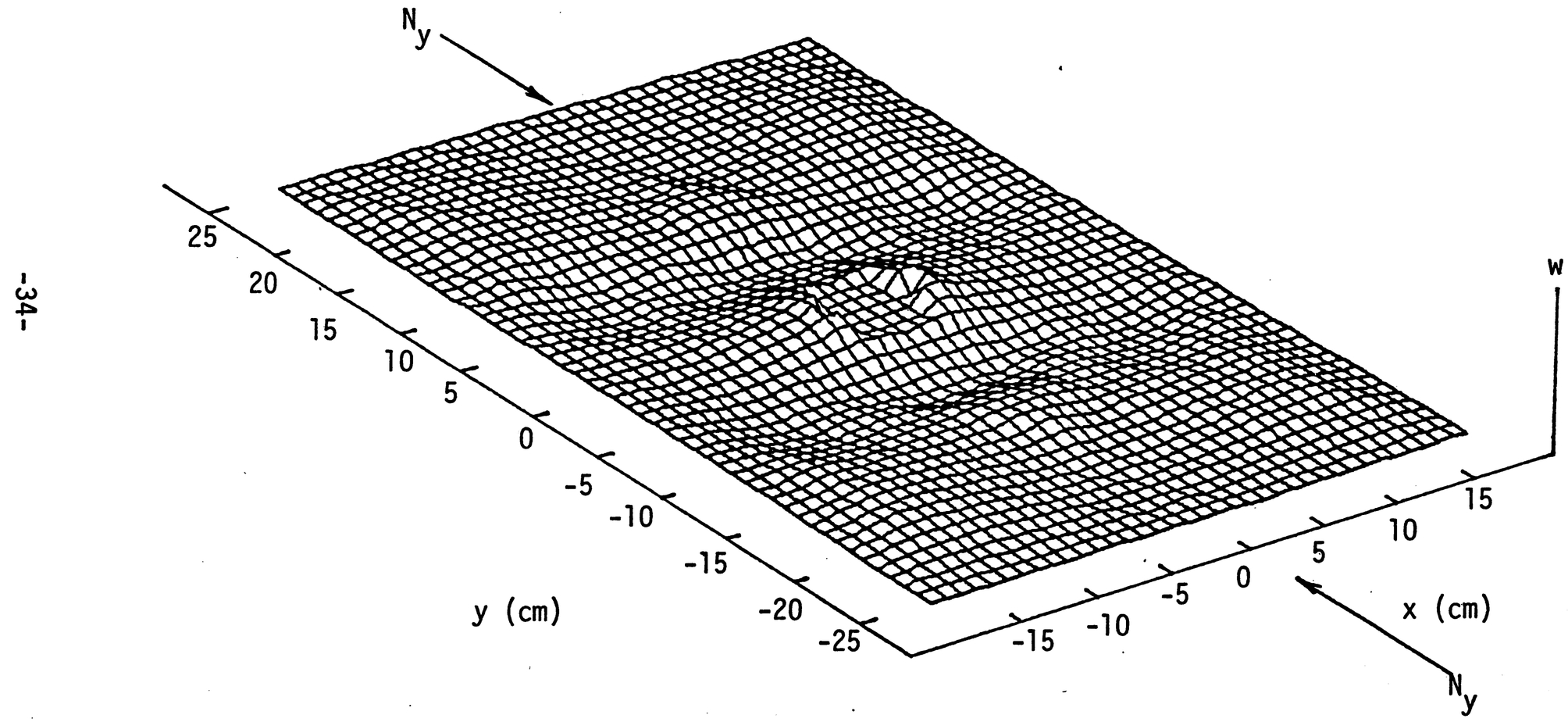

Figure 21 - The fourth lowest compressive buckling mode of a plate with a small circular hole, r = 3 cm; buckling load = 1.116 x 10^5 N/m.

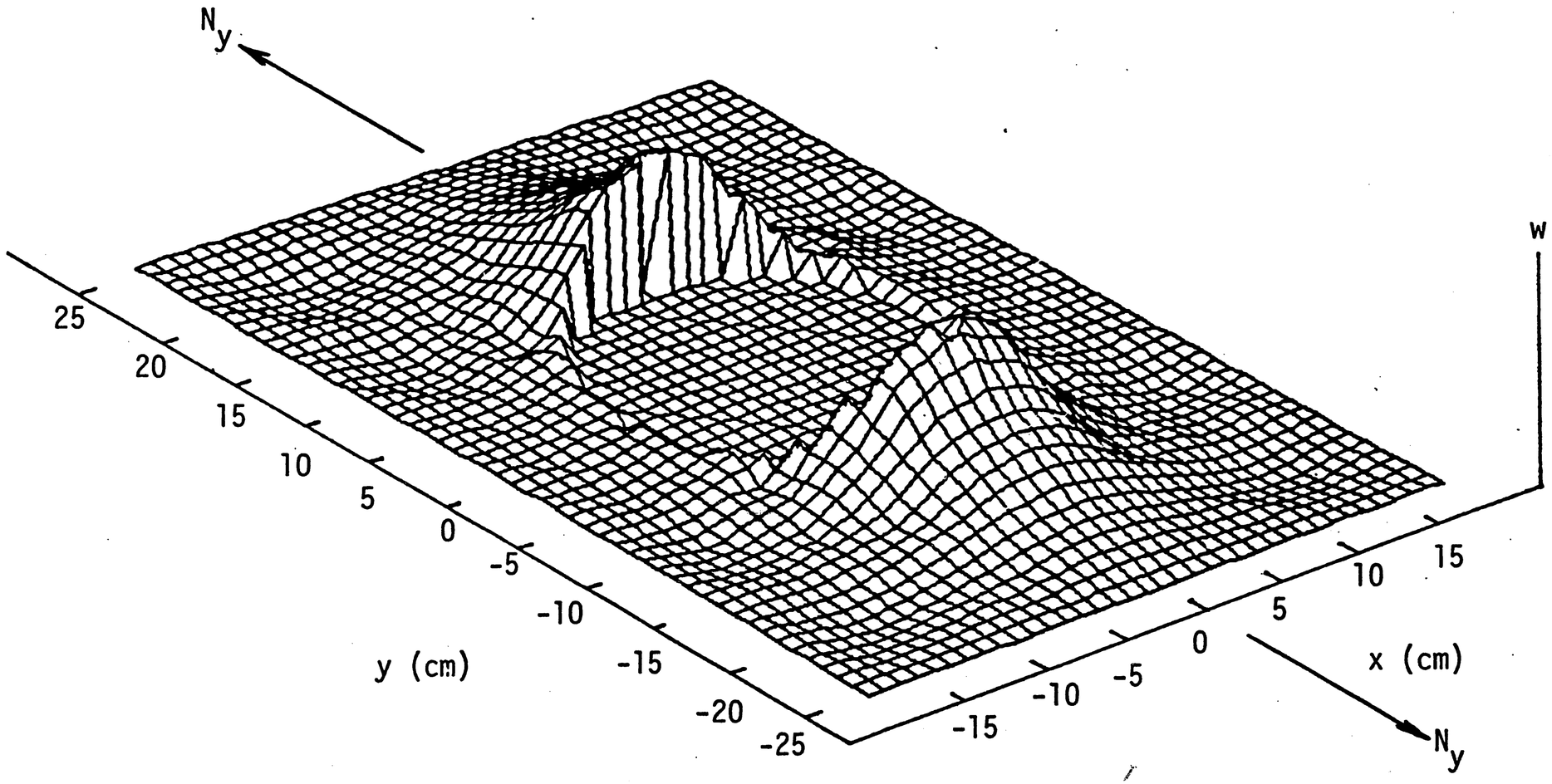

Figure 22 - The lowest tensile buckling mode of a plate with a large circular hole, r = 10 cm; buckling load = 1.140×10^5 N/m.

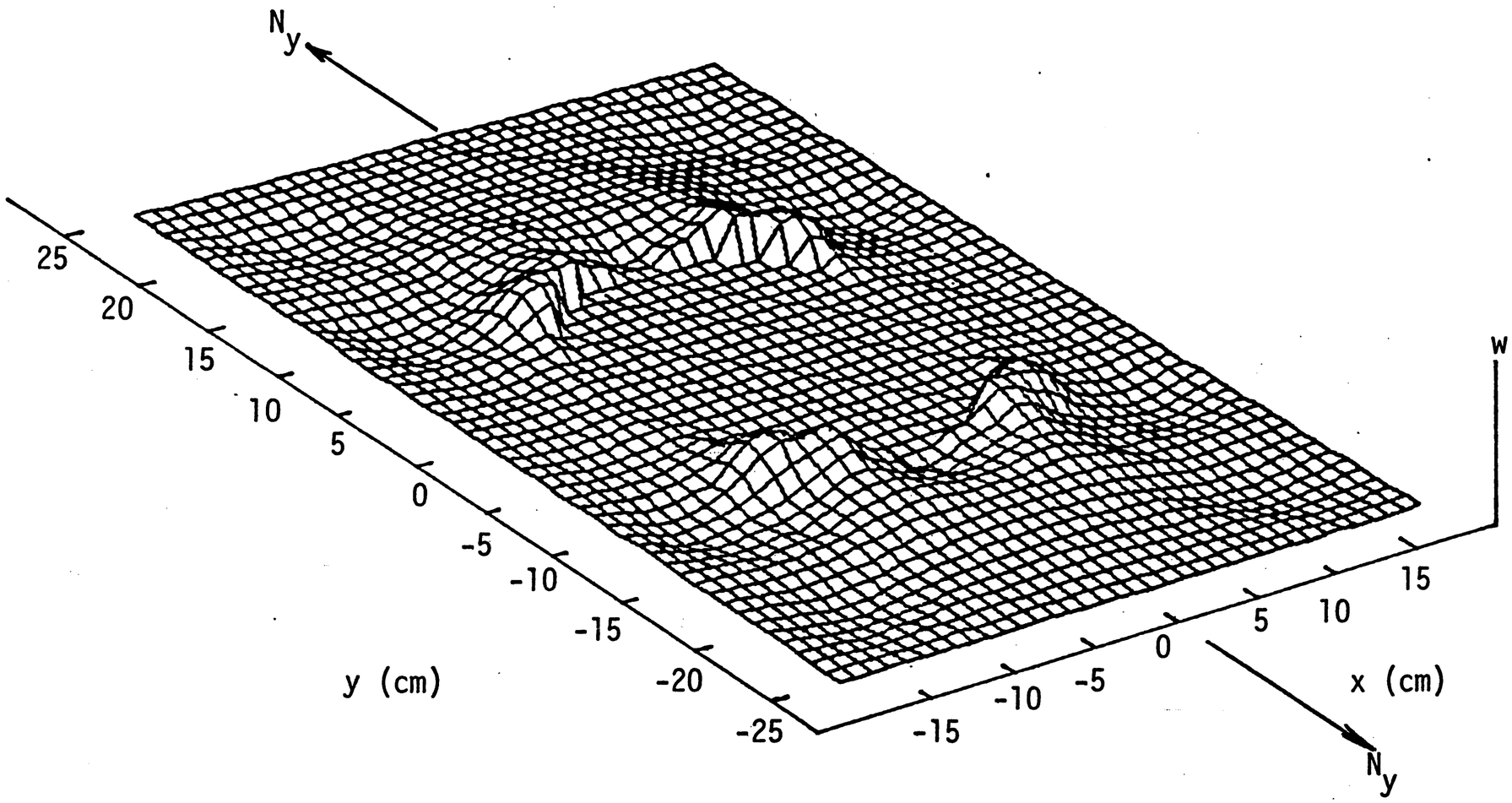

Figure 23 - The second lowest tensile buckling mode of a plate with a large circular hole, r = 10 cm; buckling load = 4.031×10^5 N/m.

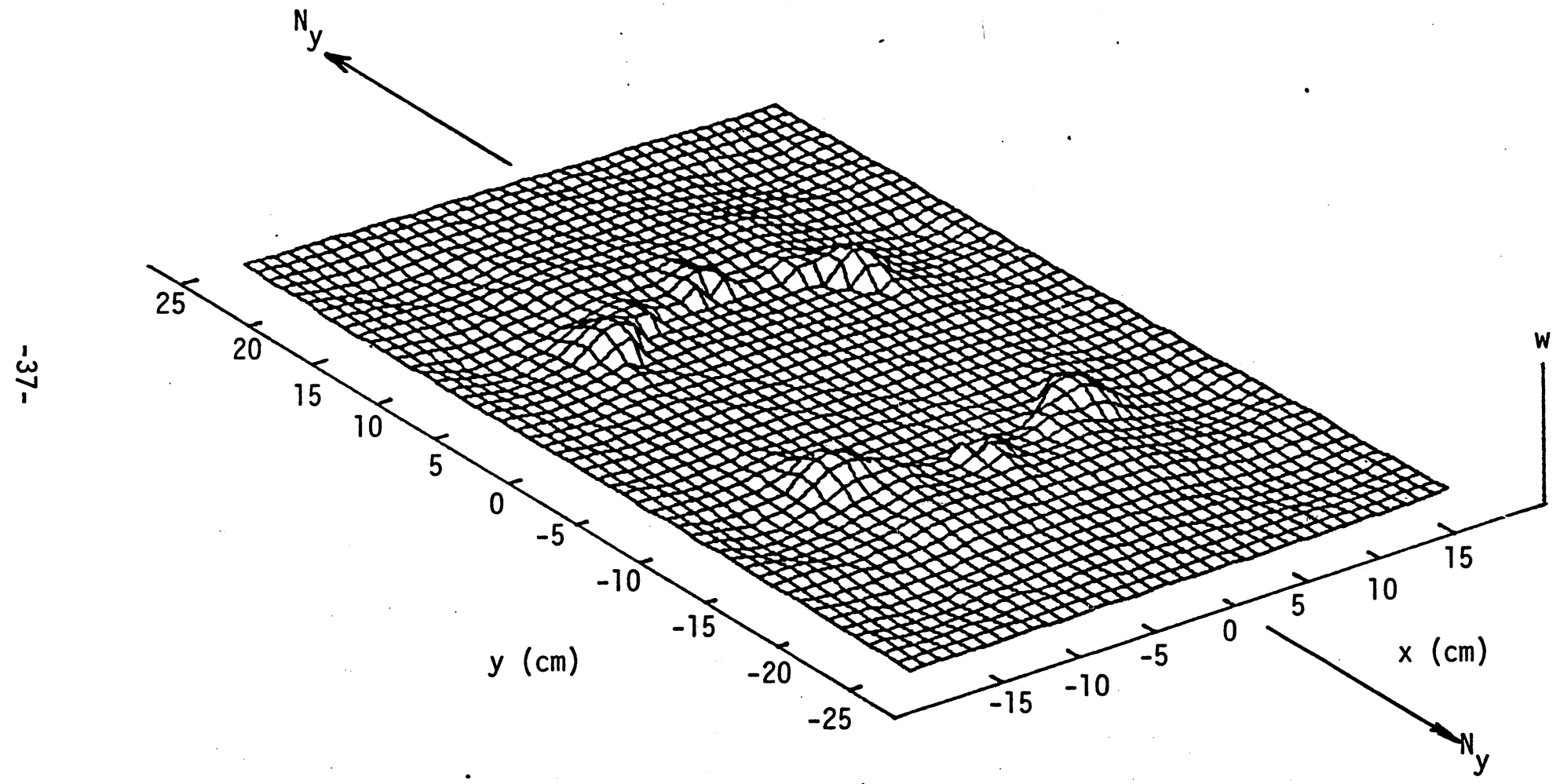

Figure 24 - The third lowest tensile buckling mode of a plate with a large circular hole, r = 10 cm; buckling load = 7.006×10^5 N/m.

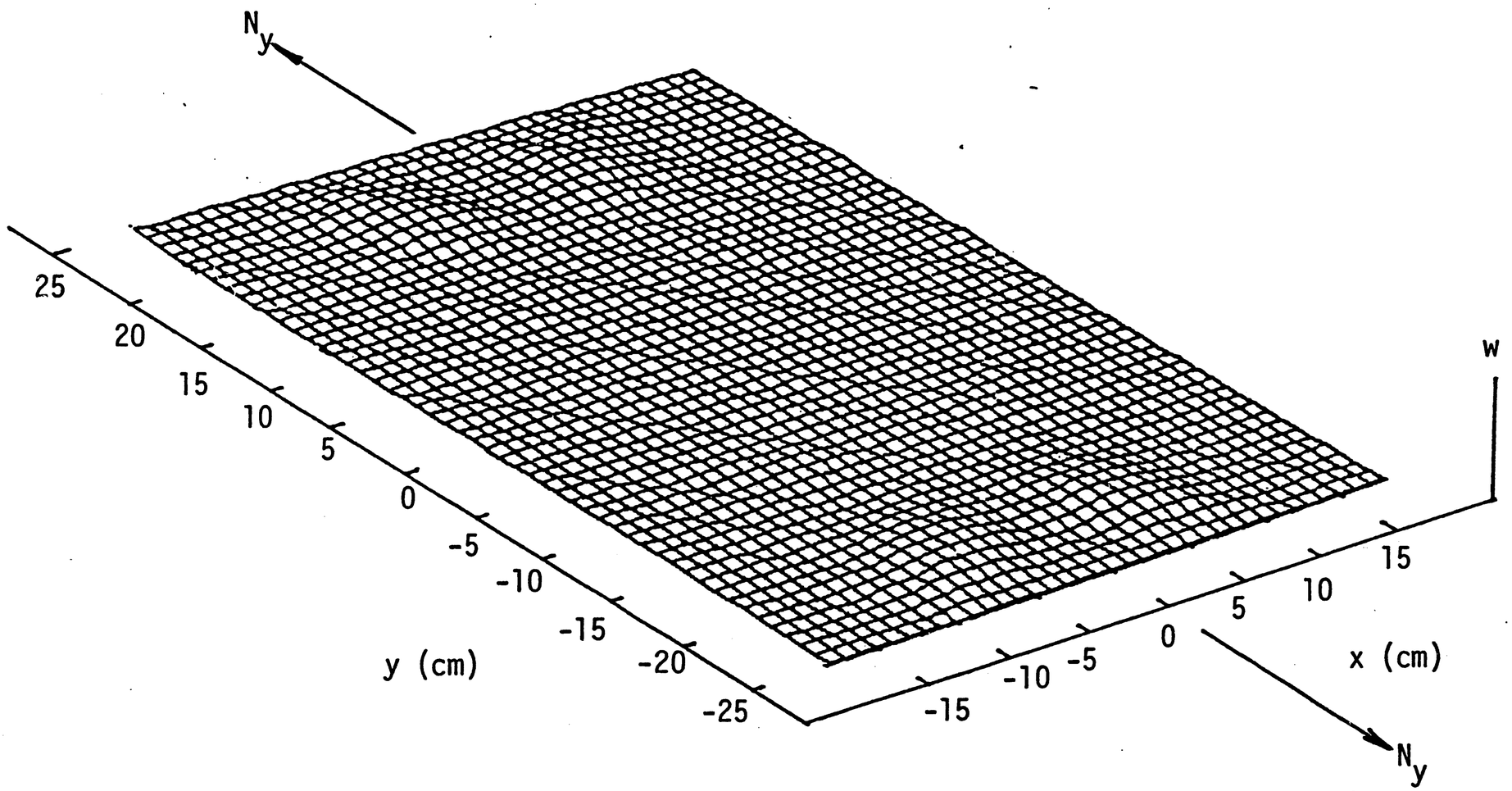

Figure 25 - The fourth lowest tensile buckling mode of a plate with a large circular hole, r = 10 cm; buckling load = 8.707×10^5 N/m.

the number of the local buckling zones increases with decreasing amplitude as the critical load is increased. The two large zones in Figure 22 switches to four in Figure 23 and eventually to six in Figure 24. At the critical load of 8.707×10^5 N/m, only slight wrinkles of the plate can be noticed.

Buckling extends to a much larger portion of the plate when the load is applied in compression, Figures 26 to 29 inclusive. The larger size hole results in a greater reduction of the average stiffness of the plate. This reduces the compressive load at which buckling occurs. They are given as 1.565×10^4, 2.624×10^4, 4.830×10^4 and 8.597×10^4 N/m which are less than those given for the small circular hole in Figures 18 to 21 inclusive. Considerable amount of bulging of the plate surface is observed in Figure 27 with a deflected zone where the hole lies. The buckled pattern of four corner zones is developed in Figure 28. Local concentration of wrinkling dies out at the higher buckling modes. This is noticeable from the results shown in Figure 29. Refer to Appendix III for the numerical values of the displacements, slopes and other parameters.

C. Narrow Horizontal Elliptical Cavity (b/a = 0.1)

Referring to Figure 8, a narrow horizontal elliptical cavity with an aspect ratio of b/a = 0.1 is considered. It is stretched up to the first buckling mode in tension at a load of 1.261×10^5 N/m. Figure 30 shows that considerable bulging occurred locally, the amplitude of which decreases at the ends of the cavity. This effect disappeared

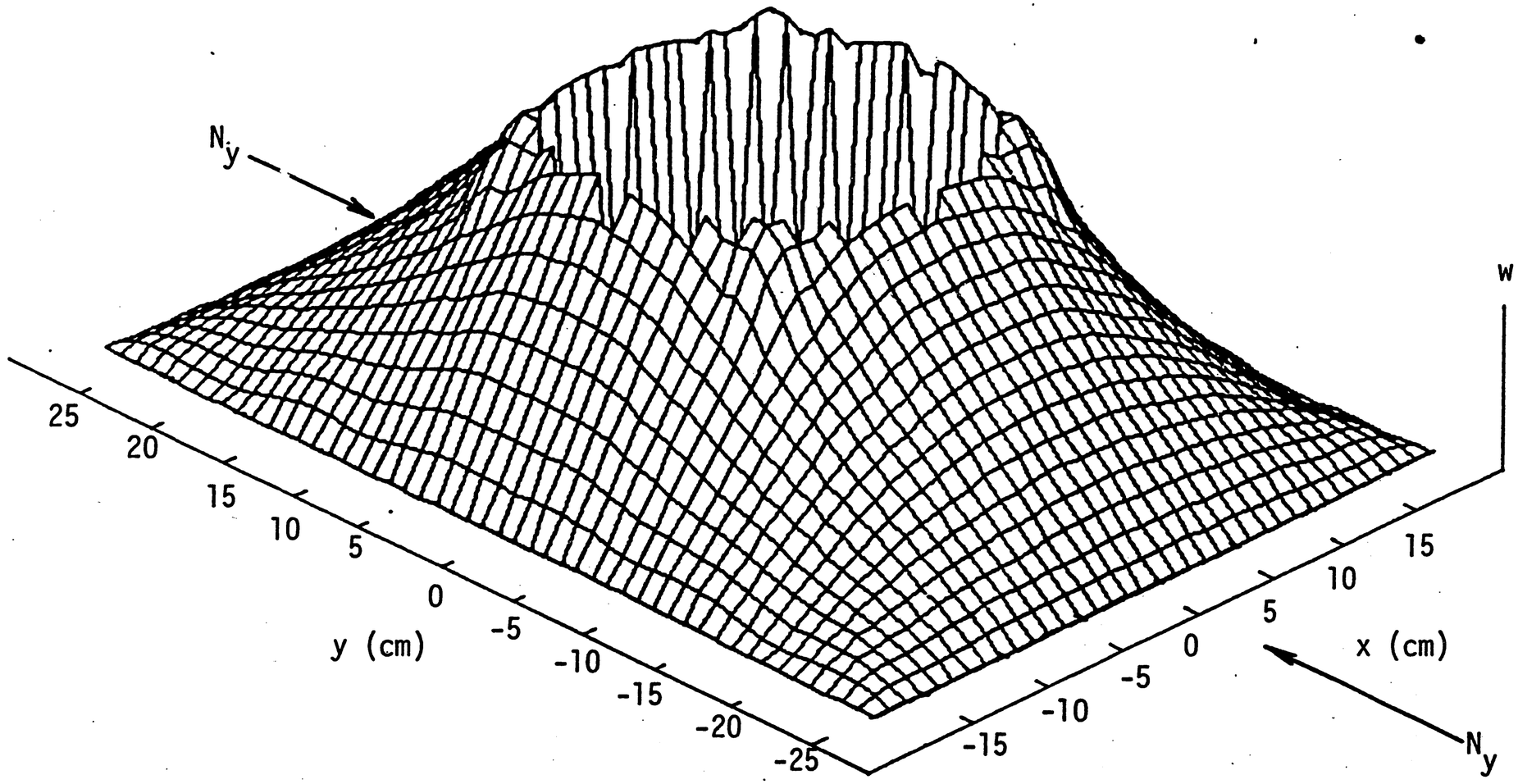

Figure 26 - The lowest compressive buckling mode of a plate with a large circular hole, r = 10 cm; buckling load = 1.565×10^4 N/m.

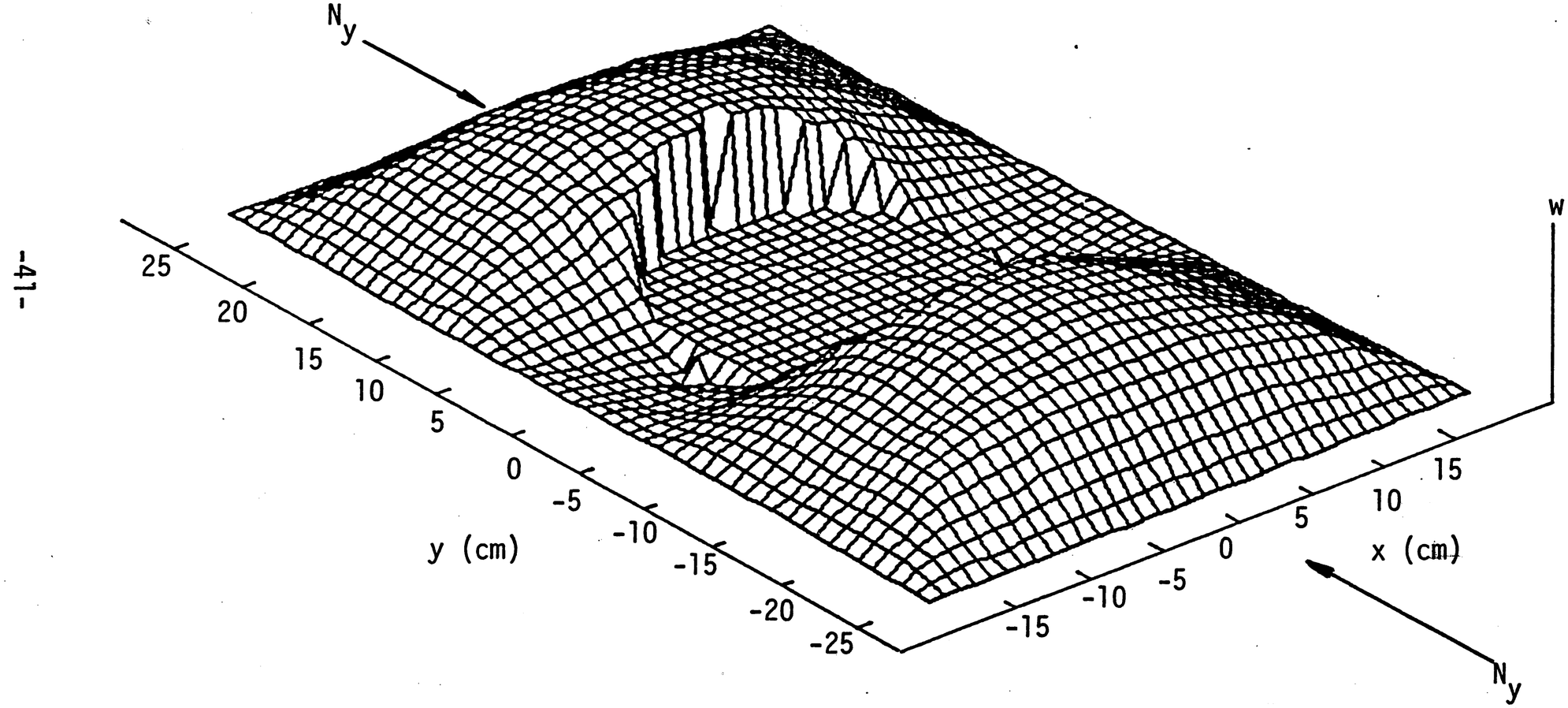

Figure 27 - The second lowest compressive buckling mode of a plate with a large circular hole, r = 10 cm; buckling load = 2.624×10^4 N/m.

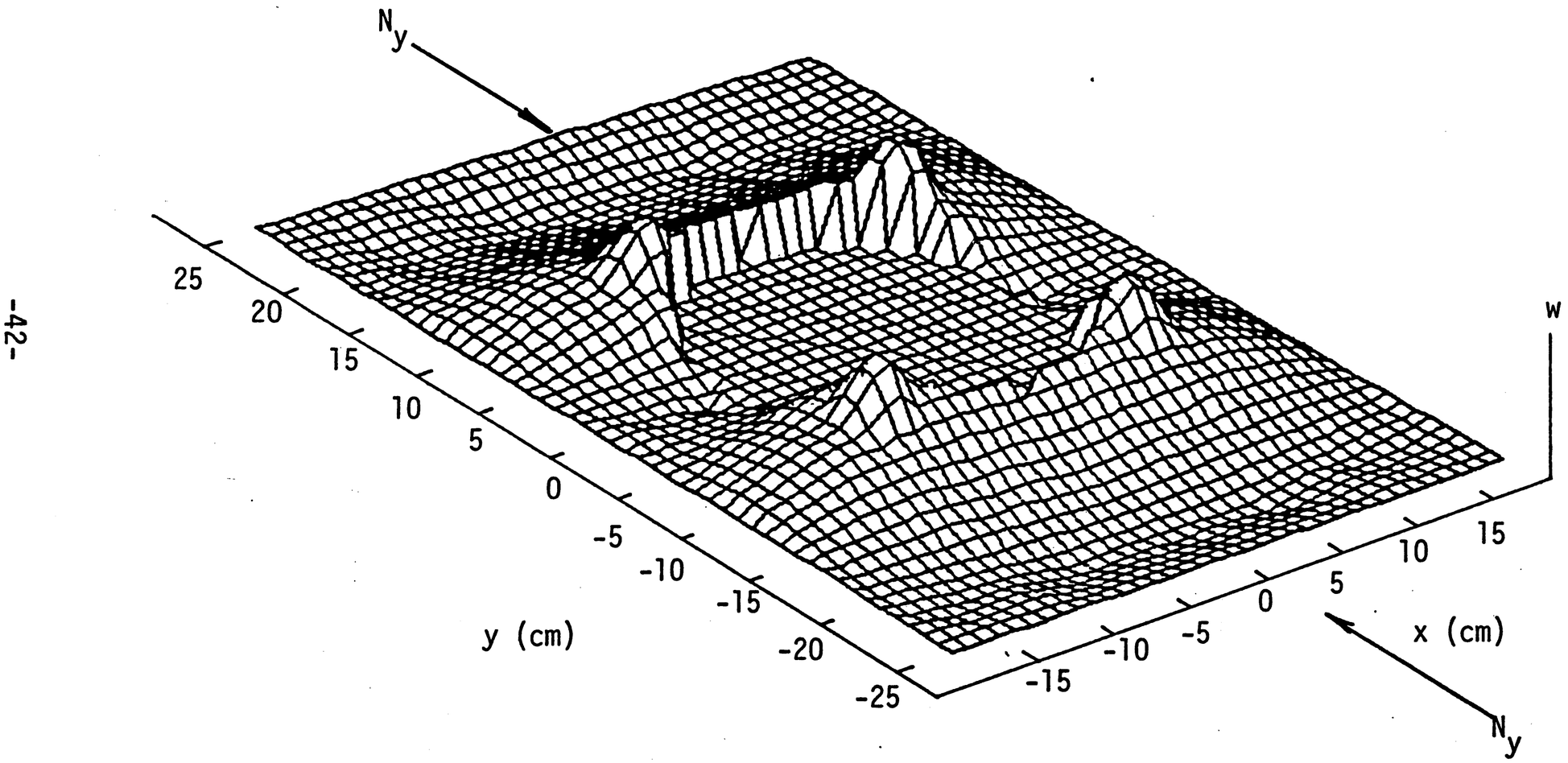

Figure 28 - The third lowest compressive buckling mode of a plate with a large circular hole, r = 10 cm; buckling load = 4.830×10^4 N/m.

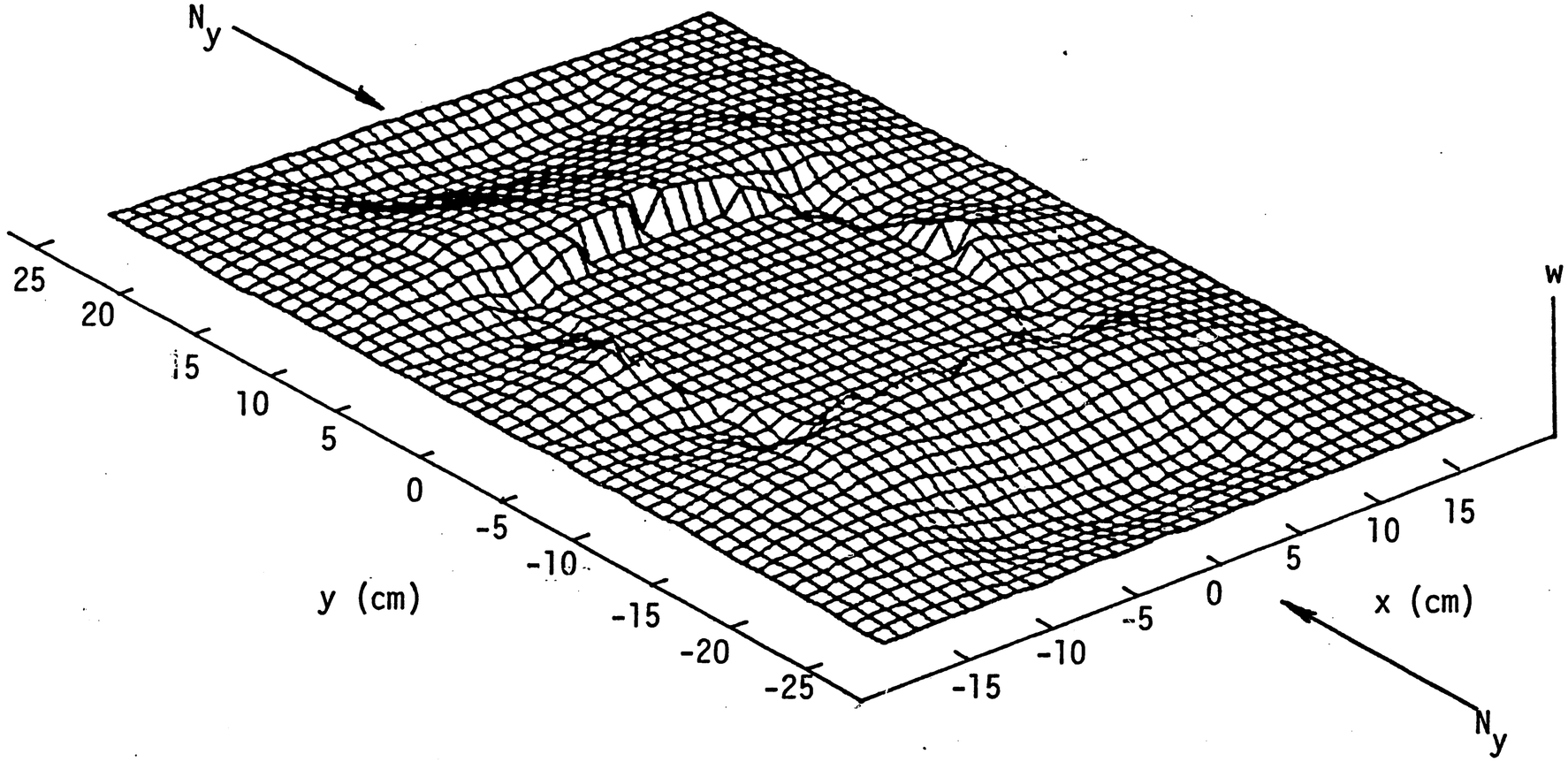

Figure 29 - The fourth lowest compressive buckling mode of a plate with a large circular hole, r = 10 cm; buckling load = 8.597×10^4 N/m.

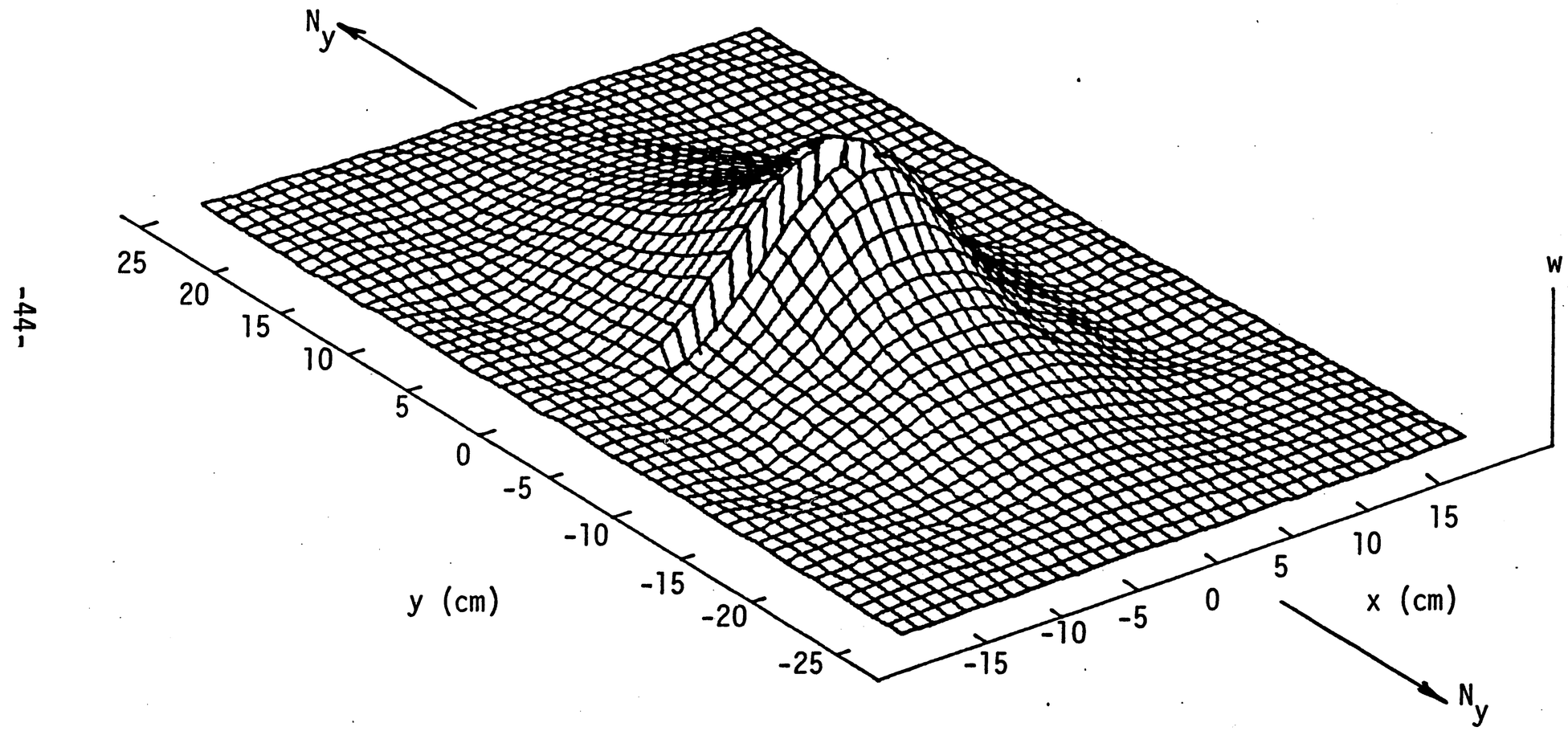

Figure 30 - The lowest tensile buckling mode of a plate with a narrow horizontal elliptical cavity, b/a = 0.1, a = 10 cm; buckling load = 1.261×10^5 N/m.

completely at the second critical tensile load of 2.417×10^5 N/m. This is shown in Figure 31 in which the plate is wrinkled slightly. A double bulge near the narrow elliptical cavity is obtained in Figure 32 corresponding to the third tensile buckling load of 3.762×10^5 N/m. More diffused pattern of local bulging is seen at the next higher mode of buckling, Figure 33.

The elliptical cavity has little influence on the buckled shape of the plate in Figure 34 for the first compressive critical load of 2.428×10^4 N/m. Local bulging becomes very pronounced in Figure 35 for the second mode of buckling in compression. Wrinkling of the plate surface at large is seen for the next two buckling loads in Figures 36 and 37. Appendix IV summarizes the numerical results of the parameters associated with the buckling modes shown in Figures 30 to 37.

D. Narrow Vertical Elliptical Cavity (b/a = 0.1)

As it is to be expected, the case of a narrow vertical elliptical notch has little effect on the buckling pattern, Figures 38 to 45. Figures 38 to 41 reveal only small amount of ripples in the plate for the first four critical tensile buckling loads. Similarly, the buckling patterns also followed those for a plate without the cavity. These results are illustrated in Figures 42 to 45 in which the out-of-plane displacements of the cavity boundary is nearly the same as those in regions undisturbed by the cavity. This is confirmed numerically in Appendix V.

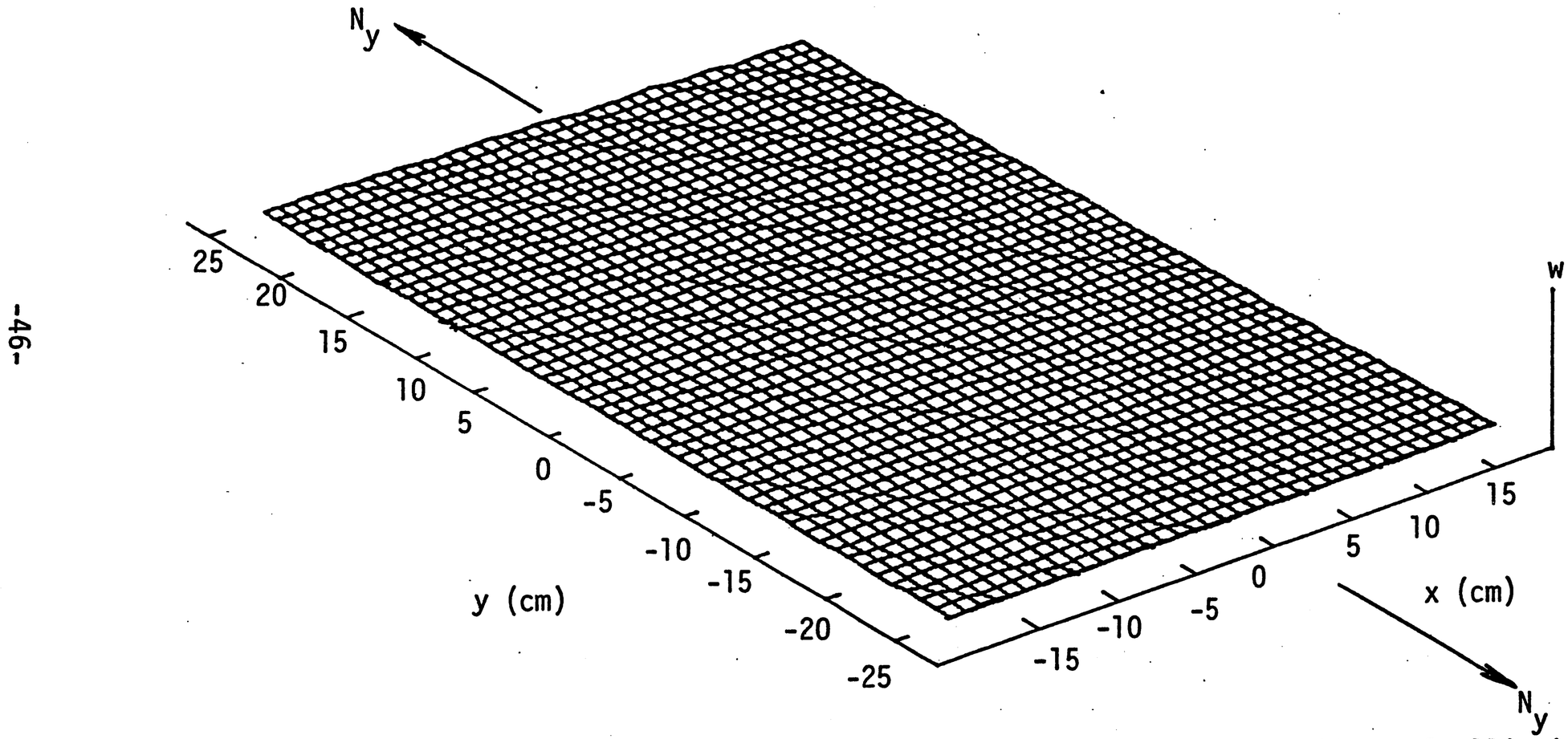

Figure 31 - The second lowest tensile buckling mode of a plate with a narrow horizontal elliptical cavity, b/a = 0.1, a = 10 cm; buckling load = 2.417×10^5 N/m.

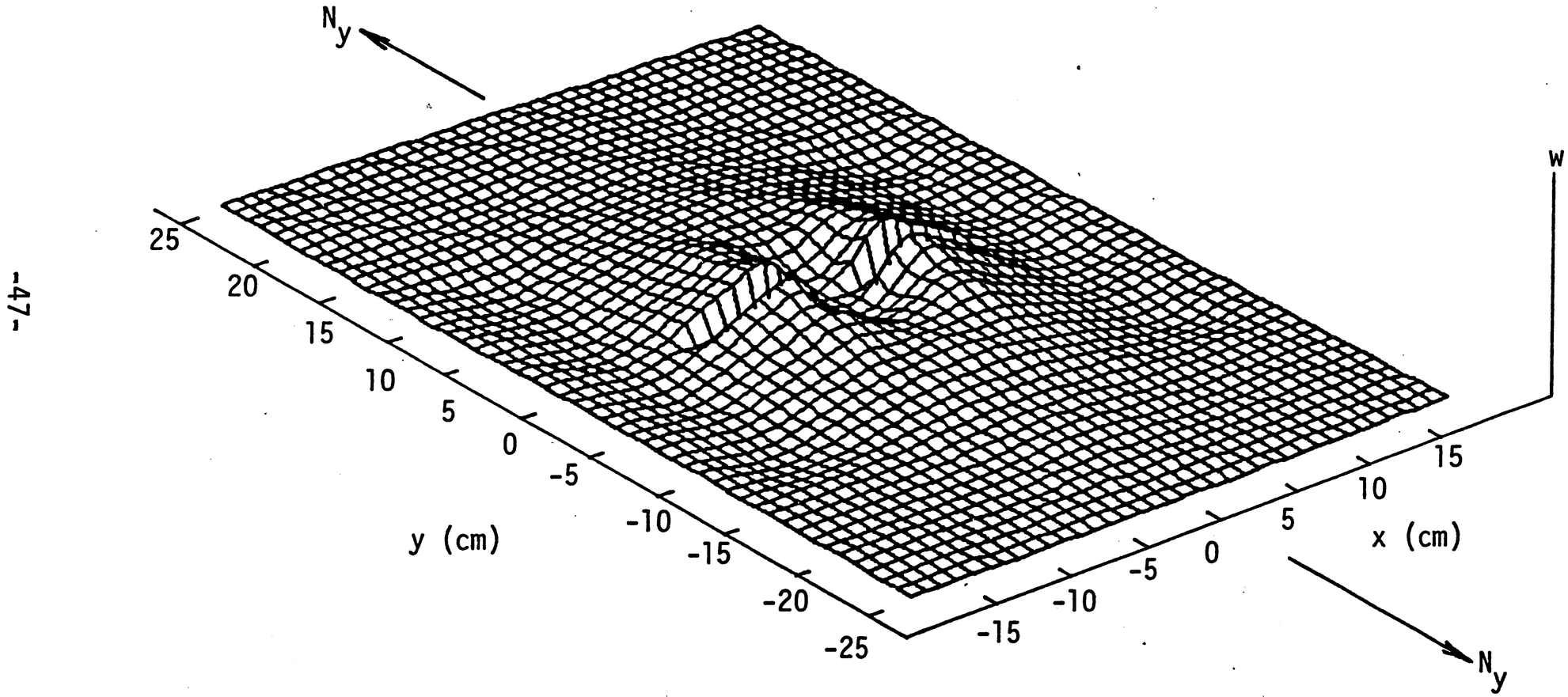

Figure 32 - The third lowest tensile buckling mode of a plate with a narrow horizontal elliptical cavity, b/a = 0.1, a = 10 cm; buckling load = 3.762×10^5 N/m.

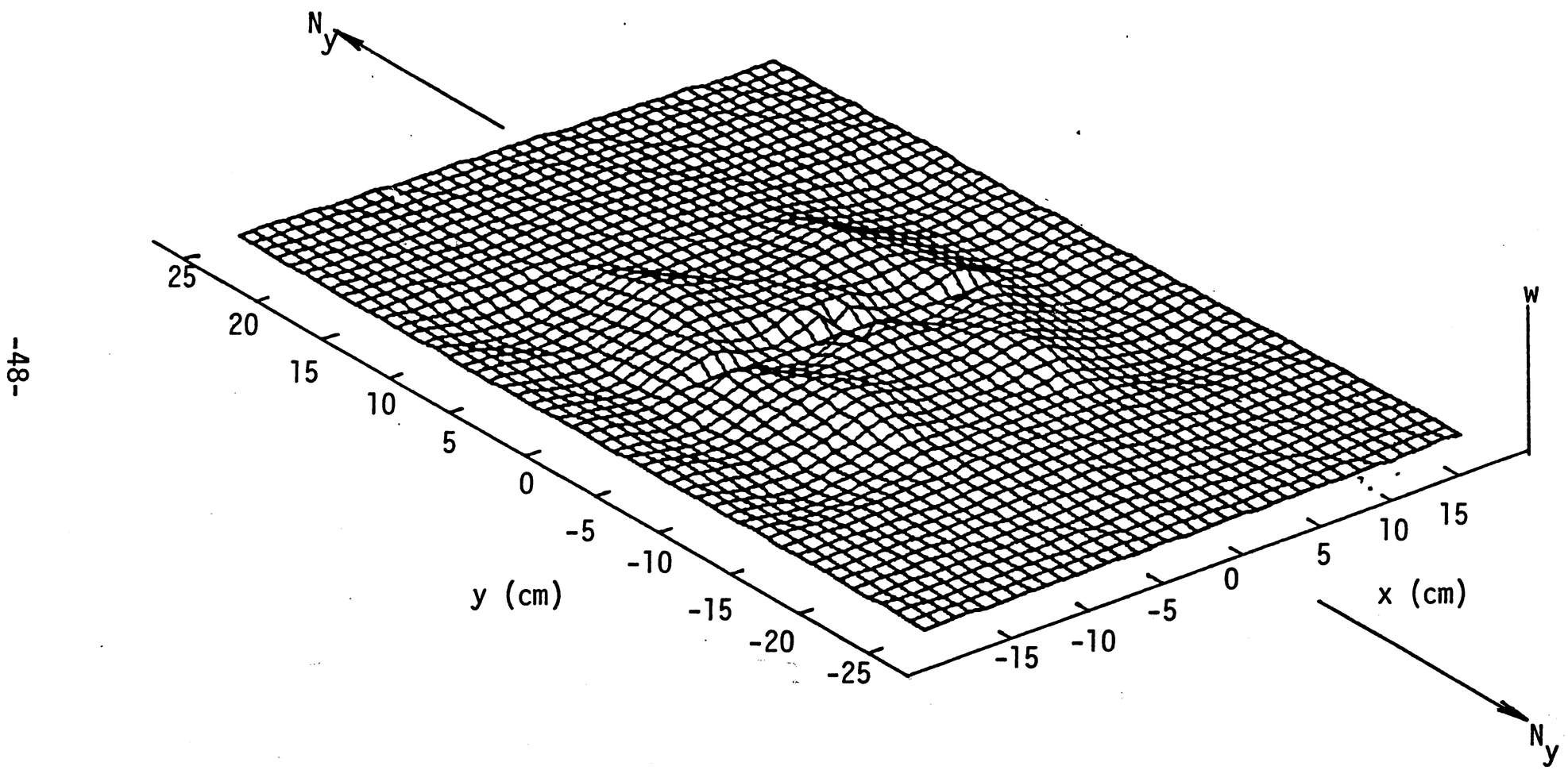

Figure 33 - The fourth lowest tensile buckling mode of a plate with a narrow horizontal elliptical cavity, b/a = 0.1, a = 10 cm; buckling load = 9.771×10^5 N/m.

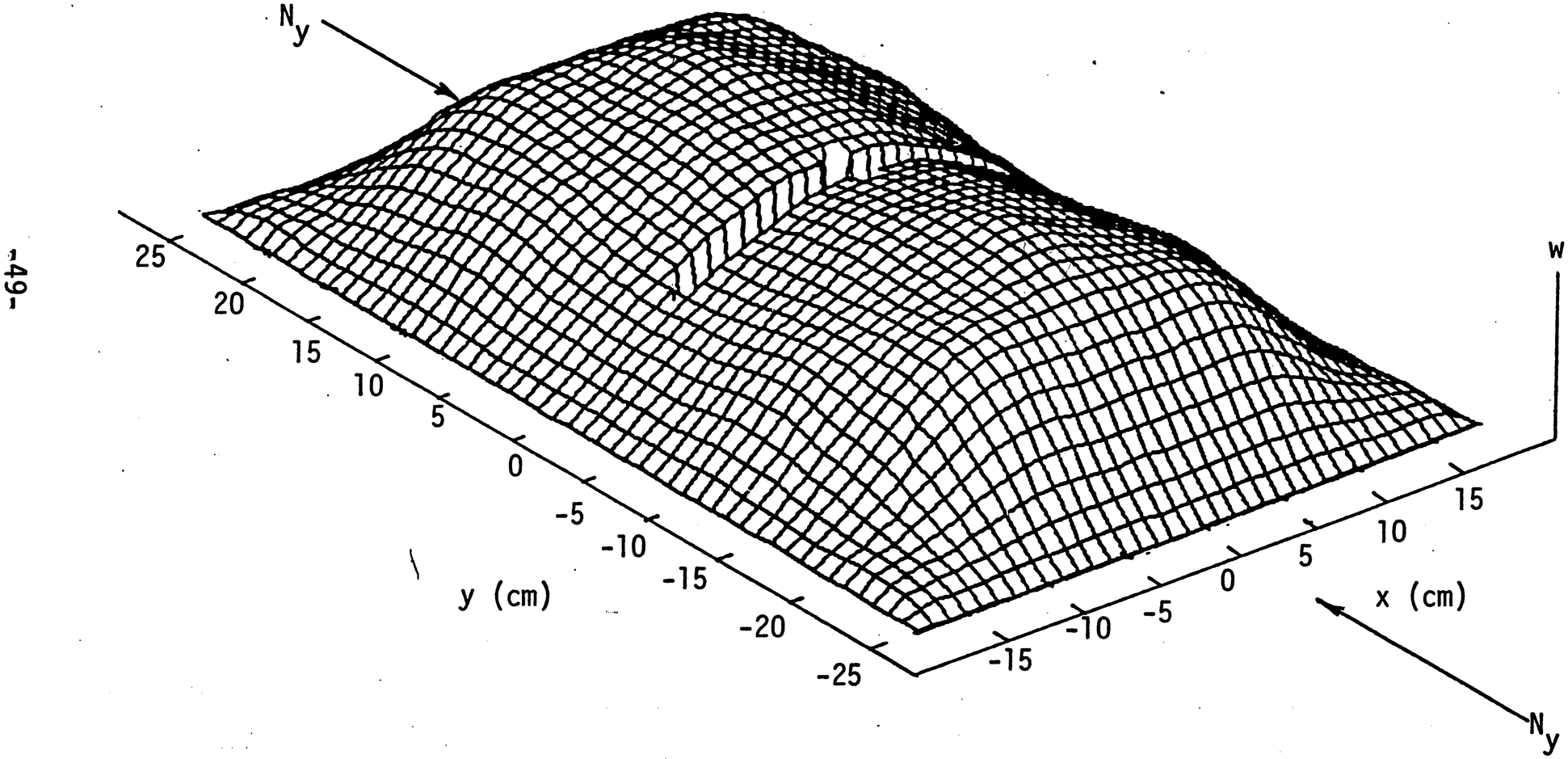

Figure 34 - The lowest compressive buckling mode of a plate with a narrow horizontal elliptical cavity, b/a = 0.1, a = 10 cm; buckling load = 2.428×10^4 N/m.

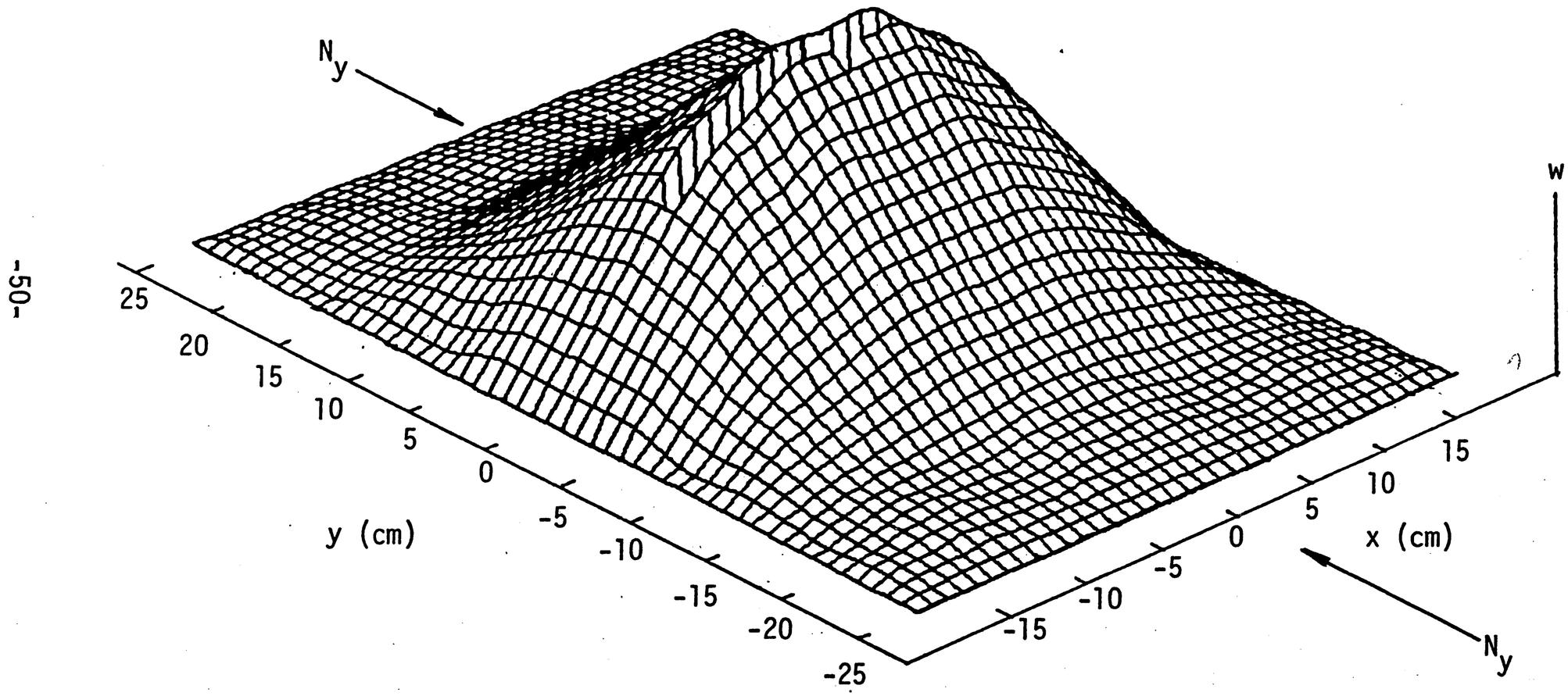

Figure 35 - The second lowest compressive buckling mode of a plate with a narrow horizontal elliptical cavity, b/a = 0.1, a = 10 cm; buckling load = 2.863×10^4 N/m.

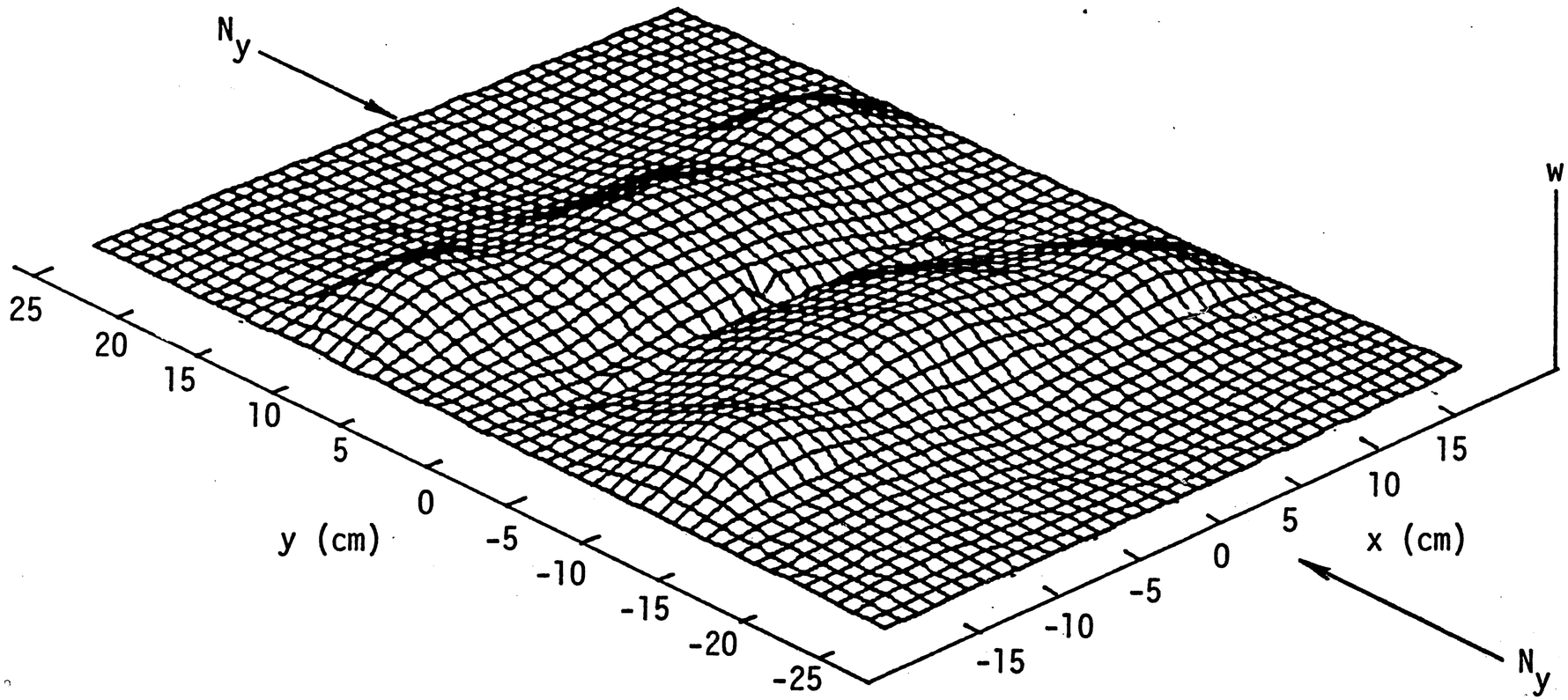

Figure 36 - The third lowest compressive buckling mode of a plate with a narrow horizontal elliptical cavity, b/a = 0.1, a = 10 cm; buckling load = 5.794×10^4 N/m.

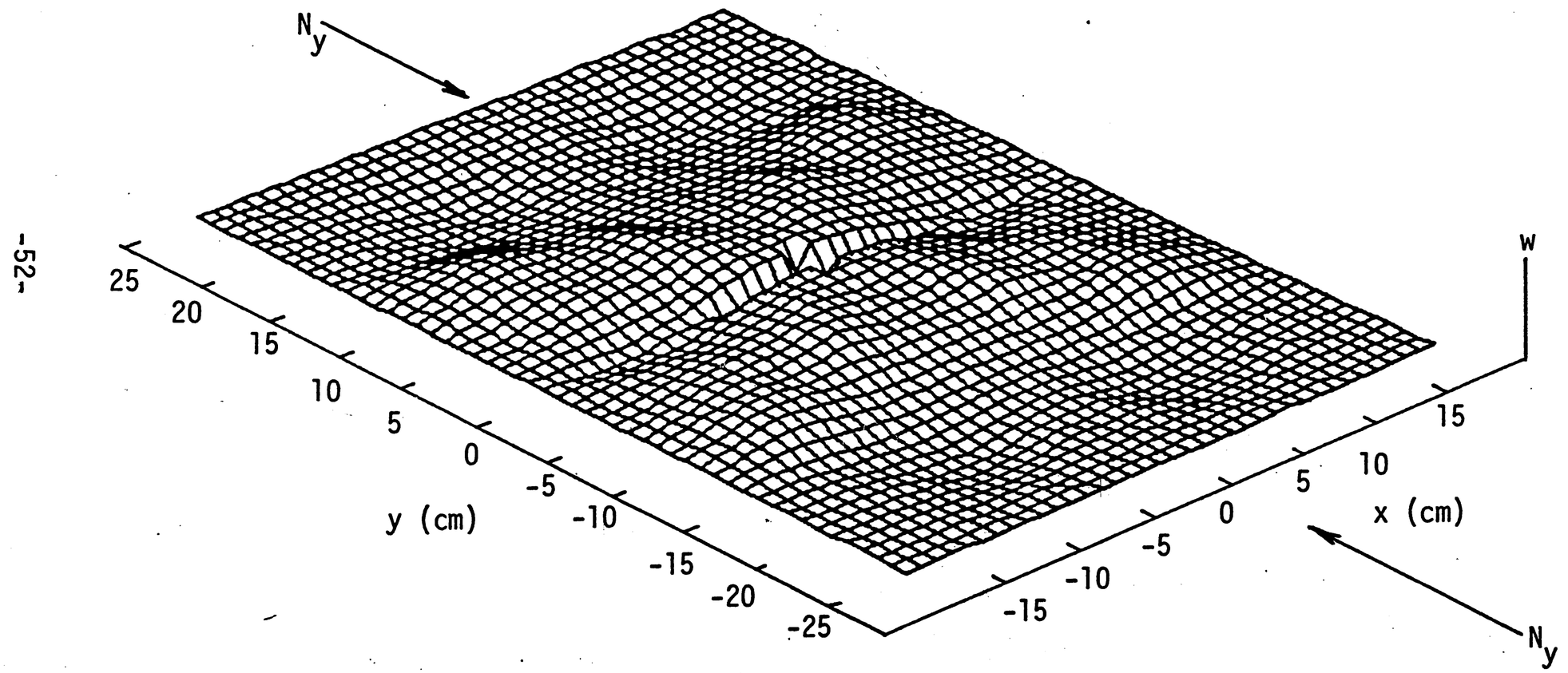

Figure 37 - The fourth lowest compressive buckling mode of a plate with a narrow horizontal elliptical cavity, b/a = 0.1, a = 10 cm; buckling load = 1.032×10^5 N/m.

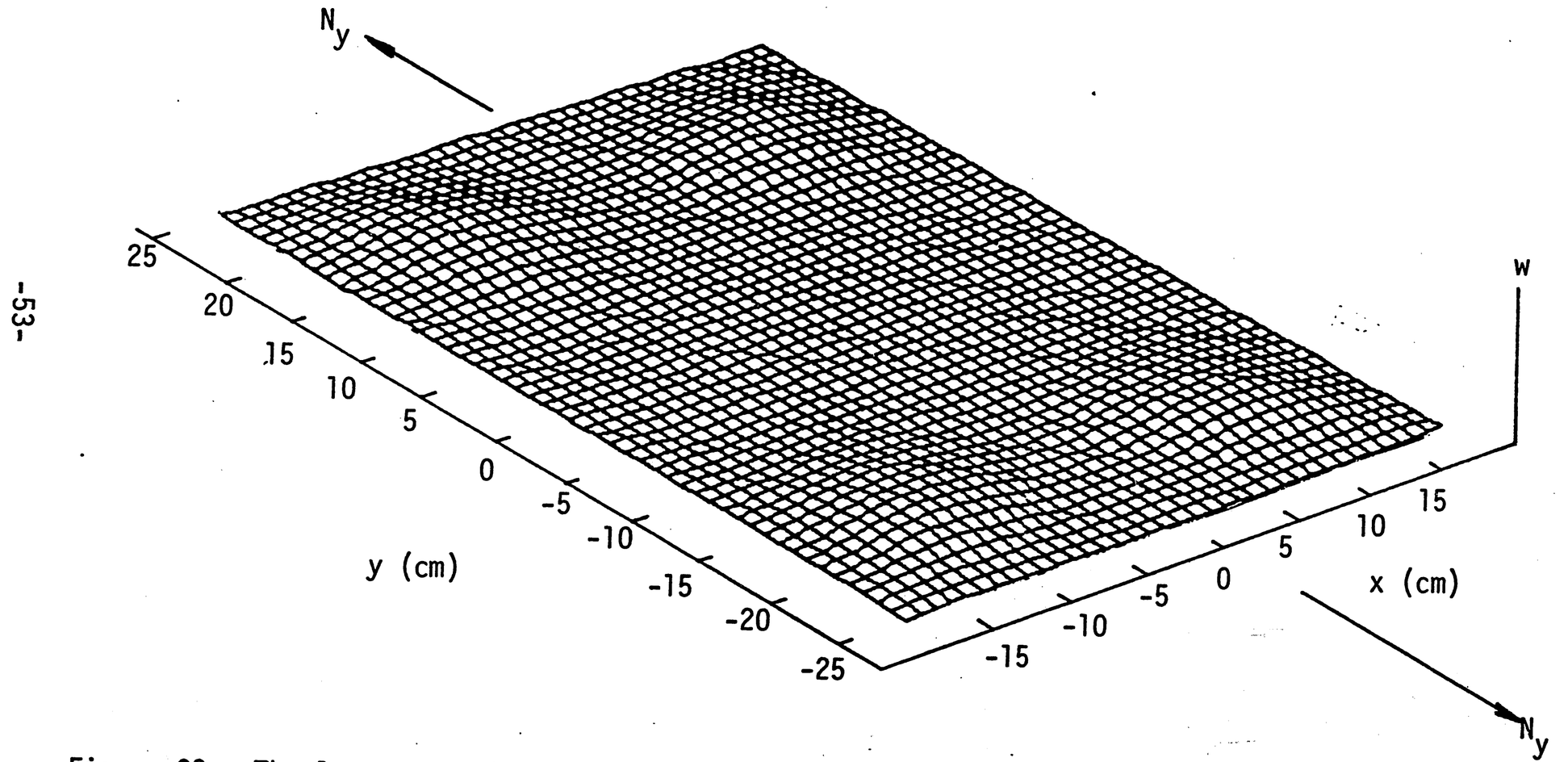

Figure 38 - The lowest tensile buckling mode of a plate with a narrow vertical elliptical cavity, b/a = 0.1, a = 10 cm; buckling load = 3.956×10^5 N/m.

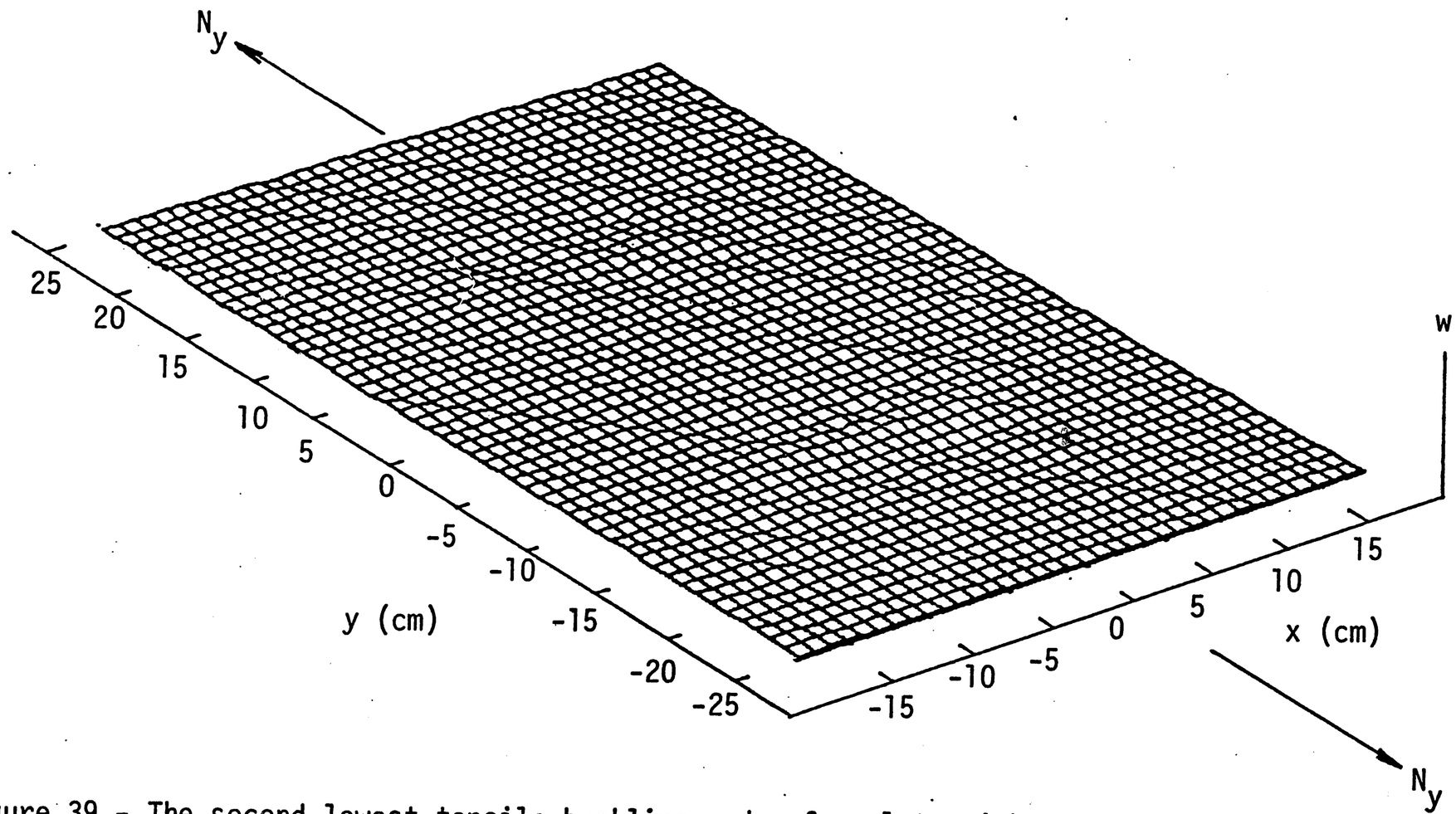

Figure 39 - The second lowest tensile buckling mode of a plate with a narrow vertical elliptical cavity, b/a = 0.1, a = 10 cm; buckling load = 1.146×10^6 N/m.

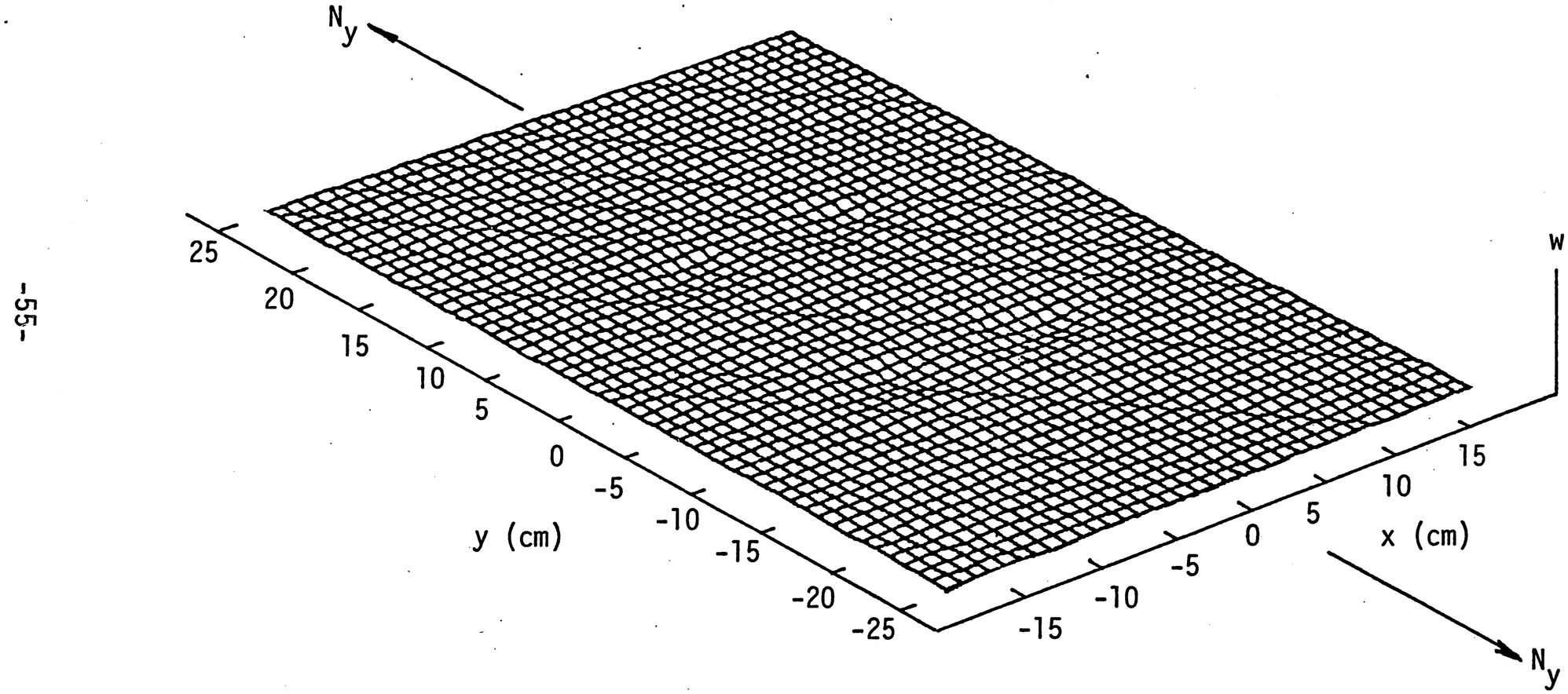

Figure 40 - The third lowest tensile buckling mode of a plate with a narrow vertical elliptical cavity, b/a = 0.1, a = 10 cm; buckling load = 2.433×10^6 N/m.

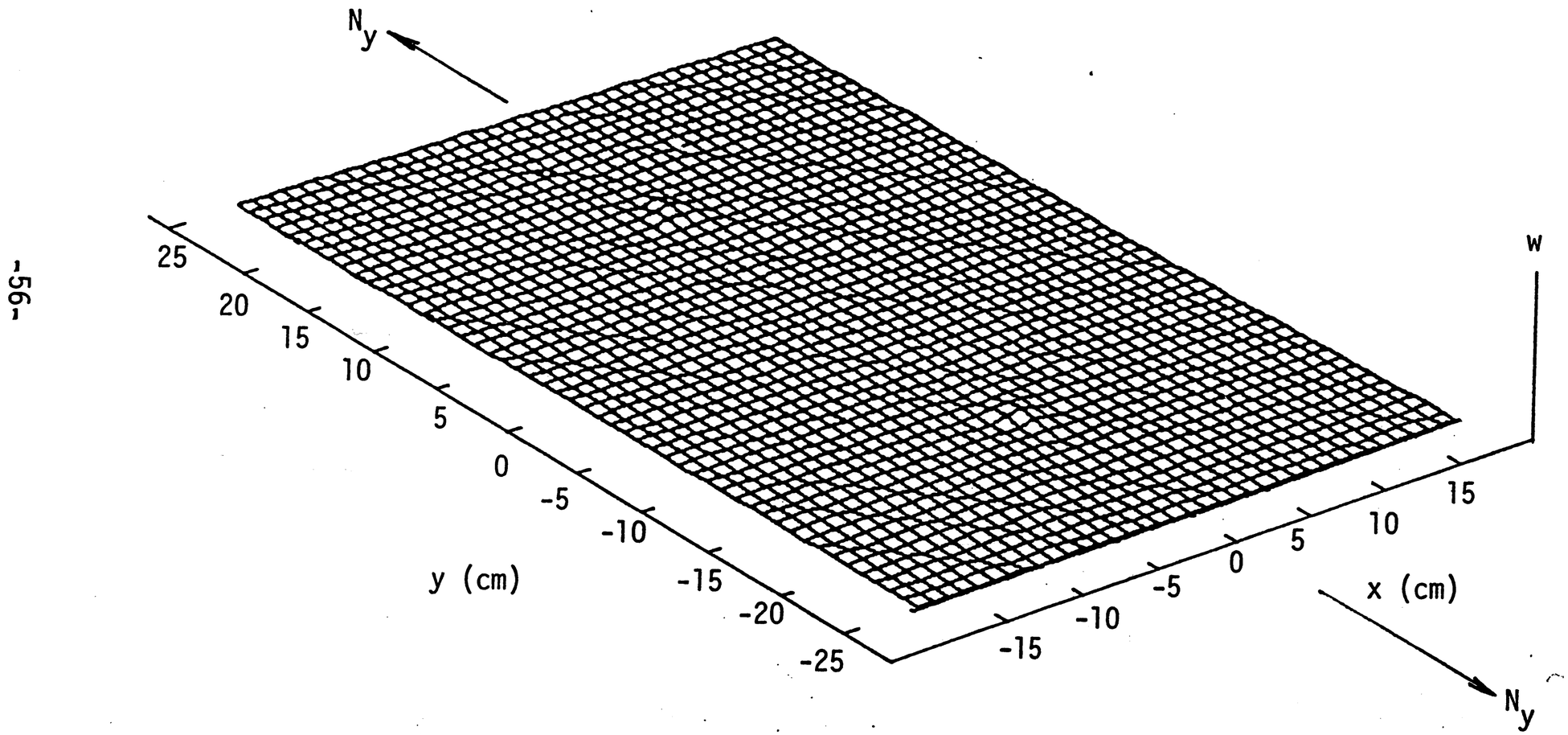

Figure 41 - The fourth lowest tensile buckling mode of a plate with a narrow vertical elliptical cavity, b/a = 0.1, a = 10 cm; buckling load = 5.002×10^6 N/m.

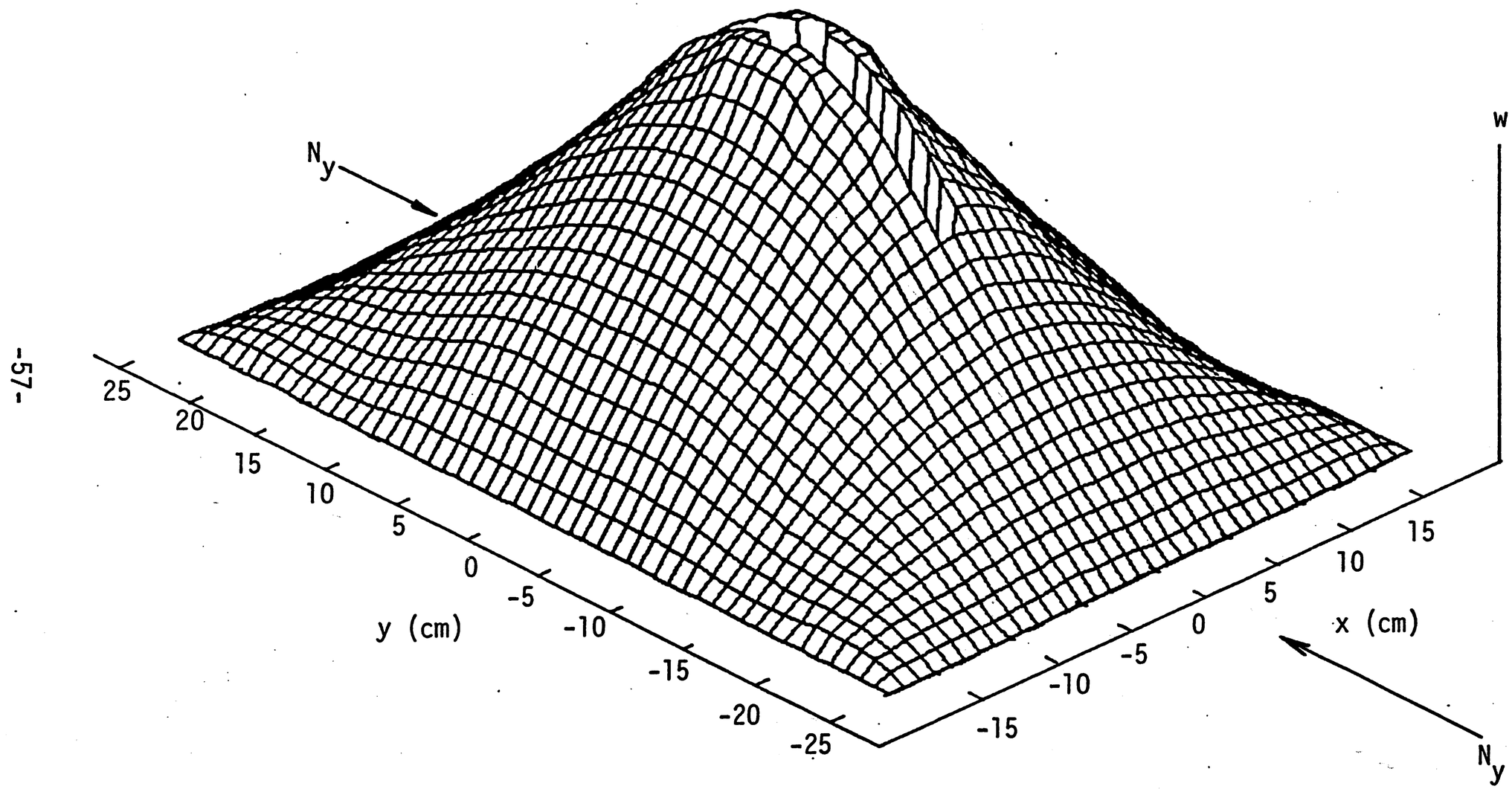

Figure 42 - The lowest compressive buckling mode of a plate with a narrow vertical elliptical cavity, b/a = 0.1, a = 10 cm; buckling load = 1.293×10^4 N/m.

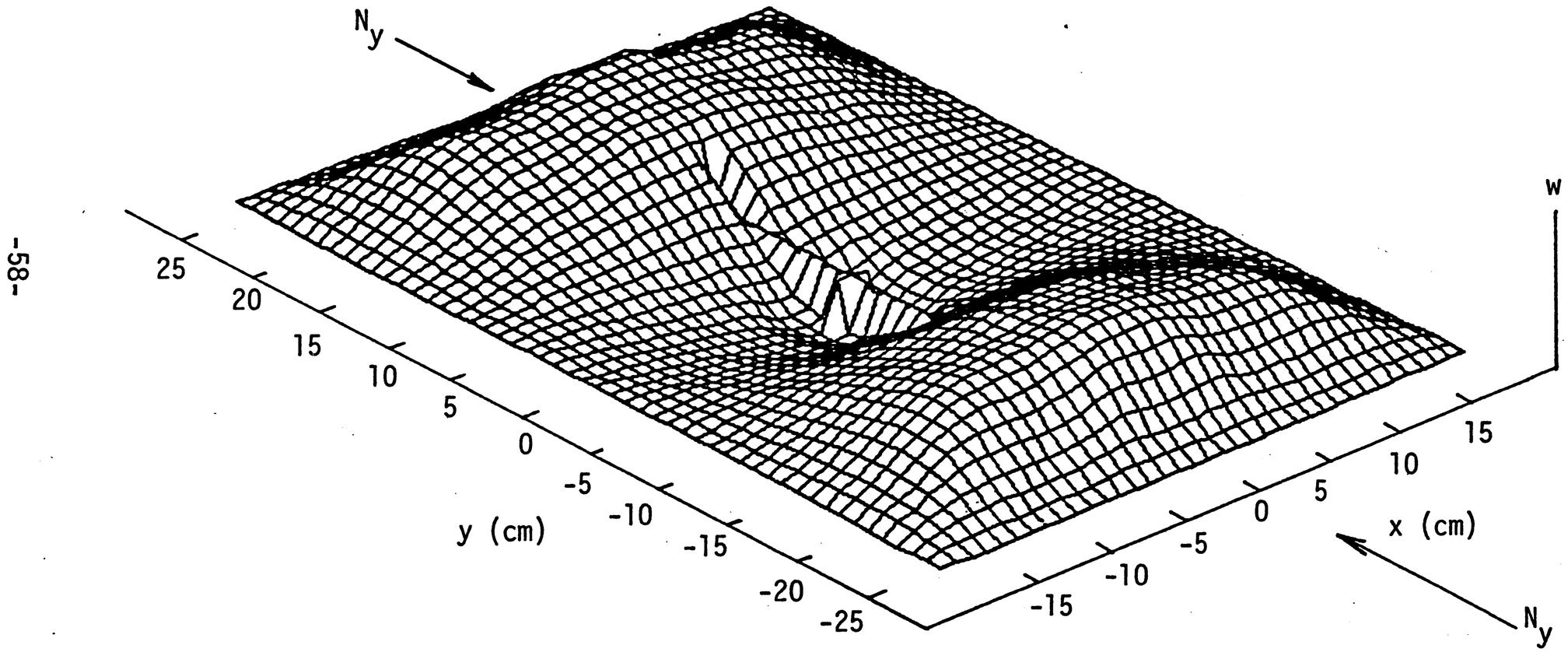

Figure 43 - The second lowest compressive buckling mode of a plate with a narrow vertical elliptical cavity, b/a = 0.1, a = 10 cm; buckling load = 2.702×10^4 N/m.

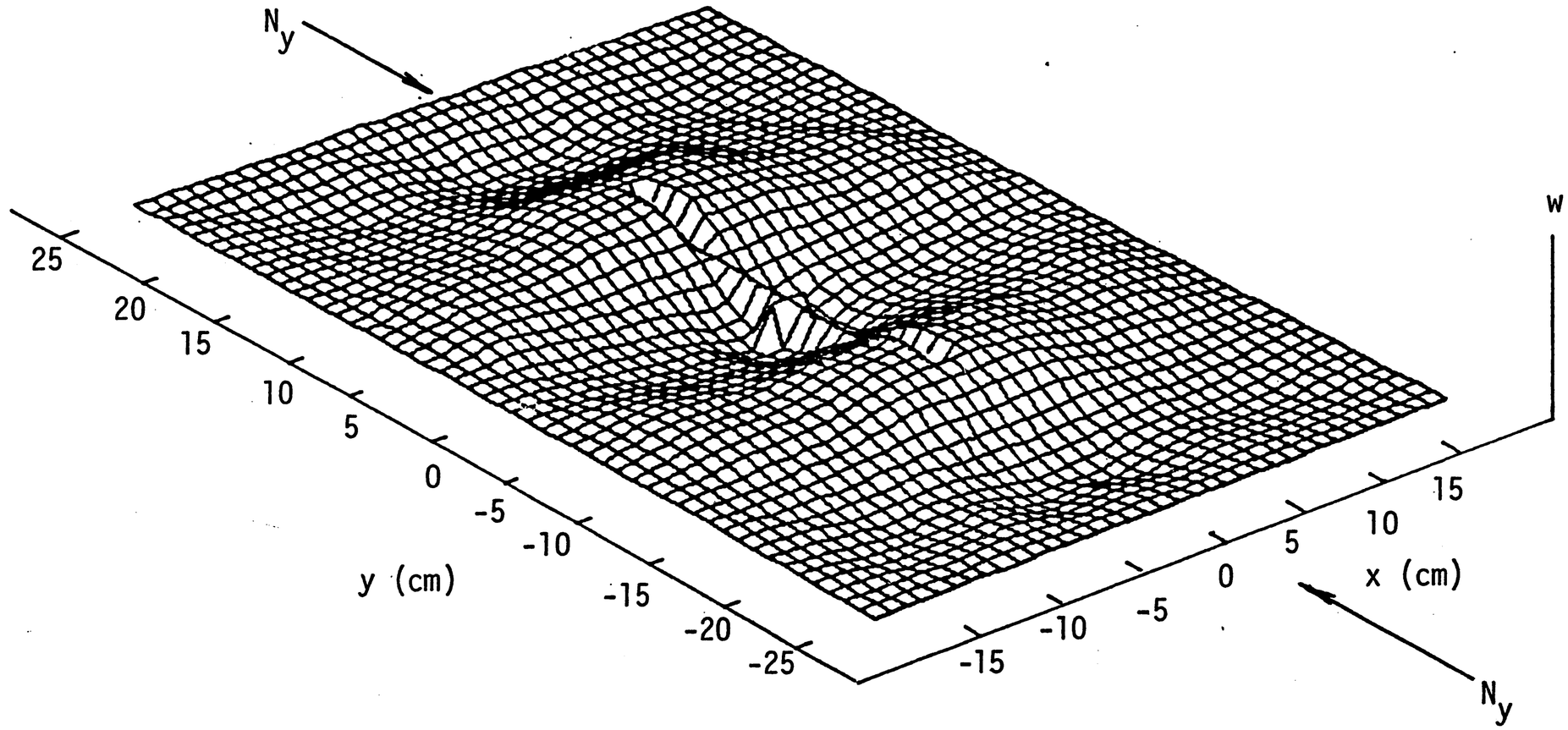

Figure 44 - The third lowest compressive buckling mode of a plate with a narrow vertical elliptical cavity, b/a = 0.1, a = 10 cm; buckling load = 6.075×10^4 N/m.

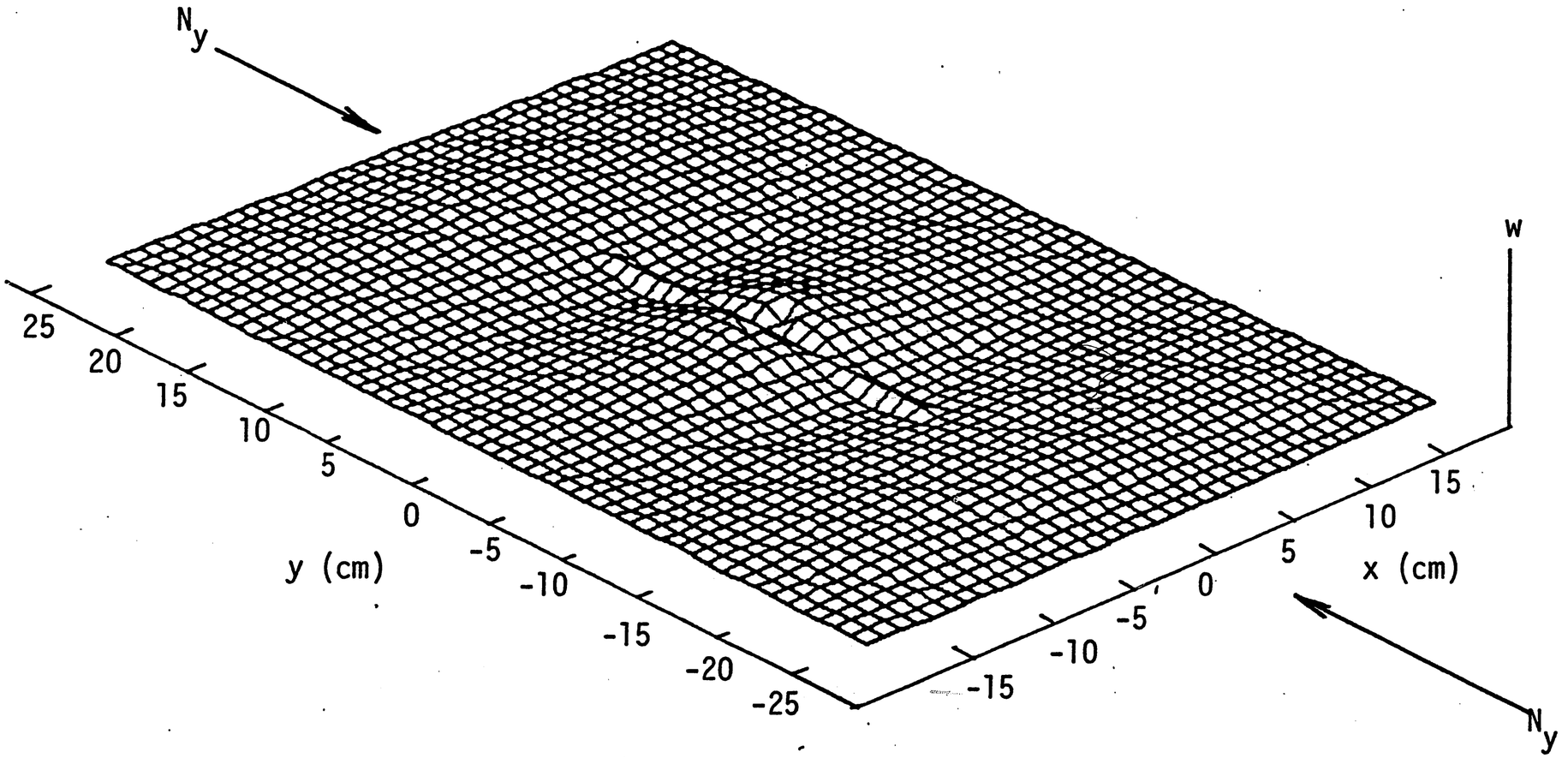

Figure 45 - The fourth lowest compressive buckling mode of a plate with a narrow vertical elliptical cavity, b/a = 0.1, a = 10 cm; buckling load = 9.458×10^4 N/m.

CONCLUDING REMARKS AND FUTURE WORK

One of the simplifying assumptions in this work is that the buckling modes occur symmetrically across the width of the plate along which the cavity lies. This condition was invoked simply to reduce the computation time. It is not a restriction on the analytical approach. Anti-symmetric buckling displacement modes can be investigated by the same procedure which should yield more information on how cavity shape and size influence the overall instability of plate-like structures.

In the case of the narrow elliptical cavity, there is the likelihood that the materials near the ends of the cavity may undergo yielding and/or fracture, especially if the remote loading is tensile. It is possible that fracture may take place prior to global or local buckling. This can be checked from the fluctuations of the strain energy density function for the condition of fracture initiation [7,8]. Moreover, in regions of high stress and energy intensification, local material elements can be easily deformed beyond their elastic limits. Such an effect can be beneficial as it tends to reduce the remaining energy available for buckling and/or the creation of new fracture surface.

Although the physical phenomena can be readily anticipated, the stress and failure analysis required for analyzing the situation may not be straightforward. Yielding, for example, is a strain rate dependent process that may differ significantly in regions near the cav-

ity from those at some distances away. Such effects cannot be consistently accounted for by the classical theory of plasticity that invokes too many simplifying assumptions, one of which is the coincidence of the uniaxial stress and strain curve with the effective stress and effective strain curve. Neglected is the dilatational effect that cannot be justified on physical grounds in regions where fracture may initiate.

Only recently, a general theory [15] has been developed by making use of the concept that failure, in general, is governed by the rate of energy dissipated in a unit volume and unit area of material. Material damage involves an exchange of volume and surface energy through rate change of volume with surface. This enables the simultaneous and consistent treatment of stress and failure analysis without invoking arbitrariness into the formulation. The application of this theory to buckling of plates weakened by cavities is a topic for future considerations.

REFERENCES

[1] Kapur, K. K. and Hartz, B. J., "Stability of plates using the finite element method", Journal of the Engineering Mechanics Division, American Society of Civil Engineers, EM2, pp. 177-195, 1966.

[2] Anderson, R. G., Irons, B. M. and Zienkiewicz, O. C., "Vibration and stability of plates using finite elements", International Journal of Solids and Structures, 4, pp. 1031-1055, 1968.

[3] Wang, C. T., Applied Elasticity, McGraw-Hill, New York, 1953.

[4] Gelfand, I. M. and Fomin, S. V., Calculus of Variations, Prentice-Hall, Englewood Cliffs, New Jersey, 1963.

[5] Zienkiewicz, O. C., The Finite Element Method, Third Edition, McGraw-Hill, London, 1977.

[6] Bathe, K. J., Finite Element Procedures in Engineering Analysis, Prentice-Hall, Englewood Cliffs, New Jersey, 1982.

[7] Sih, G. C., "Stress analysis of notch problems: strain energy density and surface layer energy for blunt cracks or notches", Mechanics of Fracture V, edited by G. C. Sih, Noordhoff International Publishing, Leyden, pp. XIII-CX, 1978.

[8] Chu, Ru-Chu, "Material damage and structural instability analysis: local and global stationary values of the strain energy density function", Unpublished Ph.D. Dissertation, Lehigh University, 1983.

[9] Timoshenko, S., Theory of Elastic Stability, First Edition, McGraw-Hill, New York, 1936.

[10] Dym, C. L. and Shames, I. H., Solid Mechanics: A Variational Approach, McGraw-Hill, New York, 1976.

[11] Washizu, K., Variational Methods in Elasticity and Plasticity, Second Edition, Pergamon Press, Oxford, 1975.

[12] Bell, K., "A refined triangular plate bending finite element", International Journal of Numerical Methods in Engineering, 1, pp. 101-122, 1969.

[13] Irons, B. M., "Engineering application of numerical integration in stiffness methods", American Institute of Aeronautics and Astronautics, 4, pp. 2035-2037, 1966.

[14] "Symmetric plate buckling analysis (SPBA)", Forthcoming Technical Report, Institute of Fracture and Solid Mechanics, Lehigh University.

[15] Sih, G. C., "Mechanics and physics of energy density theory", Journal of Theoretical and Applied Fracture Mechanics, Vol. 4, No. 3 (in press).

APPENDIX I

DERIVATION OF THE SHAPE FUNCTION

APPENDIX I - DERIVATION OF THE SHAPE FUNCTION

The out-of-plane displacement field in equation (16) can be expressed in terms of the function $p_i(x,y)$ and generalized coordinates q_i. Let the degree of freedom at each corner node be defined as in equation (15). Note that $(\frac{\partial w}{\partial n})_1$, $(\frac{\partial w}{\partial n})_2$, $(\frac{\partial w}{\partial n})_3$ correspond to each mid-side node respectively as shown in Figure 46. A 21 x 1 matrix {e} is obtained for each triangular element:

$$\{e\} = \begin{Bmatrix} \{\xi\} \\ (\frac{\partial w}{\partial n})_1 \\ (\frac{\partial w}{\partial n})_2 \\ (\frac{\partial w}{\partial n})_3 \end{Bmatrix} , \tag{30}$$

The orientation of the normal slope n of the mid-nodes is defined according to Figure 47.

$$0 \leq \beta_1, \beta_2, \beta_3 < \pi \tag{31}$$

$$0 \leq \alpha_1, \alpha_2, \alpha_3 < \frac{\pi}{2}; \frac{3\pi}{2} \leq \alpha_1, \alpha_2, \alpha_3 < 2\pi$$

The derivatives of w in the normal and tangential directions can thus be expressed as

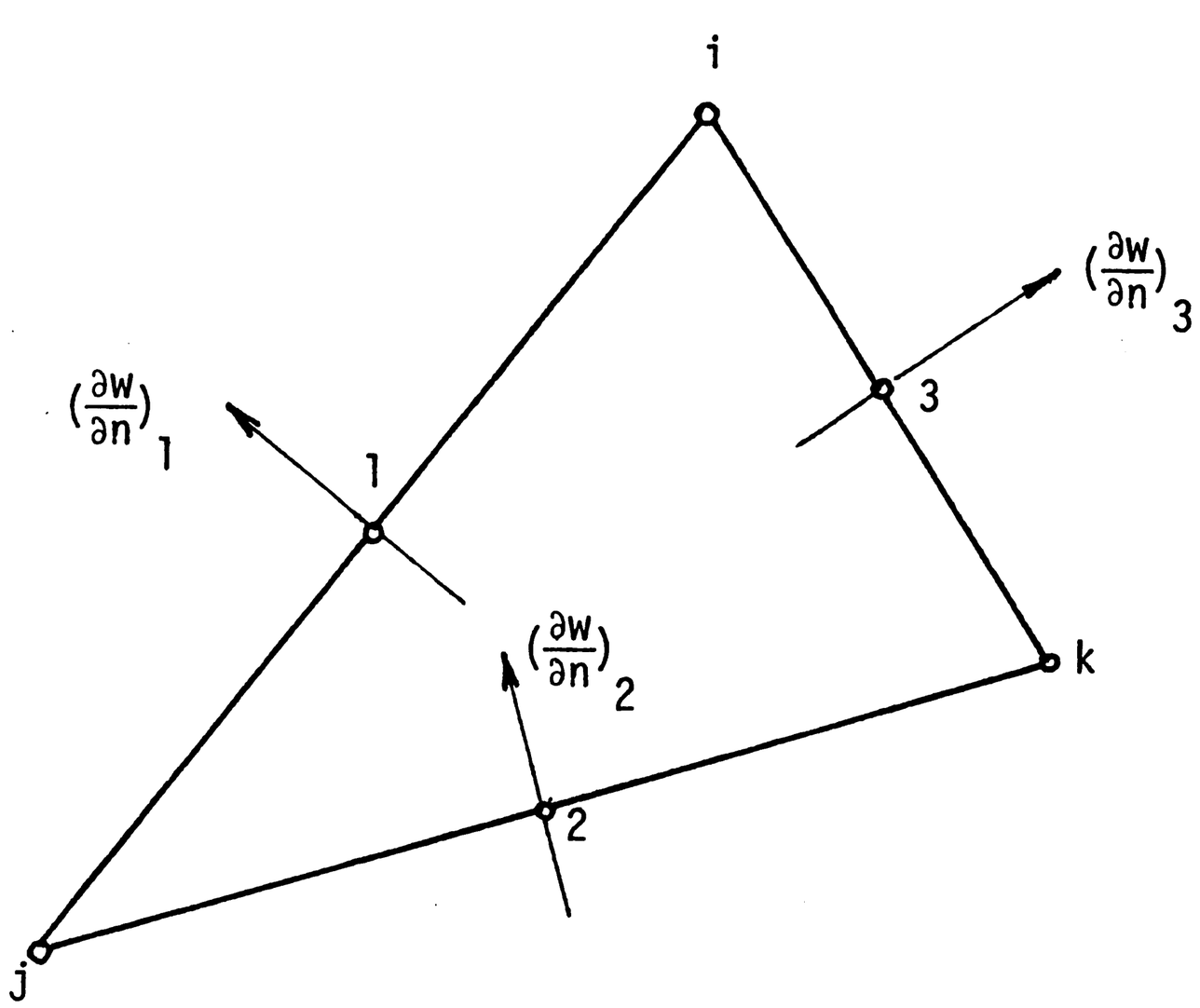

Figure 46 - Degree of freedom at the mid-side node.

$$\frac{\partial w}{\partial n} = - \sin\alpha \frac{\partial w}{\partial x} + \cos\alpha \frac{\partial w}{\partial y} \qquad (32)$$

$$\frac{\partial w}{\partial t} = \cos\alpha \frac{\partial w}{\partial x} + \sin\alpha \frac{\partial w}{\partial y}$$

The second derivative of w with respect to t and n follows

$$\frac{\partial^2 w}{\partial n \partial t} = - \sin\alpha\cos\alpha \frac{\partial^2 w}{\partial x^2} + (\cos^2\alpha - \sin^2\alpha)\frac{\partial^2 w}{\partial x \partial y} + \sin\alpha\cos\alpha \frac{\partial^2 w}{\partial y^2} \qquad (33)$$

where α is the direction angle as defined in Figures 47 and 48. By substituting the coordinates of each node into equation (16), equation (30) becomes

$$\{e\} = \begin{bmatrix} [P]_i \\ [P]_j \\ [P]_k \\ [P]_1 \\ [P]_2 \\ [P]_3 \end{bmatrix} \{q\} = [P]\{q\} \qquad (34)$$

where the $[P]_i$ matrix at the ith corner node is a 6 x 21 matrix given by

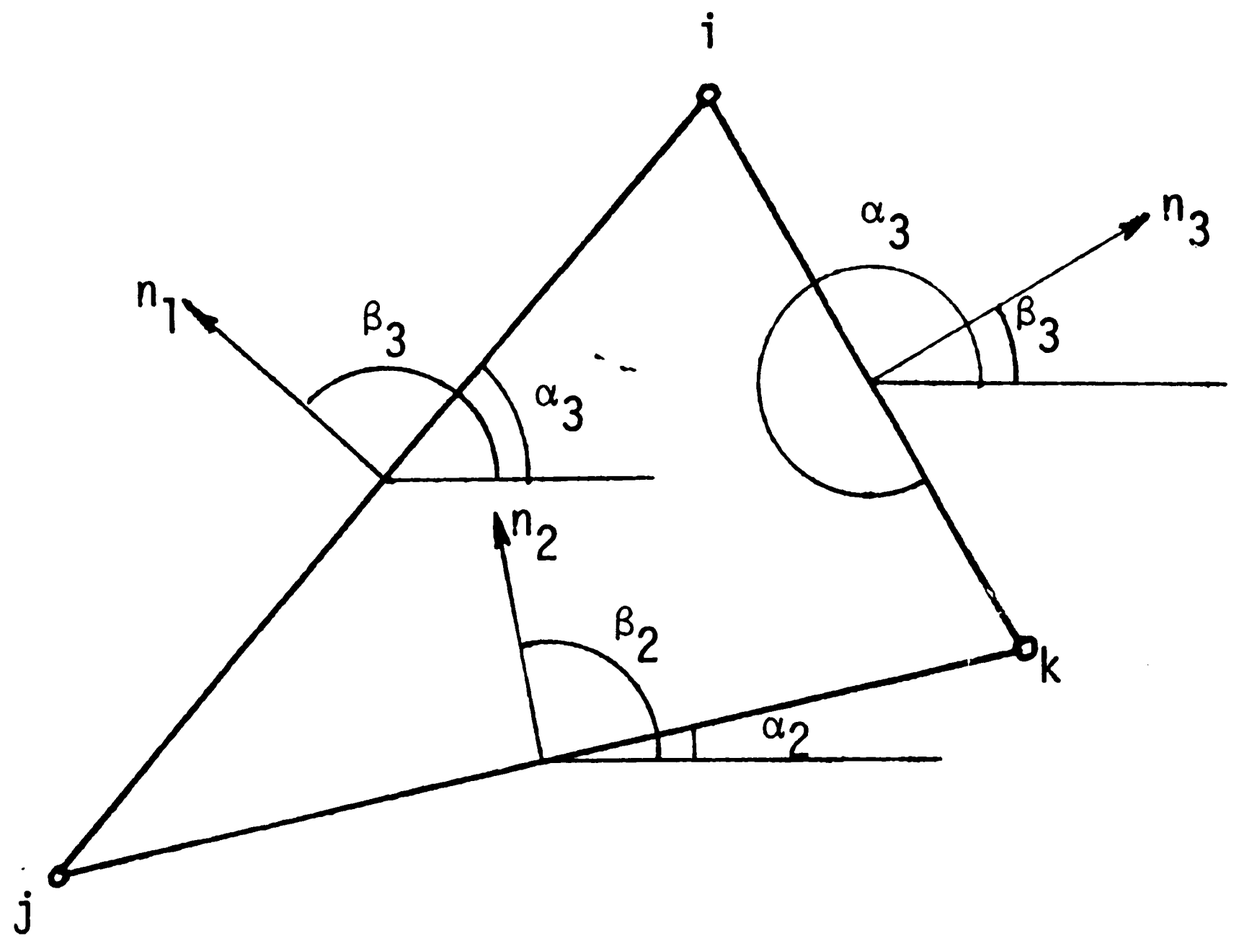

Figure 47 - Definition of the orientation of the normal slope at each mid-side node.

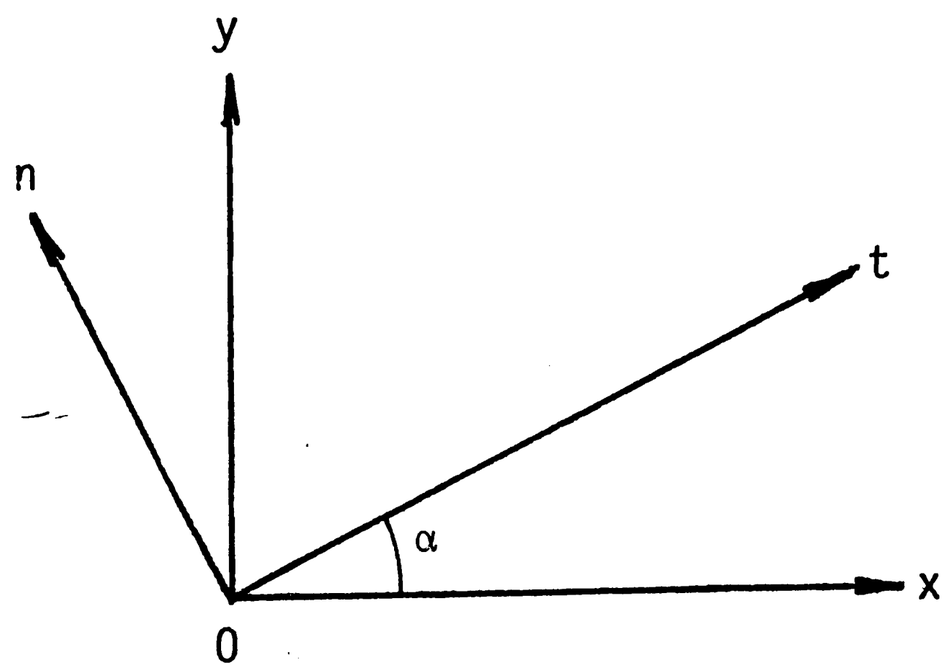

Figure 48 - Definition of the direction angle α.

$$[P]_i = \begin{bmatrix} 1, & x_i, & y_i, & x_i^2, & x_iy_i, \ldots, & x_iy_i^4, & y_i^5 \\ 0, & 1, & 0, & 2x_i, & y_i, \ldots, & y_i^4, & 0 \\ 0, & 0, & 1, & 0, & x_i, \ldots, & 4x_iy_i^3, & 5y_i^4 \\ 0, & 0, & 0, & 2, & 0, \ldots, & 0, & 0 \\ 0, & 0, & 0, & 0, & 0, \ldots, & 12x_iy_i^2, & 20y_i^3 \\ 0, & 0, & 0, & 0, & 1, \ldots, & 4y_i^3, & 0 \end{bmatrix} \tag{35}$$

The $[P]_1$ matrix at the 1th mid-side node is a 1 x 21 matrix:

$$[P]_1 = [0, -\sin\alpha_1, \cos\alpha_1, -2\sin\alpha_1 x_1, \ldots, -\sin\alpha_1 y_1^4$$

$$+ 4\cos\alpha_1 x_1 y_1^3, 5\sin\alpha_1 y_1^4] \tag{36}$$

Therefore, equation (16) becomes

$$w = \{p\}^T[P]^{-1}\{e\} \tag{37}$$

In order to condense the mid-side nodal variables, a cubic function is taken for the normal slope variation along the element boundary, i.e.,

$$\frac{\partial w}{\partial n} = a_0 + a_1 t + a_2 t^2 + a_3 t^3 \tag{38}$$

The corresponding boundary conditions are

$$t = 0,\ \frac{\partial w}{\partial n} = \left(\frac{\partial w}{\partial n}\right)_i,\ \frac{\partial^2 w}{\partial n \partial t} = \left(\frac{\partial^2 w}{\partial n \partial t}\right)_i$$

$$t = d_1,\ \frac{\partial w}{\partial n} = \left(\frac{\partial w}{\partial n}\right)_j,\ \frac{\partial^2 w}{\partial n \partial t} = \left(\frac{\partial^2 w}{\partial n \partial t}\right)_j \tag{39}$$

where d_1 is the nodal distance between the ith and jth nodes. By making use of the boundary conditions (39), the constants in equation (38) can be evaluated as

$$a_0 = \left(\frac{\partial w}{\partial n}\right)_i$$

$$a_1 = \left(\frac{\partial^2 w}{\partial n \partial t}\right)_i$$

$$a_2 = \frac{3}{d_1}\left[-\left(\frac{\partial w}{\partial n}\right)_i + \left(\frac{\partial w}{\partial n}\right)_j\right] - \frac{1}{d_1}\left[2\left(\frac{\partial^2 w}{\partial n \partial t}\right)_i + \left(\frac{\partial^2 w}{\partial n \partial t}\right)_j\right] \tag{40}$$

$$a_3 = \frac{2}{d_1^3}\left[\left(\frac{\partial w}{\partial n}\right)_i - \left(\frac{\partial w}{\partial n}\right)_j\right] + \frac{1}{d_1^2}\left[\left(\frac{\partial^2 w}{\partial n \partial t}\right)_i + \left(\frac{\partial^2 w}{\partial n \partial t}\right)_j\right]$$

Therefore, the normal slope at node 1 becomes

$$\left(\frac{\partial w}{\partial n}\right)_1 = \frac{1}{2}\left[\left(\frac{\partial w}{\partial n}\right)_i + \left(\frac{\partial w}{\partial n}\right)_j\right] + \frac{d_1}{8}\left[\left(\frac{\partial^2 w}{\partial n \partial t}\right)_i - \left(\frac{\partial^2 w}{\partial n \partial t}\right)_j\right] \tag{41}$$

Putting equations (32) and (33) into equation (41) and making use of the following notations

$$k_1^{(1)} = \frac{1}{2}\sin\alpha_1$$

$$k_2^{(1)} = \frac{1}{2}\cos\alpha_1 \qquad (42)$$

$$k_3^{(1)} = \frac{1}{8}d_1\sin\alpha_1\cos\alpha_1$$

$$k_4^{(1)} = \frac{1}{8}d_1(\cos^2\alpha_1 - \sin^2\alpha_1)$$

$(\partial w/\partial n)$ can be written in the form

$$\left(\frac{\partial w}{\partial n}\right)_1 = -k_1^{(1)}\left(\frac{\partial w}{\partial x}\right)_i + k_2^{(1)}\left(\frac{\partial w}{\partial y}\right)_i - k_3^{(1)}\left(\frac{\partial^2 w}{\partial x^2}\right)_i + k_3^{(1)}\left(\frac{\partial^2 w}{\partial y^2}\right)_i$$

$$+ k_4^{(1)}\left(\frac{\partial^2 w}{\partial x\partial y}\right)_i - k_1^{(1)}\left(\frac{\partial w}{\partial y}\right)_j + k_2^{(1)}\left(\frac{\partial w}{\partial y}\right)_j + k_3^{(1)}\left(\frac{\partial^2 w}{\partial x^2}\right)_j$$

$$- k_3^{(1)}\left(\frac{\partial^2 w}{\partial y^2}\right)_j - k_4^{(1)}\left(\frac{\partial^2 w}{\partial x\partial y}\right)_j \qquad (43)$$

The mid-side nodal variables can thus be expressed in terms of the corner nodal variables as

$$\begin{Bmatrix} \left(\frac{\partial w}{\partial n}\right)_1 \\ \left(\frac{\partial w}{\partial n}\right)_2 \\ \left(\frac{\partial w}{\partial n}\right)_3 \end{Bmatrix} = [Z]\{\xi\} \qquad (44)$$

The matrix [Z] is derived from equation (43). Therefore, {e} can be related directly to {ξ}:

$$\{e\} = \begin{bmatrix} [I] \\ [Z] \end{bmatrix}\{\xi\} = [U]\{\xi\} \tag{45}$$

in which [I] is an identity matrix. As a result, the displacement field can be explicitly expressed as

$$W = \{p\}^T[P]^{-1}[U]\{\xi\} = \{p\}^T[R]\{\xi\} \tag{46}$$

APPENDIX II

NUMERICAL RESULTS FOR THE SMALL CIRCULAR HOLE

APPENDIX II - NUMERICAL RESULTS FOR THE SMALL CIRCULAR HOLE

Table 1 - Deflection at each node of the lowest tensile buckling mode.

Node	x (cm)	y (cm)	w (cm)
1	3.000	.000	-.3435E-05
2	2.772	1.148	-.4184E-05
3	2.121	2.121	-.7136E-05
4	1.148	2.772	-.1203E-04
5	.000	3.000	-.1388E-04
6	6.000	.000	.1135E-05
7	5.500	2.500	.1022E-05
8	4.500	4.500	.3548E-06
9	2.500	5.500	-.5538E-05
10	.000	6.000	-.5792E-05
11	11.000	.000	.1267E-05
12	10.000	6.000	.1461E-05
13	6.000	10.000	.1158E-05
14	.000	12.000	.5033E-05
15	18.000	.000	.0000E+00
16	18.000	6.000	.0000E+00
17	12.000	15.000	-.3743E-06
18	.000	18.000	-.1331E-05
19	18.000	15.000	.0000E+00
20	18.000	25.000	.0000E+00
21	11.000	25.000	.0000E+00
22	4.000	25.000	.0000E+00
23	.000	25.000	.0000E+00

Table 2 - Deflection at each node of the second lowest tensile buckling mode.

Node	x (cm)	y (cm)	w (cm)
1	3.000	.000	.1523E-05
2	2.772	1.148	.3840E-05
3	2.121	2.121	.1487E-04
4	1.148	2.772	.3478E-04
5	.000	3.000	.4338E-04
6	6.000	.000	-.5059E-05
7	5.500	2.500	-.5348E-05
8	4.500	4.500	-.4215E-05
9	2.500	5.500	.3503E-05
10	.000	6.000	.1922E-04
11	11.000	.000	-.1202E-05
12	10.000	6.000	-.1869E-05
13	6.000	10.000	-.3976E-05
14	.000	12.000	.7970E-05
15	18.000	.000	.0000E+00
16	18.000	6.000	.0000E+00
17	12.000	15.000	.2420E-06
18	.000	18.000	.2074E-05
19	18.000	15.000	.0000E+00
20	18.000	25.000	.0000E+00
21	11.000	25.000	.0000E+00
22	4.000	25.000	.0000E+00
23	.000	25.000	.0000E+00

Table 3 - Continuation of Table 1, including the results of rotations and curvatures.

Node	$\frac{\partial w}{\partial x}$	$\frac{\partial w}{\partial y}$	$\frac{\partial^2 w}{\partial x^2}$	$\frac{\partial^2 w}{\partial y^2}$	$\frac{\partial^2 w}{\partial x \partial y}$
1	.1989E-05	.0000E+00	.9805E-09	.0000E+00	.0000E+00
2	.2708E-05	-.4855E-06	-.8194E-06	-.5165E-06	.9365E-06
3	.5043E-05	.7167E-07	-.3839E-05	.8641E-06	-.7901E-06
4	.4857E-05	.1918E-05	.4702E-05	.1188E-05	-.3407E-05
5	.0000E+00	.1981E-05	.0000E+00	-.1423E-05	.0000E+00
6	.7286E-06	.0000E+00	-.5082E-06	.0000E+00	.0000E+00
7	.6246E-06	.2193E-06	-.3008E-06	-.3850E-07	-.3060E-06
8	.1294E-05	-.1134E-07	-.8903E-06	.9643E-06	.1315E-06
9	.2255E-05	.3423E-06	.7992E-05	.6304E-05	-.3653E-05
10	.0000E+00	.4226E-05	.0000E+00	-.8560E-05	.0000E+00
11	-.2885E-06	.0000E+00	-.1583E-06	.0000E+00	.0000E+00
12	.8988E-07	-.4432E-06	-.2397E-06	-.8119E-06	.3557E-06
13	.3313E-08	.4639E-07	.8942E-06	-.2314E-07	-.1549E-05
14	.0000E+00	.1768E-05	.0000E+00	-.1863E-04	.0000E+00
15	-.3456E-07	.0000E+00	.0000E+00	.0000E+00	.0000E+00
16	.1416E-06	.0000E+00	.0000E+00	.0000E+00	.1451E-06
17	-.5016E-06	-.5019E-06	.9848E-06	.6268E-06	.5490E-06
18	.0000E+00	.1284E-05	.0000E+00	-.3970E-05	.0000E+00
19	-.2998E-06	.0000E+00	.0000E+00	.0000E+00	.3163E-07
20	.0000E+00	.0000E+00	.0000E+00	.0000E+00	.6229E-07
21	.0000E+00	-.4722E-07	.0000E+00	.0000E+00	-.1146E-06
22	.0000E+00	-.7960E-06	.0000E+00	.0000E+00	.3106E-06
23	.0000E+00	.8888E-06	.0000E+00	.0000E+00	.0000E+00

Table 4 - Deflection at each node of the third lowest tensile buckling mode.

Node	x (cm)	y (cm)	w (cm)
1	3.000	.000	.2696E-07
2	2.772	1.148	-.9641E-06
3	2.121	2.121	-.3901E-05
4	1.148	2.772	-.8644E-05
5	.000	3.000	-.1100E-04
6	6.000	.000	.1480E-05
7	5.500	2.500	.1888E-05
8	4.500	4.500	.4756E-05
9	2.500	5.500	-.2677E-05
10	.000	6.000	-.4645E-05
11	11.000	.000	.4814E-06
12	10.000	6.000	.2249E-06
13	6.000	10.000	.1302E-05
14	.000	12.000	-.2586E-05
15	18.000	.000	.0000E+00
16	18.000	6.000	.0000E+00
17	12.000	15.000	.6002E-06
18	.000	18.000	-.2927E-06
19	18.000	15.000	.0000E+00
20	18.000	25.000	.0000E+00
21	11.000	25.000	.0000E+00
22	4.000	25.000	.0000E+00
23	.000	25.000	.0000E+00

Table 5 - Deflection at each node of the fourth lowest tensile buckling mode.

Node	x (cm)	y (cm)	w (cm)
1	3.000	.000	.2103E-05
2	2.772	1.148	.2956E-05
3	2.121	2.121	.5720E-05
4	1.148	2.772	.6797E-05
5	.000	3.000	.6144E-05
6	6.000	.000	-.3096E-05
7	5.500	2.500	-.3670E-05
8	4.500	4.500	-.3306E-05
9	2.500	5.500	.4277E-05
10	.000	6.000	.8078E-05
11	11.000	.000	-.9281E-07
12	10.000	6.000	.1485E-05
13	6.000	10.000	-.4920E-05
14	.000	12.000	.5873E-05
15	18.000	.000	.0000E+00
16	18.000	6.000	.0000E+00
17	12.000	15.000	.2726E-05
18	.000	18.000	.9064E-06
19	18.000	15.000	.0000E+00
20	18.000	25.000	.0000E+00
21	11.000	25.000	.0000E+00
22	4.000	25.000	.0000E+00
23	.000	25.000	.0000E+00

Table 6 - Deflection at each node of the lowest compressive buckling mode.

Node	x (cm)	y (cm)	w (cm)
1	3.000	.000	-.3924E-03
2	2.772	1.148	-.3935E-03
3	2.121	2.121	-.3947E-03
4	1.148	2.772	-.3955E-03
5	.000	3.000	-.3951E-03
6	6.000	.000	-.3351E-03
7	5.500	2.500	-.3381E-03
8	4.500	4.500	-.3379E-03
9	2.500	5.500	-.3478E-03
10	.000	6.000	-.3493E-03
11	11.000	.000	-.2144E-03
12	10.000	6.000	-.2200E-03
13	6.000	10.000	-.2488E-03
14	.000	12.000	-.2499E-03
15	18.000	.000	.0000E+00
16	18.000	6.000	.0000E+00
17	12.000	15.000	-.1001E-03
18	.000	18.000	-.1369E-03
19	18.000	15.000	.0000E+00
20	18.000	25.000	.0000E+00
21	11.000	25.000	.0000E+00
22	4.000	25.000	.0000E+00
23	.000	25.000	.0000E+00

Table 7 - Deflection at each node of the second lowest compressive buckling mode.

Node	x (cm)	y (cm)	w (cm)
1	3.000	.000	-.6639E-04
2	2.772	1.148	-.6469E-04
3	2.121	2.121	-.5897E-04
4	1.148	2.772	-.5294E-04
5	.000	3.000	-.5023E-04
6	6.000	.000	-.4922E-04
7	5.500	2.500	-.4177E-04
8	4.500	4.500	-.2174E-04
9	2.500	5.500	-.8369E-05
10	.000	6.000	-.2494E-06
11	11.000	.000	-.2675E-04
12	10.000	6.000	.1135E-05
13	6.000	10.000	.5847E-04
14	.000	12.000	.9323E-04
15	18.000	.000	.0000E+00
16	18.000	6.000	.0000E+00
17	12.000	15.000	.5859E-04
18	.000	18.000	.1067E-03
19	18.000	15.000	.0000E+00
20	18.000	25.000	.0000E+00
21	11.000	25.000	.0000E+00
22	4.000	25.000	.0000E+00
23	.000	25.000	.0000E+00

Table 8 - Continuation of Table 5, including the results of rotations and curvatures.

Node	$\frac{\partial w}{\partial x}$	$\frac{\partial w}{\partial y}$	$\frac{\partial^2 w}{\partial x^2}$	$\frac{\partial^2 w}{\partial y^2}$	$\frac{\partial^2 w}{\partial x \partial y}$
1	.1871E-04	.0000E+00	-.3640E-06	.0000E+00	.0000E+00
2	.1786E-04	.6370E-05	-.3305E-06	.4176E-05	-.3244E-05
3	.1322E-04	.1190E-04	.2627E-05	.1435E-05	-.4092E-05
4	.6793E-05	.1552E-04	.4680E-05	-.1036E-05	-.2755E-05
5	.0000E+00	.1589E-04	.0000E+00	-.6025E-06	.0000E+00
6	.2047E-04	.0000E+00	.9415E-06	.0000E+00	.0000E+00
7	.1843E-04	.5918E-05	.1906E-05	.2173E-05	-.1059E-05
8	.1415E-04	.1051E-04	.2315E-05	.1373E-05	-.1116E-05
9	.7812E-05	.1375E-04	.2821E-05	.8865E-06	-.9473E-06
10	.0000E+00	.1525E-04	.0000E+00	.2089E-07	.0000E+00
11	.2770E-04	.0000E+00	.6367E-06	.0000E+00	.0000E+00
12	.2320E-04	.7184E-05	.1475E-05	.1019E-05	-.8204E-06
13	.1251E-04	.1411E-04	.1948E-05	.6309E-06	-.8870E-06
14	.0000E+00	.1790E-04	.0000E+00	.7953E-07	.0000E+00
15	.3240E-04	.0000E+00	.0000E+00	.0000E+00	.0000E+00
16	.2952E-04	.0000E+00	.0000E+00	.0000E+00	-.8539E-06
17	.1503E-04	.9463E-05	.8624E-06	.2447E-06	-.1473E-05
18	.0000E+00	.1945E-04	.0000E+00	-.3719E-06	.0000E+00
19	.1746E-04	.0000E+00	.0000E+00	.0000E+00	-.1641E-05
20	.0000E+00	.0000E+00	.0000E+00	.0000E+00	-.1796E-05
21	.0000E+00	.1184E-04	.0000E+00	.0000E+00	-.1481E-05
22	.0000E+00	.1908E-04	.0000E+00	.0000E+00	-.3891E-06
23	.0000E+00	.1984E-04	.0000E+00	.0000E+00	.0000E+00

Table 9 - Deflection at each node of the third lowest compressive buckling mode.

Node	x (cm)	y (cm)	w (cm)
1	3.000	.000	-.3486E-04
2	2.772	1.148	-.3251E-04
3	2.121	2.121	-.2526E-04
4	1.148	2.772	-.1802E-04
5	.000	3.000	-.1505E-04
6	6.000	.000	-.2282E-04
7	5.500	2.500	-.1416E-04
8	4.500	4.500	.5777E-05
9	2.500	5.500	.1786E-04
10	.000	6.000	.2398E-04
11	11.000	.000	-.9205E-05
12	10.000	6.000	.1636E-04
13	6.000	10.000	.3987E-04
14	.000	12.000	.3422E-04
15	18.000	.000	.0000E+00
16	18.000	6.000	.0000E+00
17	12.000	15.000	.5918E-06
18	.000	18.000	-.3059E-04
19	18.000	15.000	.0000E+00
20	18.000	25.000	.0000E+00
21	11.000	25.000	.0000E+00
22	4.000	25.000	.0000E+00
23	.000	25.000	.0000E+00

Table 10 - Deflection at each node of the fourth lowest compressive buckling mode.

Node	x (cm)	y (cm)	w (cm)
1	3.000	.000	.2421E-04
2	2.772	1.148	.2152E-04
3	2.121	2.121	.1367E-04
4	1.148	2.772	.6392E-05
5	.000	3.000	.3685E-05
6	6.000	.000	.1253E-04
7	5.500	2.500	.4192E-05
8	4.500	4.500	-.1147E-04
9	2.500	5.500	-.1758E-04
10	.000	6.000	-.1956E-04
11	11.000	.000	-.9445E-06
12	10.000	6.000	-.1646E-04
13	6.000	10.000	-.5635E-05
14	.000	12.000	.9424E-05
15	18.000	.000	.0000E+00
16	18.000	6.000	.0000E+00
17	12.000	15.000	.1149E-04
18	.000	18.000	-.6630E-05
19	18.000	15.000	.0000E+00
20	18.000	25.000	.0000E+00
21	11.000	25.000	.0000E+00
22	4.000	25.000	.0000E+00
23	.000	25.000	.0000E+00

APPENDIX III

NUMERICAL RESULTS FOR THE LARGE CIRCULAR HOLE

APPENDIX III - NUMERICAL RESULTS FOR THE LARGE CIRCULAR HOLE

Table 11 - Deflection at each node of the lowest tensile buckling mode.

Node	x (cm)	y (cm)	w (cm)
1	10.000	.000	.1407E-04
2	9.659	2.588	.1656E-04
3	8.660	5.000	.2745E-04
4	7.071	7.071	.5487E-04
5	5.000	8.660	.1044E-03
6	2.588	9.659	.1609E-03
7	.000	10.000	.1801E-03
8	14.000	.000	.1366E-05
9	13.500	5.500	-.7487E-06
10	12.000	9.000	-.1965E-05
11	9.000	12.000	.1131E-04
12	5.500	13.500	.5132E-04
13	.000	15.000	.8446E-04
14	18.000	.000	.0000E+00
15	18.000	6.000	.0000E+00
16	18.000	15.000	.0000E+00
17	10.700	17.000	-.2870E-05
18	5.000	18.500	.2378E-04
19	.000	20.000	.3073E-04
20	18.000	25.000	.0000E+00
21	11.000	25.000	.0000E+00
22	4.000	25.000	.0000E+00
23	.000	25.000	.0000E+00

Table 12 - Deflection at each node of the second lowest tensile buckling mode.

Node	x (cm)	y (cm)	w (cm)
1	10.000	.000	-.7000E-06
2	9.659	2.588	-.2481E-05
3	8.660	5.000	-.1104E-04
4	7.071	7.071	-.3248E-04
5	5.000	8.660	-.5199E-04
6	2.588	9.659	-.2195E-04
7	.000	10.000	.7020E-05
8	14.000	.000	.5430E-05
9	13.500	5.500	.7567E-05
10	12.000	9.000	.9635E-05
11	9.000	12.000	-.1432E-05
12	5.500	13.500	-.2531E-04
13	.000	15.000	-.1704E-04
14	18.000	.000	.0000E+00
15	18.000	6.000	.0000E+00
16	18.000	15.000	.0000E+00
17	10.700	17.000	.6548E-05
18	5.000	18.500	-.8609E-05
19	.000	20.000	-.9779E-05
20	18.000	25.000	.0000E+00
21	11.000	25.000	.0000E+00
22	4.000	25.000	.0000E+00
23	.000	25.000	.0000E+00

Table 13 - Continuation of Table 9, including the results of rotations and curvatures.

Node	$\frac{\partial w}{\partial x}$	$\frac{\partial w}{\partial y}$	$\frac{\partial^2 w}{\partial x^2}$	$\frac{\partial^2 w}{\partial y^2}$	$\frac{\partial^2 w}{\partial x \partial y}$
1	-.4071E-05	.0000E+00	-.7333E-07	.0000E+00	.0000E+00
2	-.5290E-05	.8269E-06	.3490E-06	.4074E-07	-.1027E-05
3	-.1061E-04	.1782E-05	.2544E-05	-.1395E-05	-.2110E-05
4	-.2085E-04	.2603E-06	.5340E-05	-.3573E-05	-.9450E-06
5	-.2979E-04	-.6976E-05	.3871E-05	-.3301E-05	.2561E-05
6	-.2277E-04	-.1926E-04	-.6228E-05	.7391E-06	.5245E-05
7	.0000E+00	-.2177E-04	.0000E+00	.1318E-05	.0000E+00
8	-.1628E-05	.0000E+00	.9525E-06	.0000E+00	.0000E+00
9	-.1667E-05	-.1122E-05	.1230E-05	-.1041E-06	.1979E-06
10	-.3111E-05	-.1422E-05	.1972E-05	.3387E-06	.3451E-06
11	-.9480E-05	-.2294E-05	.3318E-05	.2639E-06	.9620E-06
12	-.1565E-04	-.7674E-05	.7573E-06	.1555E-06	.2770E-05
13	.0000E+00	-.1490E-04	.0000E+00	.5159E-05	.0000E+00
14	.2661E-06	.0000E+00	.0000E+00	.0000E+00	.0000E+00
15	.1230E-05	.0000E+00	.0000E+00	.0000E+00	.2249E-06
16	.2021E-05	.0000E+00	.0000E+00	.0000E+00	-.1455E-06
17	-.2419E-05	-.3114E-07	.1310E-05	.1741E-06	.4559E-06
18	-.6475E-05	-.5029E-05	-.3690E-06	.6647E-06	.1205E-05
19	.0000E+00	-.7964E-05	.0000E+00	.1815E-05	.0000E+00
20	.0000E+00	.0000E+00	.0000E+00	.0000E+00	-.1840E-06
21	.0000E+00	.4981E-06	.0000E+00	.0000E+00	.1808E-06
22	.0000E+00	-.3906E-05	.0000E+00	.0000E+00	.9793E-06
23	.0000E+00	-.5651E-05	.0000E+00	.0000E+00	.0000E+00

Table 14 - Deflection at each node of the third lowest tensile buckling mode.

Node	x (cm)	y (cm)	w (cm)
1	10.000	.000	.3320E-06
2	9.659	2.588	.1646E-05
3	8.660	5.000	.7836E-05
4	7.071	7.071	.2107E-04
5	5.000	8.660	.1971E-04
6	2.588	9.659	.4588E-05
7	.000	10.000	.2973E-04
8	14.000	.000	-.4369E-05
9	13.500	5.500	-.5897E-05
10	12.000	9.000	-.7428E-05
11	9.000	12.000	.1333E-05
12	5.500	13.500	.1456E-04
13	.000	15.000	.1202E-04
14	18.000	.000	.0000E+00
15	18.000	6.000	.0000E+00
16	18.000	15.000	.0000E+00
17	10.700	17.000	-.5305E-05
18	5.000	18.500	.4701E-05
19	.000	20.000	.5466E-05
20	18.000	25.000	.0000E+00
21	11.000	25.000	.0000E+00
22	4.000	25.000	.0000E+00
23	.000	25.000	.0000E+00

Table 15 - Deflection at each node of the fourth lowest tensile buckling mode.

Node	x (cm)	y (cm)	w (cm)
1	10.000	.000	-.4422E-06
2	9.659	2.588	-.3924E-06
3	8.660	5.000	-.5413E-07
4	7.071	7.071	.1371E-05
5	5.000	8.660	.2860E-05
6	2.588	9.659	.1896E-06
7	.000	10.000	-.7207E-07
8	14.000	.000	-.4463E-06
9	13.500	5.500	-.5243E-06
10	12.000	9.000	-.5373E-06
11	9.000	12.000	-.2216E-06
12	5.500	13.500	-.4911E-06
13	.000	15.000	.2139E-05
14	18.000	.000	.0000E+00
15	18.000	6.000	.0000E+00
16	18.000	15.000	.0000E+00
17	10.700	17.000	-.7415E-06
18	5.000	18.500	.1249E-04
19	.000	20.000	.9770E-06
20	18.000	25.000	.0000E+00
21	11.000	25.000	.0000E+00
22	4.000	25.000	.0000E+00
23	.000	25.000	.0000E+00

Table 16 - Deflection at each node of the lowest compressive buckling mode.

Node	x (cm)	y (cm)	w (cm)
1	10.000	.000	-.3580E-03
2	9.659	2.588	-.3609E-03
3	8.660	5.000	-.3607E-03
4	7.071	7.071	-.3574E-03
5	5.000	8.660	-.3523E-03
6	2.588	9.659	-.3476E-03
7	.000	10.000	-.3447E-03
8	14.000	.000	-.1796E-03
9	13.500	5.500	-.1774E-03
10	12.000	9.000	-.1892E-03
11	9.000	12.000	-.2126E-03
12	5.500	13.500	-.2313E-03
13	.000	15.000	-.2208E-03
14	18.000	.000	.0000E+00
15	18.000	6.000	.0000E+00
16	18.000	15.000	.0000E+00
17	10.700	17.000	-.1084E-03
18	5.000	18.500	-.1315E-03
19	.000	20.000	-.1090E-03
20	18.000	25.000	.0000E+00
21	11.000	25.000	.0000E+00
22	4.000	25.000	.0000E+00
23	.000	25.000	.0000E+00

Table 17 - Deflection at each node of the second lowest compressive buckling mode.

Node	x (cm)	y (cm)	w (cm)
1	10.000	.000	-.3052E-04
2	9.659	2.588	-.1785E-04
3	8.660	5.000	.2276E-04
4	7.071	7.071	.7224E-04
5	5.000	8.660	.1139E-03
6	2.588	9.659	.1393E-03
7	.000	10.000	.1465E-03
8	14.000	.000	-.1499E-04
9	13.500	5.500	.1106E-04
10	12.000	9.000	.5381E-04
11	9.000	12.000	.1052E-03
12	5.500	13.500	.1364E-03
13	.000	15.000	.1480E-03
14	18.000	.000	.0000E+00
15	18.000	6.000	.0000E+00
16	18.000	15.000	.0000E+00
17	10.700	17.000	.8976E-04
18	5.000	18.500	.1143E-03
19	.000	20.000	.1001E-03
20	18.000	25.000	.0000E+00
21	11.000	25.000	.0000E+00
22	4.000	25.000	.0000E+00
23	.000	25.000	.0000E+00

Table 18 - Continuation of Table 13, including the results of rotations and curvatures.

Node	$\frac{\partial w}{\partial x}$	$\frac{\partial w}{\partial y}$	$\frac{\partial^2 w}{\partial x^2}$	$\frac{\partial^2 w}{\partial y^2}$	$\frac{\partial^2 w}{\partial x \partial y}$
1	.4507E-04	.0000E+00	-.9204E-06	.0000E+00	.0000E+00
2	.4316E-04	.1095E-04	-.6298E-06	.4012E-05	-.2984E-05
3	.3406E-04	.2052E-04	.1894E-05	.1029E-05	-.3574E-05
4	.2292E-04	.2535E-04	.3539E-05	-.9676E-06	-.2481E-05
5	.1306E-04	.2674E-04	.3387E-05	-.1357E-05	-.9575E-06
6	.5766E-05	.2688E-04	.2596E-05	-.8595E-06	-.4549E-06
7	.0000E+00	.2630E-04	.0000E+00	-.4321E-06	.0000E+00
8	.4470E-04	.0000E+00	-.7450E-06	.0000E+00	.0000E+00
9	.3821E-04	.8477E-05	.8047E-06	.1059E-05	-.1880E-05
10	.2911E-04	.1321E-04	.1369E-05	-.2395E-07	-.2103E-05
11	.1830E-04	.1808E-04	.1932E-05	-.5323E-06	-.1574E-05
12	.9727E-05	.2156E-04	.1923E-05	-.5303E-06	-.8580E-06
13	.0000E+00	.2332E-04	.0000E+00	-.9763E-06	.0000E+00
14	.4572E-04	.0000E+00	.0000E+00	.0000E+00	.0000E+00
15	.3884E-04	.0000E+00	.0000E+00	.0000E+00	-.1848E-05
16	.1973E-04	.0000E+00	.0000E+00	.0000E+00	-.1847E-05
17	.1264E-04	.1333E-04	.9240E-06	-.1222E-06	-.1580E-05
18	.4625E-05	.2014E-04	.1038E-05	.5729E-07	-.7354E-06
19	.0000E+00	.2196E-04	.0000E+00	-.2119E-06	.0000E+00
20	.0000E+00	.0000E+00	.0000E+00	.0000E+00	-.2128E-05
21	.0000E+00	.1341E-04	.0000E+00	.0000E+00	-.1553E-05
22	.0000E+00	.2081E-04	.0000E+00	.0000E+00	-.3994E-06
23	.0000E+00	.2168E-04	.0000E+00	.0000E+00	.0000E+00

Table 19 - Deflection at each node of the third lowest compressive buckling mode.

Node	x (cm)	y (cm)	w (cm)
1	10.000	.000	-.1392E-04
2	9.659	2.588	.5718E-05
3	8.660	5.000	.5413E-04
4	7.071	7.071	.8379E-04
5	5.000	8.660	.8402E-04
6	2.588	9.659	.7279E-04
7	.000	10.000	.6738E-04
8	14.000	.000	-.6455E-05
9	13.500	5.500	.2588E-04
10	12.000	9.000	.5071E-04
11	9.000	12.000	.4323E-04
12	5.500	13.500	.2362E-04
13	.000	15.000	.4642E-06
14	18.000	.000	.0000E+00
15	18.000	6.000	.0000E+00
16	18.000	15.000	.0000E+00
17	10.700	17.000	-.5847E-05
18	5.000	18.500	-.2434E-04
19	.000	20.000	-.3028E-04
20	18.000	25.000	.0000E+00
21	11.000	25.000	.0000E+00
22	4.000	25.000	.0000E+00
23	.000	25.000	.0000E+00

Table 20 - Deflection at each node of the fourth lowest compressive buckling mode.

Node	x (cm)	y (cm)	w (cm)
1	10.000	.000	.3380E-04
2	9.659	2.588	.1600E-04
3	8.660	5.000	-.8304E-05
4	7.071	7.071	.6385E-05
5	5.000	8.660	.3148E-04
6	2.588	9.659	.4265E-04
7	.000	10.000	.4404E-04
8	14.000	.000	.1529E-04
9	13.500	5.500	-.3811E-05
10	12.000	9.000	.9738E-05
11	9.000	12.000	.3603E-04
12	5.500	13.500	.3259E-04
13	.000	15.000	.1337E-04
14	18.000	.000	.0000E+00
15	18.000	6.000	.0000E+00
16	18.000	15.000	.0000E+00
17	10.700	17.000	.1660E-04
18	5.000	18.500	-.9879E-05
19	.000	20.000	-.2490E-04
20	18.000	25.000	.0000E+00
21	11.000	25.000	.0000E+00
22	4.000	25.000	.0000E+00
23	.000	25.000	.0000E+00

APPENDIX IV

NUMERICAL RESULTS FOR THE NARROW HORIZONTAL ELLIPTICAL CAVITY

APPENDIX IV - NUMERICAL RESULTS FOR THE NARROW HORIZONTAL ELLIPTICAL CAVITY

Table 21 - Deflection at each node of the lowest tensile buckling mode.

Node	x (cm)	y (cm)	w (cm)
1	1.000	.000	-.9166E-06
2	.968	2.500	-.9158E-06
3	.866	5.000	-.9047E-06
4	.368	9.300	-.7288E-06
5	.148	9.890	-.5622E-06
6	.126	9.920	-.5525E-06
7	.100	9.950	-.5428E-06
8	.077	9.970	-.5363E-06
9	.045	9.990	-.5299E-06
10	.000	10.000	-.5268E-06
11	6.000	.000	-.1490E-06
12	5.000	4.000	-.4348E-06
13	3.500	7.500	-.5298E-06
14	1.500	9.800	-.8631E-06
15	.240	9.990	-.5414E-06
16	.110	10.100	-.5000E-06
17	.000	10.400	-.3988E-06
18	11.000	.000	.1052E-05
19	11.000	7.000	.1647E-05
20	3.000	11.000	-.1175E-05
21	.500	10.500	-.3963E-06
22	.000	11.500	.6352E-07
23	18.000	.000	.0000E+00
24	18.000	12.000	.0000E+00
25	8.000	15.000	-.1756E-04
26	.000	16.000	-.2532E-06
27	18.000	25.000	.0000E+00
28	7.000	25.000	.0000E+00
29	.000	25.000	.0000E+00

Table 22 - Deflection at each node of the second lowest tensile buckling mode..

Node	x (cm)	y (cm)	w (cm)
1	1.000	.000	.2420E-06
2	.968	2.500	.1267E-06
3	.866	5.000	.3988E-06
4	.368	9.300	.1768E-05
5	.148	9.890	.3812E-07
6	.126	9.920	.4323E-08
7	.100	9.950	-.2583E-07
8	.077	9.970	-.3927E-07
9	.045	9.990	-.4716E-07
10	.000	10.000	-.4874E-07
11	6.000	.000	-.1507E-07
12	5.000	4.000	.2440E-08
13	3.500	7.500	.1435E-06
14	1.500	9.800	-.2132E-05
15	.240	9.990	-.6521E-08
16	.110	10.100	-.3735E-07
17	.000	10.400	.1038E-06
18	11.000	.000	-.1423E-06
19	11.000	7.000	.1126E-08
20	3.000	11.000	-.5234E-07
21	.500	10.500	.1767E-06
22	.000	11.500	.2207E-06
23	18.000	.000	.0000E+00
24	18.000	12.000	.0000E+00
25	8.000	15.000	.4364E-08
26	.000	16.000	.5895E-07
27	18.000	25.000	.0000E+00
28	7.000	25.000	.0000E+00
29	.000	25.000	.0000E+00

Table 23 - Continuation of Table 17, including the results of rotations and curvatures.

Node	$\frac{\partial w}{\partial x}$	$\frac{\partial w}{\partial y}$	$\frac{\partial^2 w}{\partial x^2}$	$\frac{\partial^2 w}{\partial y^2}$	$\frac{\partial^2 w}{\partial x \partial y}$
1	.1335E-06	.0000E+00	.5279E-09	.0000E+00	.0000E+00
2	.1178E-06	.4360E-08	.3153E-07	.3675E-07	.1032E-07
3	.1343E-06	.2426E-07	-.9262E-07	-.2441E-07	-.5801E-07
4	-.7489E-07	.2010E-06	-.3623E-06	.2160E-06	-.9663E-07
5	-.7631E-07	.2709E-06	-.1778E-06	.1094E-06	.1924E-06
6	-.6522E-07	.2722E-06	-.2704E-06	.1503E-06	.1588E-06
7	-.5117E-07	.2736E-06	-.3967E-06	.2182E-06	.1398E-06
8	-.3761E-07	.2750E-06	-.5556E-06	.3231E-06	.1191E-06
9	-.1726E-07	.2781E-06	-.5990E-06	.2784E-06	.6984E-07
10	.0000E+00	.2799E-06	.0000E+00	.2494E-06	.0000E+00
11	.2158E-06	.0000E+00	.5320E-07	.0000E+00	.0000E+00
12	.1473E-06	.7123E-07	.6131E-07	.3304E-06	.4641E-07
13	.2867E-06	.5531E-07	.3914E-06	.1511E-07	.3104E-06
14	-.2961E-06	.1481E-06	.1051E-07	.2724E-06	-.2009E-06
15	-.8975E-07	.2953E-06	-.1507E-06	.2192E-06	.1015E-06
16	-.4123E-07	.3044E-06	-.2653E-06	.2412E-06	.9271E-07
17	.0000E+00	.3617E-06	.0000E+00	.2482E-06	.0000E+00
18	-.3118E-07	.0000E+00	-.3675E-06	.0000E+00	.0000E+00
19	.9266E-06	-.2748E-06	-.1214E-05	-.6432E-06	.7317E-06
20	-.1604E-07	-.1790E-06	.1272E-05	-.8375E-07	-.8866E-06
21	-.1383E-06	.3858E-06	-.2132E-06	.7506E-07	-.4908E-07
22	.0000E+00	.4810E-06	.0000E+00	.2016E-06	.0000E+00
23	-.5057E-06	.0000E+00	.0000E+00	.0000E+00	.0000E+00
24	.1549E-05	.0000E+00	.0000E+00	.0000E+00	.1283E-06
25	-.1551E-05	-.1931E-05	.4414E-05	.9231E-05	-.1772E-05
26	.0000E+00	-.9109E-07	.0000E+00	.6783E-06	.0000E+00
27	.0000E+00	.0000E+00	.0000E+00	.0000E+00	.3645E-06
28	.0000E+00	-.2120E-05	.0000E+00	.0000E+00	-.1014E-05
29	.0000E+00	-.2637E-06	.0000E+00	.0000E+00	.0000E+00

Table 24 - Deflection at each node of the third lowest tensile buckling mode.

Node	x (cm)	y (cm)	w (cm)
1	1.000	.000	.5656E-06
2	.968	2.500	.4443E-06
3	.866	5.000	.7288E-07
4	.368	9.300	.6492E-06
5	.148	9.890	.6412E-06
6	.126	9.920	.6403E-06
7	.100	9.950	.6396E-06
8	.077	9.970	.6395E-06
9	.045	9.990	.6395E-06
10	.000	10.000	.6395E-06
11	6.000	.000	-.1065E-05
12	5.000	4.000	-.5396E-07
13	3.500	7.500	.5378E-05
14	1.500	9.800	.4096E-06
15	.240	9.990	.6473E-06
16	.110	10.100	.6464E-06
17	.000	10.400	.6267E-06
18	11.000	.000	.1040E-05
19	11.000	7.000	-.5291E-06
20	3.000	11.000	-.7367E-06
21	.500	10.500	.7462E-06
22	.000	11.500	.1008E-05
23	18.000	.000	.0000E+00
24	18.000	12.000	.0000E+00
25	8.000	15.000	-.3009E-06
26	.000	16.000	.3776E-06
27	18.000	25.000	.0000E+00
28	7.000	25.000	.0000E+00
29	.000	25.000	.0000E+00

Table 25 - Deflection at each node of the fourth lowest tensile buckling mode.

Node	x (cm)	y (cm)	w (cm)
1	1.000	.000	-.1471E-05
2	.968	2.500	-.1291E-05
3	.866	5.000	-.1758E-05
4	.368	9.300	-.2852E-05
5	.148	9.890	-.3060E-05
6	.126	9.920	-.3063E-05
7	.100	9.950	-.3063E-05
8	.077	9.970	-.3062E-05
9	.045	9.990	-.3059E-05
10	.000	10.000	-.3055E-05
11	6.000	.000	.1146E-05
12	5.000	4.000	.5118E-06
13	3.500	7.500	-.2579E-06
14	1.500	9.800	-.1092E-05
15	.240	9.990	-.2932E-05
16	.110	10.100	-.2966E-05
17	.000	10.400	-.2859E-05
18	11.000	.000	.5810E-07
19	11.000	7.000	-.4086E-07
20	3.000	11.000	-.3564E-06
21	.500	10.500	-.2261E-05
22	.000	11.500	.3862E-05
23	18.000	.000	.0000E+00
24	18.000	12.000	.0000E+00
25	8.000	15.000	.2880E-06
26	.000	16.000	-.1545E-05
27	18.000	25.000	.0000E+00
28	7.000	25.000	.0000E+00
29	.000	25.000	.0000E+00

Table 26 - Deflection at each node of the lowest compressive buckling mode.

Node	x (cm)	y (cm)	w (cm)
1	1.000	.000	-.4922E-03
2	.968	2.500	-.4838E-03
3	.866	5.000	-.4549E-03
4	.368	9.300	-.3643E-03
5	.148	9.890	-.3485E-03
6	.126	9.920	-.3477E-03
7	.100	9.950	-.3469E-03
8	.077	9.970	-.3463E-03
9	.045	9.990	-.3458E-03
10	.000	10.000	-.3455E-03
11	6.000	.000	-.3625E-03
12	5.000	4.000	-.3729E-03
13	3.500	7.500	-.3605E-03
14	1.500	9.800	-.3419E-03
15	.240	9.990	-.3454E-03
16	.110	10.100	-.3425E-03
17	.000	10.400	-.3341E-03
18	11.000	.000	-.2218E-03
19	11.000	7.000	-.1985E-03
20	3.000	11.000	-.3004E-03
21	.500	10.500	-.3306E-03
22	.000	11.500	-.3051E-03
23	18.000	.000	.0000E+00
24	18.000	12.000	.0000E+00
25	8.000	15.000	-.1656E-03
26	.000	16.000	-.1975E-03
27	18.000	25.000	.0000E+00
28	7.000	25.000	.0000E+00
29	.000	25.000	.0000E+00

Table 27 - Deflection at each node of the second lowest compressive buckling mode.

Node	x (cm)	y (cm)	w (cm)
1	1.000	.000	-.6272E-04
2	.968	2.500	-.5266E-04
3	.866	5.000	-.2074E-04
4	.368	9.300	.5569E-04
5	.148	9.890	.6531E-04
6	.126	9.920	.6578E-04
7	.100	9.950	.6625E-04
8	.077	9.970	.6656E-04
9	.045	9.990	.6687E-04
10	.000	10.000	.6703E-04
11	6.000	.000	-.3758E-04
12	5.000	4.000	-.2115E-04
13	3.500	7.500	.2557E-04
14	1.500	9.800	.6351E-04
15	.240	9.990	.6684E-04
16	.110	10.100	.6855E-04
17	.000	10.400	.7307E-04
18	11.000	.000	-.1984E-04
19	11.000	7.000	.1455E-04
20	3.000	11.000	.7988E-04
21	.500	10.500	.7451E-04
22	.000	11.500	.8837E-04
23	18.000	.000	.0000E+00
24	18.000	12.000	.0000E+00
25	8.000	15.000	.9163E-04
26	.000	16.000	.1175E-03
27	18.000	25.000	.0000E+00
28	7.000	25.000	.0000E+00
29	.000	25.000	.0000E+00

Table 28 - Continuation of Table 21, including the results of rotations and curvatures.

Node	$\frac{\partial w}{\partial x}$	$\frac{\partial w}{\partial y}$	$\frac{\partial^2 w}{\partial x^2}$	$\frac{\partial^2 w}{\partial y^2}$	$\frac{\partial^2 w}{\partial x \partial y}$
1	.2645E-04	.0000E+00	-.7550E-06	.0000E+00	.0000E+00
2	.2599E-04	.8300E-05	-.9105E-06	.3368E-05	-.1018E-05
3	.2232E-04	.1676E-04	-.7339E-06	.3149E-05	-.2182E-05
4	.8146E-05	.2808E-04	.1933E-05	.5014E-06	-.5314E-05
5	.3171E-05	.2939E-04	.5989E-05	-.3020E-05	-.8604E-05
6	.2624E-05	.2950E-04	.1226E-04	-.4467E-05	-.9402E-05
7	.1989E-05	.2956E-04	.1578E-04	-.6322E-05	-.7971E-05
8	.1435E-05	.2958E-04	.1978E-04	-.1051E-04	-.6181E-05
9	.6407E-06	.2956E-04	.2216E-04	-.9661E-05	-.3901E-05
10	.0000E+00	.2954E-04	.0000E+00	-.9453E-05	.0000E+00
11	.2650E-04	.0000E+00	.1029E-06	.0000E+00	.0000E+00
12	.2402E-04	.8437E-05	.7152E-06	.2022E-05	-.1011E-05
13	.1795E-04	.1682E-04	.1164E-05	.1446E-05	-.1732E-05
14	.9159E-05	.2362E-04	.2951E-05	.3121E-06	-.2764E-05
15	.3222E-05	.2845E-04	.7610E-05	-.2758E-05	-.5664E-05
16	.1360E-05	.2875E-04	.1006E-04	-.5427E-05	-.3756E-05
17	.0000E+00	.2776E-04	.0000E+00	-.4106E-05	.0000E+00
18	.3000E-04	.0000E+00	.4231E-06	.0000E+00	.0000E+00
19	.2637E-04	.6821E-05	.8149E-06	.8850E-06	-.1017E-05
20	.1055E-04	.2111E-04	.2316E-05	.5809E-06	-.1849E-05
21	.2964E-05	.2653E-04	.4529E-05	-.1775E-05	-.3536E-05
22	.0000E+00	.2513E-04	.0000E+00	-.1611E-05	.0000E+00
23	.3285E-04	.0000E+00	.0000E+00	.0000E+00	.0000E+00
24	.2318E-04	.0000E+00	.0000E+00	.0000E+00	-.1461E-05
25	.1299E-04	.1572E-04	.1205E-05	.3192E-06	-.1280E-05
26	.0000E+00	.2304E-04	.0000E+00	-.1145E-05	.0000E+00
27	.0000E+00	.0000E+00	.0000E+00	.0000E+00	-.1897E-05
28	.0000E+00	.1784E-04	.0000E+00	.0000E+00	-.1075E-05
29	.0000E+00	.2183E-04	.0000E+00	.0000E+00	.0000E+00

Table 29 - Deflection at each node of the third lowest compressive buckling mode.

Node	x (cm)	y (cm)	w (cm)
1	1.000	.000	.4645E-04
2	.968	2.500	.3349E-04
3	.866	5.000	-.1836E-05
4	.368	9.300	-.4370E-04
5	.148	9.890	-.4319E-04
6	.126	9.920	-.4312E-04
7	.100	9.950	-.4304E-04
8	.077	9.970	-.4298E-04
9	.045	9.990	-.4292E-04
10	.000	10.000	-.4289E-04
11	6.000	.000	.2840E-04
12	5.000	4.000	.8225E-05
13	3.500	7.500	-.2975E-04
14	1.500	9.800	-.4161E-04
15	.240	9.990	-.4280E-04
16	.110	10.100	-.4251E-04
17	.000	10.400	-.4136E-04
18	11.000	.000	.1479E-04
19	11.000	7.000	-.1592E-04
20	3.000	11.000	-.3638E-04
21	.500	10.500	-.4081E-04
22	.000	11.500	-.3513E-04
23	18.000	.000	.0000E+00
24	18.000	12.000	.0000E+00
25	8.000	15.000	.2768E-05
26	.000	16.000	.1350E-04
27	18.000	25.000	.0000E+00
28	7.000	25.000	.0000E+00
29	.000	25.000	.0000E+00

Table 30 - Deflection at each node of the fourth lowest compressive buckling mode.

Node	x (cm)	y (cm)	w (cm)
1	1.000	.000	.1692E-04
2	.968	2.500	.9960E-05
3	.866	5.000	-.6444E-05
4	.368	9.300	-.1260E-04
5	.148	9.890	-.1022E-04
6	.126	9.920	-.1008E-04
7	.100	9.950	-.9944E-05
8	.077	9.970	-.9852E-05
9	.045	9.990	-.9760E-05
10	.000	10.000	-.9712E-05
11	6.000	.000	.8983E-05
12	5.000	4.000	-.5389E-06
13	3.500	7.500	-.1215E-04
14	1.500	9.800	-.9776E-05
15	.240	9.990	-.9710E-05
16	.110	10.100	-.9221E-05
17	.000	10.400	-.7779E-05
18	11.000	.000	.3258E-05
19	11.000	7.000	-.5862E-05
20	3.000	11.000	-.3892E-05
21	.500	10.500	-.7229E-05
22	.000	11.500	-.2455E-05
23	18.000	.000	.0000E+00
24	18.000	12.000	.0000E+00
25	8.000	15.000	.5507E-05
26	.000	16.000	.9464E-05
27	18.000	25.000	.0000E+00
28	7.000	25.000	.0000E+00
29	.000	25.000	.0000E+00

APPENDIX V

NUMERICAL RESULTS FOR THE NARROW VERTICAL ELLIPTICAL CAVITY

APPENDIX V - NUMERICAL RESULTS FOR THE NARROW VERTICAL ELLIPTICAL CAVITY

Table 31 - Deflection at each node of the lowest tensile buckling mode.

Node	x (cm)	y (cm)	w (cm)
1	18.000	25.000	.0000E+00
2	18.000	.000	.0000E+00
3	18.000	6.000	.0000E+00
4	18.000	15.000	.0000E+00
5	11.000	25.000	.0000E+00
6	4.000	25.000	.0000E+00
7	.000	25.000	.0000E+00
8	11.500	.000	-.7823E-05
9	10.400	.500	-.1884E-04
10	11.000	3.000	-.8089E-05
11	10.000	9.000	-.6744E-05
12	6.000	14.000	-.2222E-04
13	.000	15.000	-.3587E-04
14	10.400	.000	-.1913E-04
15	10.100	.110	-.2314E-04
16	9.990	.240	-.2462E-04
17	9.800	1.500	-.2448E-04
18	5.500	4.000	-.8977E-04
19	.000	6.000	-.1207E-03
20	10.100	.000	-.2316E-04
21	10.000	.000	-.2459E-04
22	9.990	.045	-.2473E-04
23	9.970	.077	-.2501E-04
24	9.950	.100	-.2530E-04
25	9.920	.126	-.2573E-04
26	9.890	.148	-.2617E-04
27	9.300	.368	-.3567E-04
28	5.000	.866	-.1439E-03
29	.000	1.000	-.2225E-03

Table 32 - Deflection at each node of the second lowest tensile buckling mode.

Node	x (cm)	y (cm)	w (cm)
1	18.000	25.000	.0000E+00
2	18.000	.000	.0000E+00
3	18.000	6.000	.0000E+00
4	18.000	15.000	.0000E+00
5	11.000	25.000	.0000E+00
6	4.000	25.000	.0000E+00
7	.000	25.000	.0000E+00
8	11.500	.000	.8219E-07
9	10.400	.500	.2272E-06
10	11.000	3.000	.3770E-06
11	10.000	9.000	-.7806E-07
12	6.000	14.000	.2139E-06
13	.000	15.000	.3775E-06
14	10.400	.000	.2821E-06
15	10.100	.110	.3801E-06
16	9.990	.240	.4411E-06
17	9.800	1.500	.9161E-06
18	5.500	4.000	.9921E-06
19	.000	6.000	.1131E-05
20	10.100	.000	.3993E-06
21	10.000	.000	.5312E-06
22	9.990	.045	.5451E-06
23	9.970	.077	.5742E-06
24	9.950	.100	.6058E-06
25	9.920	.126	.6597E-06
26	9.890	.148	.7172E-06
27	9.300	.368	.9197E-06
28	5.000	.866	.1608E-05
29	.000	1.000	.1954E-05

Table 33 - Continuation of Table 25, including the results of rotations and curvatures.

Node	$\frac{\partial w}{\partial x}$	$\frac{\partial w}{\partial y}$	$\frac{\partial^2 w}{\partial x^2}$	$\frac{\partial^2 w}{\partial y^2}$	$\frac{\partial^2 w}{\partial x \partial y}$
1	.0000E+00	.0000E+00	.0000E+00	.0000E+00	.4886E-07
2	-.1874E-05	.0000E+00	.0000E+00	.0000E+00	.0000E+00
3	-.1883E-05	.0000E+00	.0000E+00	.0000E+00	.7707E-07
4	-.7788E-06	.0000E+00	.0000E+00	.0000E+00	.1120E-06
5	.0000E+00	.2440E-06	.0000E+00	.0000E+00	-.2103E-06
6	.0000E+00	.2369E-05	.0000E+00	.0000E+00	-.3696E-06
7	.0000E+00	.3016E-05	.0000E+00	.0000E+00	.0000E+00
8	.7973E-05	.0000E+00	-.3721E-05	.0000E+00	.0000E+00
9	.1237E-04	.1181E-05	-.4609E-05	.1683E-05	-.1321E-05
10	.7664E-05	.1935E-05	-.3203E-05	-.1297E-06	-.7913E-06
11	.5896E-05	.1077E-05	-.1874E-05	-.2000E-06	-.7584E-06
12	.5516E-05	.2598E-05	-.1342E-06	-.8339E-07	-.9330E-06
13	.0000E+00	.5636E-05	.0000E+00	-.1011E-05	.0000E+00
14	.1272E-04	.0000E+00	-.4969E-05	.0000E+00	.0000E+00
15	.1406E-04	.4086E-06	-.4770E-05	.3575E-05	-.8975E-06
16	.1449E-04	.9365E-06	-.5321E-05	.3193E-05	-.9239E-06
17	.1376E-04	.3017E-05	-.4583E-05	.6872E-06	-.1362E-05
18	.2030E-04	.1007E-04	.6266E-06	-.1545E-05	-.2460E-05
19	.0000E+00	.1659E-04	.0000E+00	-.4807E-05	.0000E+00
20	.1410E-04	.0000E+00	-.4819E-05	.0000E+00	.0000E+00
21	.1443E-04	.0000E+00	-.9661E-06	.0000E+00	.0000E+00
22	.1451E-04	.1460E-06	-.3153E-05	.3907E-05	.1516E-05
23	.1464E-04	.2792E-06	-.4511E-05	.5558E-05	.7481E-06
24	.1477E-04	.3874E-06	-.6201E-05	.5488E-05	.3032E-06
25	.1496E-04	.5284E-06	-.6853E-05	.5427E-05	-.3112E-06
26	.1512E-04	.6795E-06	-.5764E-05	.3785E-05	-.1213E-05
27	.1821E-04	.2408E-05	-.5804E-05	.2132E-05	-.2204E-05
28	.2940E-04	.1548E-04	.4894E-06	-.6277E-06	-.3216E-05
29	.0000E+00	.2328E-04	.0000E+00	-.5251E-05	.0000E+00

Table 34 - Deflection at each node of the third lowest tensile buckling mode.

Node	x (cm)	y (cm)	w (cm)
1	18.000	25.000	.0000E+00
2	18.000	.000	.0000E+00
3	18.000	6.000	.0000E+00
4	18.000	15.000	.0000E+00
5	11.000	25.000	.0000E+00
6	4.000	25.000	.0000E+00
7	.000	25.000	.0000E+00
8	11.500	.000	-.3565E-05
9	10.400	.500	.4301E-05
10	11.000	3.000	-.3992E-05
11	10.000	9.000	-.3846E-05
12	6.000	14.000	.6490E-05
13	.000	15.000	.1341E-04
14	10.400	.000	.4633E-05
15	10.100	.110	.7787E-05
16	9.990	.240	.8952E-05
17	9.800	1.500	.8156E-05
18	5.500	4.000	.4186E-04
19	.000	6.000	.2735E-04
20	10.100	.000	.7812E-05
21	10.000	.000	.8969E-05
22	9.990	.045	.9084E-05
23	9.970	.077	.9314E-05
24	9.950	.100	.9547E-05
25	9.920	.126	.9902E-05
26	9.890	.148	.1026E-04
27	9.300	.368	.1812E-04
28	5.000	.866	.6448E-04
29	.000	1.000	.2763E-05

Table 35 - Deflection at each node of the fourth lowest tensile buckling mode.

Node	x (cm)	y (cm)	w (cm)
1	18.000	25.000	.0000E+00
2	18.000	.000	.0000E+00
3	18.000	6.000	.0000E+00
4	18.000	15.000	.0000E+00
5	11.000	25.000	.0000E+00
6	4.000	25.000	.0000E+00
7	.000	25.000	.0000E+00
8	11.500	.000	.4400E-05
9	10.400	.500	-.3023E-05
10	11.000	3.000	.5253E-05
11	10.000	9.000	.6625E-05
12	6.000	14.000	-.3487E-05
13	.000	15.000	-.7476E-05
14	10.400	.000	-.3295E-05
15	10.100	.110	-.6047E-05
16	9.990	.240	-.7054E-05
17	9.800	1.500	-.6829E-05
18	5.500	4.000	-.1969E-04
19	.000	6.000	-.1236E-04
20	10.100	.000	-.6067E-05
21	10.000	.000	-.7060E-05
22	9.990	.045	-.7159E-05
23	9.970	.077	-.7359E-05
24	9.950	.100	-.7561E-05
25	9.920	.126	-.7867E-05
26	9.890	.148	-.8176E-05
27	9.300	.368	-.1444E-04
28	5.000	.866	-.1989E-06
29	.000	1.000	-.1998E-04

Table 36 - Deflection at each node of the lowest compressive buckling mode.

Node	x (cm)	y (cm)	w (cm)
1	18.000	25.000	.0000E+00
2	18.000	.000	.0000E+00
3	18.000	6.000	.0000E+00
4	18.000	15.000	.0000E+00
5	11.000	25.000	.0000E+00
6	4.000	25.000	.0000E+00
7	.000	25.000	.0000E+00
8	11.500	.000	-.1064E-03
9	10.400	.500	-.1220E-03
10	11.000	3.000	-.1183E-03
11	10.000	9.000	-.1522E-03
12	6.000	14.000	-.1950E-03
13	.000	15.000	-.2113E-03
14	10.400	.000	-.1218E-03
15	10.100	.110	-.1258E-03
16	9.990	.240	-.1273E-03
17	9.800	1.500	-.1318E-03
18	5.500	4.000	-.1903E-03
19	.000	6.000	-.2214E-03
20	10.100	.000	-.1258E-03
21	10.000	.000	-.1270E-03
22	9.990	.045	-.1272E-03
23	9.970	.077	-.1274E-03
24	9.950	.100	-.1277E-03
25	9.920	.126	-.1281E-03
26	9.890	.148	-.1285E-03
27	9.300	.368	-.1361E-03
28	5.000	.866	-.1822E-03
29	.000	1.000	-.2003E-03

Table 37 - Deflection at each node of the second lowest compressive buckling mode.

Node	x (cm)	y (cm)	w (cm)
1	18.000	25.000	.0000E+00
2	18.000	.000	.0000E+00
3	18.000	6.000	.0000E+00
4	18.000	15.000	.0000E+00
5	11.000	25.000	.0000E+00
6	4.000	25.000	.0000E+00
7	.000	25.000	.0000E+00
8	11.500	.000	.2132E-03
9	10.400	.500	.2447E-03
10	11.000	3.000	.2081E-03
11	10.000	9.000	.1315E-03
12	6.000	14.000	.7998E-04
13	.000	15.000	.7321E-04
14	10.400	.000	.2456E-03
15	10.100	.110	.2546E-03
16	9.990	.240	.2575E-03
17	9.800	1.500	.2531E-03
18	5.500	4.000	.2724E-03
19	.000	6.000	.2449E-03
20	10.100	.000	.2547E-03
21	10.000	.000	.2578E-03
22	9.990	.045	.2580E-03
23	9.970	.077	.2586E-03
24	9.950	.100	.2592E-03
25	9.920	.126	.2600E-03
26	9.890	.148	.2609E-03
27	9.300	.368	.2764E-03
28	5.000	.866	.3423E-03
29	.000	1.000	.3583E-03

Table 38 - Continuation of Table 29, including the results of rotations and curvatures.

Node	$\frac{\partial w}{\partial x}$	$\frac{\partial w}{\partial y}$	$\frac{\partial^2 w}{\partial x^2}$	$\frac{\partial^2 w}{\partial y^2}$	$\frac{\partial^2 w}{\partial x \partial y}$
1	.0000E+00	.0000E+00	.0000E+00	.0000E+00	-.2646E-05
2	.1705E-04	.0000E+00	.0000E+00	.0000E+00	.0000E+00
3	.1898E-04	.0000E+00	.0000E+00	.0000E+00	.5193E-06
4	.1917E-04	.0000E+00	.0000E+00	.0000E+00	-.7392E-06
5	.0000E+00	.1649E-04	.0000E+00	.0000E+00	-.1852E-05
6	.0000E+00	.2585E-04	.0000E+00	.0000E+00	-.7405E-06
7	.0000E+00	.2713E-04	.0000E+00	.0000E+00	.0000E+00
8	.1471E-04	.0000E+00	.9973E-06	.0000E+00	.0000E+00
9	.1356E-04	-.8096E-06	.1108E-05	-.1219E-05	.8520E-06
10	.1525E-04	-.2813E-05	.8204E-06	-.6083E-06	.4403E-06
11	.1604E-04	-.1747E-05	.1297E-05	.8823E-06	.1262E-06
12	.9199E-05	.6641E-05	.1626E-05	.2382E-05	-.2794E-06
13	.0000E+00	.1053E-04	.0000E+00	.2524E-05	.0000E+00
14	.1332E-04	.0000E+00	.1526E-05	.0000E+00	.0000E+00
15	.1292E-04	-.3031E-06	.1610E-05	-.2559E-05	.8776E-06
16	.1290E-04	-.7154E-06	.1276E-05	-.1870E-05	.1079E-05
17	.1360E-04	-.2229E-05	.9843E-06	-.8924E-06	.4605E-06
18	.8598E-05	-.4623E-05	.1843E-05	-.3174E-06	.1632E-06
19	.0000E+00	-.4225E-05	.0000E+00	-.4505E-06	.0000E+00
20	.1287E-04	.0000E+00	.1933E-05	.0000E+00	.0000E+00
21	.1272E-04	.0000E+00	.7259E-06	.0000E+00	.0000E+00
22	.1270E-04	-.1719E-06	.1810E-05	-.3750E-05	.5314E-06
23	.1268E-04	-.3146E-06	.1785E-05	-.3839E-05	.1128E-05
24	.1267E-04	-.4192E-06	.1989E-05	-.3387E-05	.1365E-05
25	.1265E-04	-.5469E-06	.1852E-05	-.2911E-05	.1656E-05
26	.1264E-04	-.6631E-06	.1436E-05	-.1600E-05	.1625E-05
27	.1232E-04	-.1695E-05	.1003E-05	-.4515E-06	.9451E-06
28	.7893E-05	-.3114E-05	.1686E-05	-.5584E-06	-.1705E-06
29	.0000E+00	-.3658E-05	.0000E+00	-.8441E-06	.0000E+00

Table 39 - Deflection at each node of the third lowest compressive buckling mode.

Node	x (cm)	y (cm)	w (cm)
1	18.000	25.000	.0000E+00
2	18.000	.000	.0000E+00
3	18.000	6.000	.0000E+00
4	18.000	15.000	.0000E+00
5	11.000	25.000	.0000E+00
6	4.000	25.000	.0000E+00
7	.000	25.000	.0000E+00
8	11.500	.000	-.1145E-04
9	10.400	.500	-.1163E-04
10	11.000	3.000	.3171E-05
11	10.000	9.000	.4476E-04
12	6.000	14.000	.1345E-04
13	.000	15.000	-.2226E-05
14	10.400	.000	-.1229E-04
15	10.100	.110	-.1270E-04
16	9.990	.240	-.1261E-04
17	9.800	1.500	-.5906E-05
18	5.500	4.000	.3398E-04
19	.000	6.000	.5336E-04
20	10.100	.000	-.1275E-04
21	10.000	.000	-.1296E-04
22	9.990	.045	-.1297E-04
23	9.970	.077	-.1298E-04
24	9.950	.100	-.1299E-04
25	9.920	.126	-.1300E-04
26	9.890	.148	-.1301E-04
27	9.300	.368	-.1246E-04
28	5.000	.866	.7721E-05
29	.000	1.000	.1981E-04

Table 40 - Deflection at each node of the fourth lowest compressive buckling mode.

Node	x (cm)	y (cm)	w (cm)
1	18.000	25.000	.0000E+00
2	18.000	.000	.0000E+00
3	18.000	6.000	.0000E+00
4	18.000	15.000	.0000E+00
5	11.000	25.000	.0000E+00
6	4.000	25.000	.0000E+00
7	.000	25.000	.0000E+00
8	11.500	.000	-.8032E-05
9	10.400	.500	-.6037E-05
10	11.000	3.000	.9222E-05
11	10.000	9.000	.2002E-04
12	6.000	14.000	-.1129E-04
13	.000	15.000	-.6555E-05
14	10.400	.000	-.6766E-05
15	10.100	.110	-.6472E-05
16	9.990	.240	-.6099E-05
17	9.800	1.500	.1302E-05
18	5.500	4.000	.3048E-04
19	.000	6.000	.2489E-04
20	10.100	.000	-.6535E-05
21	10.000	.000	-.6503E-05
22	9.990	.045	-.6487E-05
23	9.970	.077	-.6447E-05
24	9.950	.100	-.6403E-05
25	9.920	.126	-.6332E-05
26	9.890	.148	-.6255E-05
27	9.300	.368	-.4008E-05
28	5.000	.866	.2238E-04
29	.000	1.000	.3258E-04

VITA

Yi-Der Lee, son of Juei-Chen Lee and Huey-Lan Huang, was born on November 24, 1958 in Tainan, Taiwan, Republic of China. He graduated from Kaohsiung High School in June 1976. He attended the National Cheng Kung University in Tainan, Taiwan from 1976 and received the Bachelor of Science degree in Mechanical Engineering with high honors in June 1980. In August 1983, he was accepted as a graduate student in the Department of Mechanical Engineering and Mechanics at Lehigh University.